2 (mix)

MCR 74-93
May 24, 1974

Technical Report

Payload/Orbiter Contamination Control Requirement Study

Final Report

Contract NAS8-30452

Authors

L. E. Bareiss
R. O. Rantanen
E. B. Ress

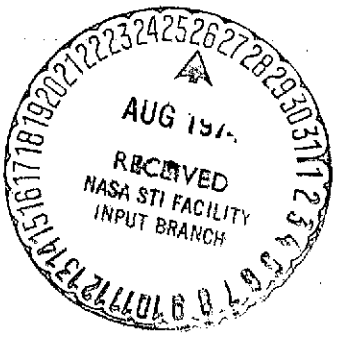

Prepared for

George C. Marshall Space Flight Center
Marshall Space Flight Center, Alabama 35812
by

Martin Marietta Aerospace, Denver Division
Denver, Colorado 80201

154

CONTENTS

CONTENTS (continued)

Figures

CONTENTS (continued)

CONTENTS (continued)

CONTENTS (continued)

1. SCOPE

1.1 Purpose - The purpose of this study is to determine and quantify the expected particulate and molecular on orbit contaminant environment for selected Shuttle Payloads as a result of major Shuttle Orbiter contaminant sources. This study reviews individual Payload susceptibilities to contamination, identifies the risk of Payload data degradation, and provides preliminary recommendations and establishes limiting factors which may depend upon operational activities associated with the Payload/Orbiter interface or upon independent Payload functional activities.

This report begins to define the contamination environment of selected planned Shuttle Payloads, determines the impact of the contamination environment on Payload feasibility design and operation, and the requirements of Payloads on Orbiter contamination control procedures. This study will begin to support the definition of the Orbiter and furnish a basis for Payload/Orbiter interface definition in the area of contamination control.

1.2 Scope - This report presents the development of a basic working computer model of the Shuttle Orbiter which includes a representative Payload configuration. The Orbiter and Payload configuration have been synthesized by developing nodal descriptions of the important geometric surfaces. These nodal surfaces have been identified numerically and have been given an optical or material characterization. The area of each nodal surface, the distance between nodal surfaces, the angular relationships, and geometric shadowing between nodal surfaces have been established. Based upon these geometrical considerations, nine lines-of-sight, which encompass viewing requirements for both the contaminants and the Payloads, have been established.

Major Orbiter contamination sources, locations, and flux characteristics based upon available data have been defined and modeled. The principle contamination sources considered were outgassing, offgassing, leakage, evaporator, Reaction Control Subsystem 25 lb thrust vernier engines, and the returned flux. Other Orbiter and/or operational contaminant sources have been identified and presented to indicate potential additional sources

which could impact a Payload. These additional sources include those peculiar to the Orbiter, reflection and resublimation from Orbiter surfaces, and boost and reentry contamination sources.

Individual Payload configurations were reviewed to identify their susceptibility to contamination. Those Payloads reviewed were:

a. 1.5 Meter Cryogenically Cooled Infrared Telescope,
b. Deep Sky Ultraviolet Survey Telescope,
c. 1.0 Meter Ultraviolet Diffraction Limited Telescope,
d. 2.5 Meter Cryogenically Cooled Infrared Telescope,
e. Dedicated Solar Sortie Mission,
f. Communications/Navigations Sortie Mission,
g. Upper Atmosphere Explorer,
h. Large Space Telescope,
i. Extra Corona Lyman Alpha Explorer,
j. Large X-Ray Telescope Facility,
k. Mars Hard Lander.

Comparisons of the determined susceptibilities to susceptibilities observed from comparable experiments on Skylab were developed. Based upon the developed contamination susceptibility review and the contaminant induced environment description as a result of the surface and source modeling, the risk of Payload data degradation from contamination was established. The risk factors or assessments were based upon contamination standards from the Woods' Hole Summer Study Work Sheets (July 1973), the Astronomy Working Group Report (May 1973), and upon value judgments gained as a result of available Skylab experience and data.

Recommendations with respect to payload feasibility, design, and operational aspects are presented. These recommendations are also with respect to support of the definition of the Orbiter and begin to develop a basis for overall Payload/Orbiter interface definition in the area of contamination control.

1.3 Summary - This study was established to determine if a contamination potential exists for the proposed Shuttle Orbiter/Payload concept. The sources and configurations modeled and analyzed are considered typical of expected situations. However, many of these source impacts on contamination levels as defined by this study can be minimized by relocating of sources, using alternate approaches, or proper mission timelining of experiment exposure times and source rates. Additional studies will be required in those areas identified as potential contaminant problems in order to establish the necessary changes or improvements consistent to program requirements and objectives to minimize or eliminate the impact of contamination upon those sensitive Payloads.

This initial Payload/Orbiter contamination control requirement study has shown that the induced contaminant environment from the Orbiter will require program contamination controls which may impact both the Orbiter and some of the many envisioned Payloads. Those Payloads which have been shown by this study to be especially sensitive to contamination were the infrared and the ultraviolet Payloads.

For those major Orbiter contamination sources modeled and under the assumptions made for this study, the induced Shuttle Orbiter contaminant environment will be at least that or greater than that anticipated and essentially observed on Skylab. A significant difference between the Shuttle Orbiter and Skylab is that on Skylab the majority of experiments were constrained to view unidirectional and those sources which required venting could be positioned so as not to particularly impact any given line-of-sight. On the Shuttle Orbiter many of the Payloads have off axis viewing requirements that encompass approximately 100 degrees of a 180 degree hemisphere which may allow some lines-of-sight to be directly impacted by contamination. In addition (due to reentry requirements for the Orbiter), the present defined major vent type sources are all located on the top portion of the Orbiter constrained to venting into the same hemisphere as the Payloads are looking. The baselined evaporator, leakage rates, and the RCS vernier engine effluent rates exceed similar activities on Skylab.

As a result of this, the elimination of any one of these sources does not uniquely reduce its impact as established by this study. The results of this study strongly suggest that further analysis of those overboard ventings (evaporator and the 25 lb thrust RCS vernier engines) should be performed along with refined analysis and testing for cabin atmosphere leakage, outgassing of non-metallic materials, off-gassing, and the production of particulates (ground handling and on orbit operations).

Leakage and outgassing are continuous sources which for all intent and purpose cannot be directly controlled on orbit. Leakage will be highly dependent upon the structural integrity of the Orbiter. Repeated launches and reentries will most likely make this source hard to assess and establish control over. Material selection, quantity, location, and qualification for usage on the Orbiter and the Payload must be controlled to specifications at least that or better than those materials considered acceptable for Skylab. Outgassing was the major source of deposition on Skylab and will be an important source of contaminants on Shuttle.

Exposure times for many of the Shuttle Payloads may exceed that of similar experiments on Skylab when multiple flights or long duration missions are contemplated.

Offgassing is somewhat the result of non-metallic materials but it is also dependent upon design factors such as compartmentization of modules, multilayer insulations, experiment bay linear, ground handling, and launch environment. Improvements to decrease the amount and/or the duration of offgassing will be required. Unlike Skylab where essentially 10 days were available for the ATM canister to reach a stable pressure, the Orbiter and Payload will be required to be operational within hours or in a few days to maximize mission objectives. This is not such a critical problem for deployed systems where delays on the order of 10 days will not necessarily impact their long term mission profiles unless Orbiter tending is necessary to establish Payload operation or checkout.

The repeated ground handling in refurbishing Payloads, changing Payloads, and the repeated launching and reentry of the Orbiter will increase the particulate potential. On orbit activities such as experiment bay doors opening, gimbaling of large Payloads, and the use of large movable aperture shades or doors will all tend to increase the particulate environment.

This study and summary must also be weighed against the Payloads and their sensitivity to contamination. By far, the infrared Payloads are the most sensitivie and the levels of contamination identified in this study will greatly impact these types of Payloads. These systems have sensitivities 5 orders of magnitude greater than infrared experiments on Skylab (S191 and S192) and also will be cryogenically cooled trapping everything that comes in contact with the cooled surfaces.

Ultraviolet and Deep Space Survey Payloads have been shown to be the next most sensitive to the levels of induced environment established by this study. Basic improvements in the locations of those sources such as the evaporator and the RCS 25 lb thrust vernier engines and improvements in the other sources will probably suffice for these Payloads. Additional on orbit constraints for vents on the Orbiter and establishing Payload

operational constraints as established for Skylab will probably bring the necessary contamination control to these Payloads.

The Solar Payloads and the Communications and Navigation Payloads will probably not be directly affected by the induced environment. Although these Payloads may be periodically effected by particulates, they as a whole should not be affected.

Automated or Free Flying Payloads are susceptible to contamination while in the experiment bay and during deployment from the Orbiter. Protective measures are being studied to minimize contamination during this period, however the Orbiter RCS impingement could cause physical damage and/or leave large amounts of deposition on the external surfaces of the Payloads. Free Flying Payloads will have their own environments to be concerned with more than the Orbiter. This has been demonstrated previously on many unmanned satellite systems (much smaller and less sensitive than those Free Flying Payloads envisioned for Shuttle). The Free Flying Payloads require independent studies to assess the free flying impact of self-contamination. This latter point is also important in that this study did not address the individual Payloads contribution to the Orbiter induced environment which could be significant because of physical size.

One important side aspect of this study has pointed out the need of adequate criteria for each independent Payload to establish their relative susceptibilities to contamination. Those criteria, standards and in fact correlation with previous space programs have been found to be inadequate in establishing baseline criteria for contamination decisions.

If the infrared Payloads are baselined as sortie modes, then the contamination control on the Orbiter and on the Payload will be rigorous to meet the requirements for mission success. If the induced environment is controlled to be acceptable for the infrared Payloads, it will most assuredly be acceptable for other proposed Payloads.

2. APPLICABLE DOCUMENTS

2.1 Program Documents - The following documents shown form a part of this report in the extent that they were used for Program information and/or are referenced for supporting technical material relevant to this study.

PROGRAM DOCUMENTS

SD-72-SH-0071B	"Orbiter Definition Handbook", Preliminary Design Review Configuration, February 4, 1974, Space Division Rockwell International.
Preliminary	"Summarized NASA Payload Descriptions - Automated Payloads", October 1973, George C. Marshall Space Flight Center.
Preliminary	"Summarized NASA/ESRO Payload Descriptions", October 1973, George C. Marshall Space Flight Center.
JSC 07700 Vol. XIV Revision B	"Space Shuttle Program Space Shuttle System Payload Accommodations", December 21, 1973, Lyndon B. Johnson Space Center.
JSC 08500 Volumes A through G	"Space Shuttle and Spacelab Discussions", October 11 and 12, 1973, Lyndon B. Johnson Space Center.
ES3-11263-1	"Status Briefing of Orbiter Purge and Vent System to Particles and Gases Working Group", November 11, 1973, Lyndon B. Johnson Space Center.

(No Number)	"Final Report of the Space Shuttle Payload Planning Working Groups", Volumes 1 through 10 including Executive Summaries, May 1973, Goddard Space Flight Center.
Technical Letter ASD-PD-18743	"Contamination Sensitivity of Selected Space Shuttle Payloads", Program Development Branch Systems Engineering Department Aerospace Support Division, George C. Marshall Space Flight Center.
50M02442 Revision W	"ATM Material Control for Contamination Due to Outgassing," March 1, 1972, George C. Marshall Space Flight Center.
CR-61173	"Apollo Telescope Mount Extended Applications Study Program - ATM Contamination Study Final Report," March 10, 1967, Ball Brothers Research Corporation.

3. ORBITER/PAYLOAD CONFIGURATION MODEL

3.1 Surface Description - The Shuttle Orbiter and a representative Payload configuration was three dimensionally synthesized on a CDC 6500 computer using a Scope 3.4 format system. The maximum number of surfaces and/or nodes that can be defined using this technique is 1100. The area of any one surface can be accurately identified down to fractions of a square meter. However, dependent upon the number of nodes available for surface definition and the number of surfaces to be described, the minimum area size must be considered a variable depending upon the resolution required and number of surfaces to be defined. It is possible to separately subdivide any surface configuration and treat specific cases singularly or uniquely.

For this study, the Shuttle Orbiter and representative Payload were described geometrically by 114 basic surface shapes. These surfaces were further subdivided into a total of 181 nodes. The physical shape of the surfaces input to the model to define the configurations are drawn graphically by scale computer plots and will be discussed in the following section. These graphical displays are used to verify the location and geometrical shape of any specific surface or relationships between surfaces or contaminant sources.

Four basic computer listings are developed with respect to the configuration modeling. These listings provide the necessary visibility to all the geometrical considerations used in establishing the model. Typical examples of these computer listings are presented in Figures 1 through 4 . Descriptions of each of these computer listings are presented below:

a. Surface orientation (input data), Figure 1 which includes;

   1) surface number (node number),
   2) X, Y, Z coordinate,
   3) rotation about major axes,
   4) sensitive side of surface in question,
   5) shadowing considerations,
   6) surface optical characteristics,
   7) surface type.

```
INPUT CARD COL. = 12345678 1 2345678 2 2345678 3 2345678 4 2345678 5 2345678 6 2345678 7 2345678 8 EDIT NO. CLC EDIT NO.  LABEL
                  P2=-644.,191.,-90.                                                                                    BB
                  P3=-463.,191.,-65.                                                                                    BA
                  PROP=0.,0.                                                                                            BA
                  COM=*   INNER WING C RECT*                                                                            BA
            $     SURF=4,TYPE=POLY,ACTIVE=BOTTOM,SHADE=BOTH,BSHADE=BOTH                                                 BA
                  P1=-698.,102.,-102.                                                                                   BA
                  P2=-644.,466.,-90.                                                                                    BA
                  P3=-644.,102.,-90.                                                                                    BA
                  PROP=0.,0.                                                                                            BA
                  COM=*...WING TAIL FLAP RT 1453,1507*                                                                  BA
            $     SURFN=  150,SHADE=BOTH,BSHADE=BOTH,ALPHA=-0.   ,EMISS=-0.                                             BA
                  TRANS=-0.   ,TRANI=-0.   ,COM=*BAY FREE CYLINDER                                                      BA
                  TYPE=CYLINDER  ,ACTIVE=INSIDE ,ALPH= 1.02000E+02                                                      BA
                  BMIN= 0.          ,BMAX= 7.60000E+02,GMIN= 0.                                                         BA
                  GMAX= 1.03000E+02,NNX=    2,NNY=    4,ICSN=   -0                                                    BA
                  POSITION=-4.72000E+02, 0.         , 0.                                                              BA
                  ROTZ    =   -0.    , ROTY    =   90.0000, ROTX    =    0.                                          BA
            $     SURFN=  140,SHADE=BOTH,BSHADE=BOTH,ALPHA=-0.   ,EMISS=-0.                                             BA
                  TRANS=-0.   ,TRANI=-0.   ,COM=*  END  BAY AREA DISK                                                   BA
                  TYPE=DISC      ,ACTIVE=TOP    ,ALPH= 0.                                                             BA
                  BMIN= 0.          ,BMAX= 1.62000E+02,GMIN= 0.                                                         BA
                  GMAX= 3.6300CE+02,NNX=    1,NNY=    1,ICSN=   -0                                                    BA
                  POSITION=-4.72000E+02, 0.         , 0.                                                              BA
                  ROTZ    =   -0.    , ROTY    =   90.0000, ROTX    =    0.                                          BA
            $     SURFN=  135,SHADE=BOTH,BSHADE=BOTH,ALPHA=-0.   ,EMISS=-0.                                             BA
                  TRANS=-0.   ,TRANI=-0.   ,COM=* FRONT BAY AREA DISK                                                   BA
                  TYPE=DISC      ,ACTIVE=TOP    ,ALPH= 0.                                                             BA
                  BMIN= 0.          ,BMAX= 1.02000E+02,GMIN= 0.                                                         BA
                  GMAX= 3.6000CE+02,NNX=    1,NNY=    1,ICSN=   -0                                                    BA
                  POSITION= 2.30000E+02, 0.         , 0.                                                              BA
                  ROTZ    =   -0.    , ROTY    =  -90.0000, ROTX    =    0.                                          BA
            $     SURFN=  122,SHADE=BOTH,BSHADE=BOTH,ALPHA=-0.   ,EMISS=-0.                                             BA
                  TRANS=-0.   ,TRANI=-0.   ,COM=* VERY ACSE CONE                                                        BA
                  TYPE=PARABOLOID,ACTIVE=OUTSIDE,ALPH= 6.13000E+00                                                      BA
                  BMIN= 0.          ,BMAX= 2.60000E+02,GMIN= 0.                                                         BA
                  GMAX= 3.60000E+02,NNX=    4,NNY=    1,ICSN=    1                                                    BA
                  POSITION= 2.00000E+02, 0.         ,-3.60000E+01                                                     BA
                  ROTZ    = -180.0000, ROTY    =  -90.0000, ROTX    =    0.                                          BA
            $     SURFN= 3200,SHADE=BOTH,BSHADE=BOTH,ALPHA=-0.   ,EMISS=-0.                                             BA
                  TRANS=-0.   ,TRANI=-0.   ,COM=*   NOSE CYLINDER                                                       BA
                  TYPE=CYLINDER  ,ACTIVE=OUTSIDE,ALPH= 7.00000E+01                                                      BA
                  BMIN= 0.          ,BMAX= 1.70000E+02,GMIN= 0.                                                         BA
                  GMAX= 3.60000E+02,NNX=    4,NNY=    1,ICSN=    1                                                    BA
                  POSITION= 4.00000E+02, 0.         ,-3.00000E+01                                                     BA
                  ROTZ    = -180.0000, ROTY    =  -90.0000, ROTX    =    0.                                          BA
            $     SURFN= 3400,SHADE=BOTH,BSHADE=BOTH,ALPHA=-0.   ,EMISS=-0.                                             BA
                  TRANS=-0.   ,TRANI=-0.   ,COM=*   NOSE PARTIAL BACK                                                  BA
                  TYPE=PARABOLOID,ACTIVE=OUTSIDE,ALPH= 7.00000E+00                                                      BA
                  BMIN= 2.60000E+02,BMAX= 3.70000E+02,GMIN= 0.                                                         BA
                  GMAX= 3.60000E+02,NNX=    4,NNY=    1,ICSN=    1                                                    BA
                  POSITION= 2.00000E+02, 0.         , 0.                                                              BA
```

Figure 1 . Surface Orientation (Input Data) Computer Printout

MODEL = CONTAM STEP = 1 SHUTTLE CONTAMINATION STUDY
PROCESSSING OPERATION DATA

NODE	PCS	AREA	ALPH	EMISS	SURF. TYPE	ACTIVE	--------COMMENTS----------
147	BODY	1.855E+04	0.	0.	PARABOLOID	OUTSID	TOP ENGIN
148	BODY	1.855E+04	0.	0.	PARABOLOID	OUTSID	+ Y ENGIN
149	BODY	1.855E+04	0.	0.	PARABOLOID	OUTSID	-Y ENGIN...
20	BODY	3.711E+03	0.	0.	DISC	TOP	...+Y OMS SEALER ...
21	BODY	3.711E+03	0.	0.	DISC	TOP	..+Y OMS SEALER ...
222	BODY	2.573E+04	0.	0.	RECTANGLE	BOTTOM	BACK RECT 7.35CEG
23	BODY	1.634E+04	0.	0.	DISC	TOP	REAR END HALF DISK
14	BODY	2.827E+01	0.	0.	DISC	TOP	BACK SIDE EVAPORAT
15	BODY	2.827E+01	0.	0.	DISC	TOP	REAR END EVAPORATOR
10	BODY	1.553E+04	0.	0.	TRAPEZOID	BOTTOM	....LEFT FRONT WING A ...
11	BODY	3.730E+04	0.	0.	TRAPEZOID	TOP	.....LEFT MIDDLE WING BACK.B
141	BODY	2.397E+04	0.	0.	RECTANGLE	TOP	BS INNER WING
12	BODY	4.513E+04	0.	0.	RECTANGLE	TOP	..... LEFT BACK RECT. WING C
142	BODY	1.455E+04	0.	0.	RECTANGLE	TOP	INNER WING C
13	BODY	1.012E+04	0.	0.	TRAPEZOID	TOP	..... LEFT WING TAIL EDGE
1	BODY	1.553E+04	0.	0.	TRAPEZOID	TOP	...FRONT WING TRIANGLE RT.A.58
2	BODY	3.730E+04	0.	0.	TRAPEZOID	BOTTOM	.....MIDDLE WING TRAP, RT B ..
143	BODY	2.397E+04	0.	0.	RECTANGLE	BOTTOM	B +Y RECTANGLE WING
3	BODY	4.513E+04	0.	0.	RECTANGLE	BOTTOM	.... BACK WING RECT. RTC .129
144	BODY	1.455E+04	0.	0.	RECTANGLE	BOTTOM	INNER WING C RECT
4	BODY	1.012E+04	0.	0.	TRAPEZOID	BOTTOM	...WING TAIL FLAP RT 1453,1507
150	BODY	2.804E+04	-0.	-0.	CYLINDER	INSIDE	BAY AREA CYLINDER
151	BODY	2.804E+04	-0.	-0.	CYLINDER	INSIDE	BAY AREA CYLINDER
152	BODY	2.804E+04	-0.	-0.	CYLINDER	INSIDE	BAY AREA CYLINDER
153	BODY	2.804E+04	-0.	-0.	CYLINDER	INSIDE	BAY AREA CYLINDER
154	BODY	2.804E+04	-0.	-0.	CYLINDER	INSIDE	BAY AREA CYLINDER
155	BODY	2.804E+04	-0.	-0.	CYLINDER	INSIDE	BAY AREA CYLINDER
156	BODY	2.804E+04	-0.	-0.	CYLINDER	INSIDE	BAY AREA CYLINDER
157	BODY	2.804E+04	-0.	-0.	CYLINDER	INSIDE	BAY AREA CYLINDER
160	BODY	3.269E+04	-0.	-0.	DISC	TOP	END BAY AREA DISK
135	BODY	3.269E+04	-0.	-0.	DISC	TOP	FRONT BAY AREA DISK
122	BODY	1.527E+04	-0.	-0.	PARABOLOID	OUTSID	VERY NOSE CONE
123	BODY	1.527E+04	-0.	-0.	PARABOLOID	OUTSID	VERY NOSE CONE
124	BODY	1.527E+04	-0.	-0.	PARABOLOID	OUTSID	VERY NOSE CONE
125	BODY	1.527E+04	-0.	-0.	PARABOLOID	OUTSID	VERY NOSE CONE
3200	BODY	4.673E+03	-0.	-0.	CYLINDER	OUTSID	NOSE CYLINDER
3201	BODY	4.673E+03	-0.	-0.	CYLINDER	OUTSID	NOSE CYLINDER
3202	BODY	4.673E+03	-0.	-0.	CYLINDER	OUTSID	NOSE CYLINDER
3203	BODY	4.673E+03	-0.	-0.	CYLINDER	OUTSID	NOSE CYLINDER
3204	BODY	4.673E+03	-0.	-0.	CYLINDER	OUTSID	NOSE CYLINDER
3205	BODY	4.673E+03	-0.	-0.	CYLINDER	OUTSID	NOSE CYLINDER
3206	BODY	4.673E+03	-0.	-0.	CYLINDER	OUTSID	NOSE CYLINDER
3207	BODY	4.673E+03	-0.	-0.	CYLINDER	OUTSID	NOSE CYLINDER
3208	BODY	4.673E+03	-0.	-0.	CYLINDER	OUTSID	NOSE CYLINDER
3209	BODY	4.673E+03	-0.	-0.	CYLINDER	OUTSID	NOSE CYLINDER
3210	BODY	4.673E+03	-0.	-0.	CYLINDER	OUTSID	NOSE CYLINDER

Figure 2. Surface Description Computer Printout

MODEL = CONTAM STEP = 1 SHUTTLE CONTAMINATION STUDY
FORM FACTOR CALCULATION LINK.

(* INDICATES NODE PAIR HAS BEEN SUBDIVIDED)

NODE I	NODE J	COMPUTATION	FE(I,J) W/SHAD	FE(J,I) W/SHAD	FA(I,J) W/SHAD	F (I,J) NO/SHAD	SHAD. E FACTOR	SHAD. A FACTOR	CP TIME (SEC)
5002	2031	CAL.	.000110	.000000	.000110	.000110	1.000000	1.000000	17.281
5002	2021	CAL.	.000542	.000002	.000542	.000542	1.000000	1.000000	17.691
5002	FF SUM =	.5410	ROW CP TIME =		17.697		*SPHERE	1 SPHERE	
5003	20	CAL.	.002241	.000009	.002241	.002241	1.000000	1.000000	.719
5003	11	CAL.	.000664	.000000	.000664	.003543	.187521	.187521	1.317
5003	12	CAL.	.000667	.000000	.000667	.001305	.510884	.510884	1.540
5003	1	CAL.	.006414	.000005	.006414	.008372	.766121	.766121	1.906
5003	143	CAL.	.000008	.000000	.000008	.000008	1.000000	1.000000	2.107
5003	151	CAL.	.034100	.000002	.034100	.034100	1.000000	1.000000	2.499
5003	152	CAL.	.008511	.000004	.008511	.008511	1.000000	1.000000	2.652
5003	153	CAL.	.003887	.000002	.003887	.003887	1.000000	1.000000	2.823
5003	155	CAL.	.006782	.000003	.006782	.006782	1.000000	1.000000	3.000
5003	156	CAL.	.008504	.000004	.008504	.008504	1.000000	1.000000	3.161
5003	157	CAL.	.003267	.000002	.003267	.003267	1.000000	1.000000	3.344
5003	135	CAL.	.011281	.000005	.011281	.011281	1.000000	1.000000	3.628
5003	182	CAL.	.000453	.000000	.000453	.000453	1.000000	1.000000	7.653
5003	771	CAL.	.001036	.000001	.001036	.001036	1.000000	1.000000	8.024
5003	772	CAL.	.001975	.000001	.001975	.001975	1.000000	1.000000	8.218
5003	773	CAL.	.004626	.000003	.004626	.004626	1.000000	1.000000	8.599
5003	774	CAL.	.008262	.000005	.008262	.008262	1.000000	1.000000	8.691
5003	775	CAL.	.006768	.000004	.006768	.006768	1.000000	1.000000	9.297
5003	776	CAL.	.007797	.000005	.007797	.007797	1.000000	1.000000	9.504
5003	777	CAL.	.003615	.000002	.003615	.003615	1.000000	1.000000	9.809
5003	778	CAL.	.006486	.000004	.006486	.006486	1.000000	1.000000	10.005
5003	2001	CAL.	.001166	.000001	.001166	.001166	1.000000	1.000000	10.664
5003	2031	CAL.	.000313	.000000	.000313	.000313	1.000000	1.000000	10.874
5003	2021	CAL.	.001057	.000004	.001057	.001057	1.000000	1.000000	11.444
5003	FF SUM =	.0999	ROW CP TIME =		11.449		*SPHERE	1 SPHERE	
5005	20	CAL.	.007642	.000033	.007642	.007642	1.000000	1.000000	1.253
5005	21	CAL.	.016115	.000070	.016115	.016115	1.000000	1.000000	1.712
5005	11	CAL.	.001760	.000001	.001760	.012707	.138490	.138490	2.411
5005	12	CAL.	.005200	.000002	.005200	.007607	.683635	.683635	2.792
5005	1	CAL.	.008435	.000037	.008435	.017475	.482694	.482694	3.520
5005	143	CAL.	.065280	.000284	.065280	.091453	.713805	.713805	4.405
5005	144	CAL.	.009070	.000040	.009070	.011973	.757581	.757581	4.842
5005	4	CAL.	.001906	.000008	.001906	.002888	.660142	.660142	5.236
5005	150	CAL.	.083259	.000368	.083259	.083259	1.000000	1.000000	6.149
5005	151	CAL.	.051017	.000029	.051017	.051017	1.000000	1.000000	6.609
5005	152	CAL.	.008495	.000305	.008495	.008495	1.000000	1.000000	6.865
5005	153	CAL.	.001567	.000001	.001567	.001567	1.000000	1.000000	7.113

Figure 3. View Factor Computer Printout

MODEL = CONTAM STEP = 1 SHUTTLE CONTAMINATION STUDY
PROCESSSING OPERATION DATA

NODE I	NODE J	F(I,J)	AREA	THETI	THETJ	RADIUS	NORMAL VECTOR I			POSITION VECTOR I		
5003	11	.000664	1.44E+01	106.85	65.47	3.31979E+02	7.19E+00	-2.22E+00	1.23E+01	-2.94E+02	4.45E+01	9.88E+01
5003	12	.000667	1.44E+01	117.40	74.40	4.93880E+02	7.19E+00	-2.22E+00	1.23E+01	-2.94E+02	4.49E+01	9.88E+01
5003	1	.000414	1.44E+01	86.10	69.41	3.44911E+02	7.19E+00	-2.22E+00	1.23E+01	-2.94E+02	4.49E+01	9.88E+01
5003	143	.000308	1.44E+01	154.30	42.38	1.86590E+02	7.19E+00	-2.22E+00	1.23E+01	-2.94E+02	4.49E+01	9.88E+01
5003	151	.000100	1.44E+01	112.00	24.89	2.24449E+02	7.19E+00	-2.22E+00	1.23E+01	-2.94E+02	4.49E+01	9.88E+01
5003	152	.000511	1.44E+01	89.46	52.38	3.33546E+02	7.19E+00	-2.22E+00	1.23E+01	-2.94E+02	4.49E+01	9.88E+01
5003	153	.000867	1.44E+01	79.19	65.07	4.83093E+02	7.19E+00	-2.22E+00	1.23E+01	-2.94E+02	4.49E+01	9.88E+01
5003	155	.000782	1.44E+01	123.45	43.59	1.93460E+02	7.19E+00	-2.22E+00	1.23E+01	-2.94E+02	4.49E+01	9.88E+01
5003	156	.000504	1.44E+01	93.50	63.45	3.13532E+02	7.19E+00	-2.22E+00	1.23E+01	-2.94E+02	4.49E+01	9.88E+01
5003	157	.000267	1.44E+01	81.63	72.64	4.69497E+02	7.19E+00	-2.22E+00	1.23E+01	-2.94E+02	4.49E+01	9.88E+01
5003	135	.001281	1.44E+01	69.18	14.72	5.41718E+02	7.19E+00	-2.22E+00	1.23E+01	-2.94E+02	4.49E+01	9.88E+01
5003	182	.000453	1.44E+01	112.35	111.28	3.33546E+02	7.19E+00	-2.22E+00	1.23E+01	-2.94E+02	4.49E+01	9.88E+01
5003	771	.001036	1.44E+01	71.86	86.07	4.01538E+02	7.19E+00	-2.22E+00	1.23E+01	-2.94E+02	4.49E+01	9.88E+01
5003	772	.001975	1.44E+01	104.57	82.04	1.98701E+02	7.19E+00	-2.22E+00	1.23E+01	-2.94E+02	4.49E+01	9.88E+01
5003	773	.004626	1.44E+01	71.87	67.71	4.34726E+02	7.19E+00	-2.22E+00	1.23E+01	-2.94E+02	4.49E+01	9.88E+01
5003	774	.008262	1.44E+01	98.81	50.51	2.59295E+02	7.19E+00	-2.22E+00	1.23E+01	-2.94E+02	4.49E+01	9.88E+01
5003	775	.006768	1.44E+01	79.03	69.50	3.91568E+02	7.19E+00	-2.22E+00	1.23E+01	-2.94E+02	4.49E+01	9.88E+01
5003	776	.007797	1.44E+01	124.60	40.48	1.77737E+02	7.19E+00	-2.22E+00	1.23E+01	-2.94E+02	4.49E+01	9.88E+01
5003	777	.003615	1.44E+01	76.86	81.23	3.70748E+02	7.19E+00	-2.22E+00	1.23E+01	-2.94E+02	4.49E+01	9.88E+01
5003	778	.010486	1.44E+01	136.37	63.17	1.25312E+02	7.19E+00	-2.22E+00	1.23E+01	-2.94E+02	4.49E+01	9.88E+01
5003	2001	.001166	1.44E+01	99.72	83.23	3.81763E+02	7.19E+00	-2.22E+00	1.23E+01	-2.94E+02	4.49E+01	9.88E+01
5003	2031	.000313	1.44E+01	103.75	84.54	4.71545E+02	7.19E+00	-2.22E+00	1.23E+01	-2.94E+02	4.49E+01	9.88E+01
5003	2021	.001057	1.44E+01	95.82	68.41	3.22591E+02	7.19E+00	-2.22E+00	1.23E+01	-2.94E+02	4.49E+01	9.88E+01
5005	20	.007642	1.60E+01	68.70	39.81	2.26354E+02	-8.02E+00	2.48E+00	-1.37E+01	-2.96E+02	4.81E+01	1.00E+02
5005	21	.016115	1.60E+01	51.99	16.50	1.81340E+02	-8.02E+00	2.48E+00	-1.37E+01	-2.96E+02	4.81E+01	1.00E+02
5005	11	.001760	1.60E+01	71.36	65.35	3.35261E+02	-8.02E+00	2.48E+00	-1.37E+01	-2.96E+02	4.81E+01	1.00E+02
5005	12	.005200	1.60E+01	62.74	74.21	4.95733E+02	-8.02E+00	2.48E+00	-1.37E+01	-2.96E+02	4.81E+01	1.00E+02
5005	1	.008435	1.60E+01	91.92	69.26	3.46842E+02	-8.02E+00	2.48E+00	-1.37E+01	-2.96E+02	4.81E+01	1.00E+02
5005	143	.065280	1.60E+01	25.14	41.11	1.89554E+02	-8.02E+00	2.48E+00	-1.37E+01	-2.96E+02	4.81E+01	1.00E+02
5005	144	.009070	1.60E+01	26.53	66.33	3.39928E+02	-8.02E+00	2.48E+00	-1.37E+01	-2.96E+02	4.81E+01	1.00E+02
5005	4	.001906	1.60E+01	31.51	75.12	4.39314E+02	-8.02E+00	2.48E+00	-1.37E+01	-2.96E+02	4.81E+01	1.00E+02
5005	150	.083259	1.60E+01	40.96	24.41	2.27356E+02	-8.02E+00	2.48E+00	-1.37E+01	-2.96E+02	4.81E+01	1.00E+02
5005	151	.051017	1.60E+01	68.35	24.89	2.28266E+02	-8.02E+00	2.48E+00	-1.37E+01	-2.96E+02	4.81E+01	1.00E+02
5005	152	.008495	1.60E+01	90.56	52.12	3.37270E+02	-8.02E+00	2.48E+00	-1.37E+01	-2.96E+02	4.81E+01	1.00E+02
5005	153	.001567	1.60E+01	100.75	64.81	4.86463E+02	-8.02E+00	2.48E+00	-1.37E+01	-2.96E+02	4.81E+01	1.00E+02
5005	154	.114068	1.60E+01	4.18	44.37	1.94503E+02	-8.02E+00	2.48E+00	-1.37E+01	-2.96E+02	4.81E+01	1.00E+02
5005	155	.078645	1.60E+01	57.00	44.67	1.95517E+02	-8.02E+00	2.48E+00	-1.37E+01	-2.96E+02	4.81E+01	1.00E+02
5005	156	.010778	1.60E+01	86.56	63.90	3.16026E+02	-8.02E+00	2.48E+00	-1.37E+01	-2.96E+02	4.81E+01	1.00E+02
5005	157	.001932	1.60E+01	98.35	72.87	4.71983E+02	-8.02E+00	2.48E+00	-1.37E+01	-2.96E+02	4.81E+01	1.00E+02
5005	140	.109580	1.60E+01	45.39	39.07	2.23942E+02	-8.02E+00	2.48E+00	-1.37E+01	-2.96E+02	4.81E+01	1.00E+02
5005	135	.001873	1.60E+01	110.72	15.02	5.44731E+02	-8.02E+00	2.48E+00	-1.37E+01	-2.96E+02	4.81E+01	1.00E+02
5005	182	.001977	1.60E+01	67.66	111.49	3.33188E+02	-8.02E+00	2.48E+00	-1.37E+01	-2.96E+02	4.81E+01	1.00E+02
5005	771	.000261	1.60E+01	107.99	86.03	4.05252E+02	-8.02E+00	2.48E+00	-1.37E+01	-2.96E+02	4.81E+01	1.00E+02
5005	772	.004916	1.60E+01	75.74	82.33	2.02332E+02	-8.02E+00	2.48E+00	-1.37E+01	-2.96E+02	4.81E+01	1.00E+02
5005	773	.001044	1.60E+01	107.99	67.54	4.38643E+02	-8.02E+00	2.48E+00	-1.37E+01	-2.96E+02	4.81E+01	1.00E+02

Figure 4 . Surface Geometric Relationships Printout

b. Surface description, Figure 2 , which includes;

1) surface number (node number),
2) word description,
3) surface area,
4) surface optical characteristics,
5) surface geometrical shape,
6) active surface,
7) comments.

c. View factor information, Figure 3 , which includes;

1) surface number (node I),
2) surface numbers in the field-of-view (node J),
3) computation indicator (calculation performed),
4) configuration factor, FE (I,J), which is the fraction of mass leaving I capable of striking J with shadowing,
5) configuration factor, FE (J,I), which is the fraction of mass leaving J capable of striking I with shadowing,
6) configuration factor FA (I,J) with shadowing which is a nomenclature change and is the same as the FE (I,J) factor,
7) configuration factor FA (I,J) which is the fraction of mass leaving I capable of striking J without shadowing (item 6 and 7 show difference due to shadowing),
8) shadow factor for the FE configuration factors,
9) shadow factor for a nomenclature change to FA configuration factors,
10) accumulative computational time for performing the indicated calculation.

d. Surface geometric relationships, Figure 4, which includes:

1) surface number (node I),
2) surface numbers in the field-of-view (node J),
3) configuration factor, F (I,J), which is the fraction of mass leaving I capable of striking J with shadowing,
4) area of surface number (node I),
5) Thet I, angle a line from surface I center to surface J center makes with respect to node I surface normal,
6) Thet J, angle a line from surface J center to surface I center makes with respect to node J surface normal,
7) radius, the distance between node I and node J center points in inches,
8) normal vector I is the (X,Y,Z) components of surface normal node I whose magnitude is node I surface area,
9) position vector I is the (X,Y,Z) coordinate of node I center point.

These computer listings are related to the present Orbiter and Payload model surfaces. As surface locations are changed, surface definitions are changed, and as surfaces are subdivided to obtain better resolution or surface definition, the various factors presented will change depending upon the specific surface impacted.

This systematic approach provides a unique approach to spacecraft contamination evaluation and begins to establish the basis for a fundamental technical and programmatic background for timely contamination control on the proposed Shuttle Payloads.

3.2 Graphic Display - As mentioned in the previous section, the physical shapes of the surfaces input to the computer to define the configuration are drawn graphically by scale computer plots. These are used to verify the location and geometrical shape of any specific surface or relationships between surfaces or contamination sources.

Figures 5 through 9 are typical graphic displays drawn by the computer. Figures 5 through 7 present normal configuration drawings of a top view, side view, and three dimensional view, respectively. Figure 8 presents a configuration with the typical Payload positioned and Figure 9 is an isolation display showing the location of the 25 pound thrust Reaction Control Subsystem vernier engine and evaporator exit planes.

Figure 9 demonstrates an important aspect of the computer model in that specific surfaces can be displayed whether they are a source or a receiver and the spatial interaction can be shown without addressing the entire configuration. This latter point is useful in surface mapping a configuration for surface and/or material categorization and location studies.

For graphic displays, the coordinate system has been positioned so that the size of the displays are maximized on the cathode ray displays. Microfilm records of these displays are also available and are on file for additional display copies as required.

3.3 Payload Lines-of-Sight - In order to define the mass and number column densities and the returned flux of the contaminants, a line-of-sight must be established for the Payload or experiment surface in question. The contaminants along a given line-of-sight will be a function of many variables. The major variables are:

a. species of the contributing contaminants,
b. spatial and temporal nature of the contamination sources,
c. location of the line-of-sight with respect to the experiment bay (position of the Payload),
d. pointing requirements of the Payload,
e. emission rates and velocities of the contaminant source.

For this study, the Payload was positioned approximately three-quarters of the way aft in the Orbiter experiment bay. This position was selected since it is the most representative

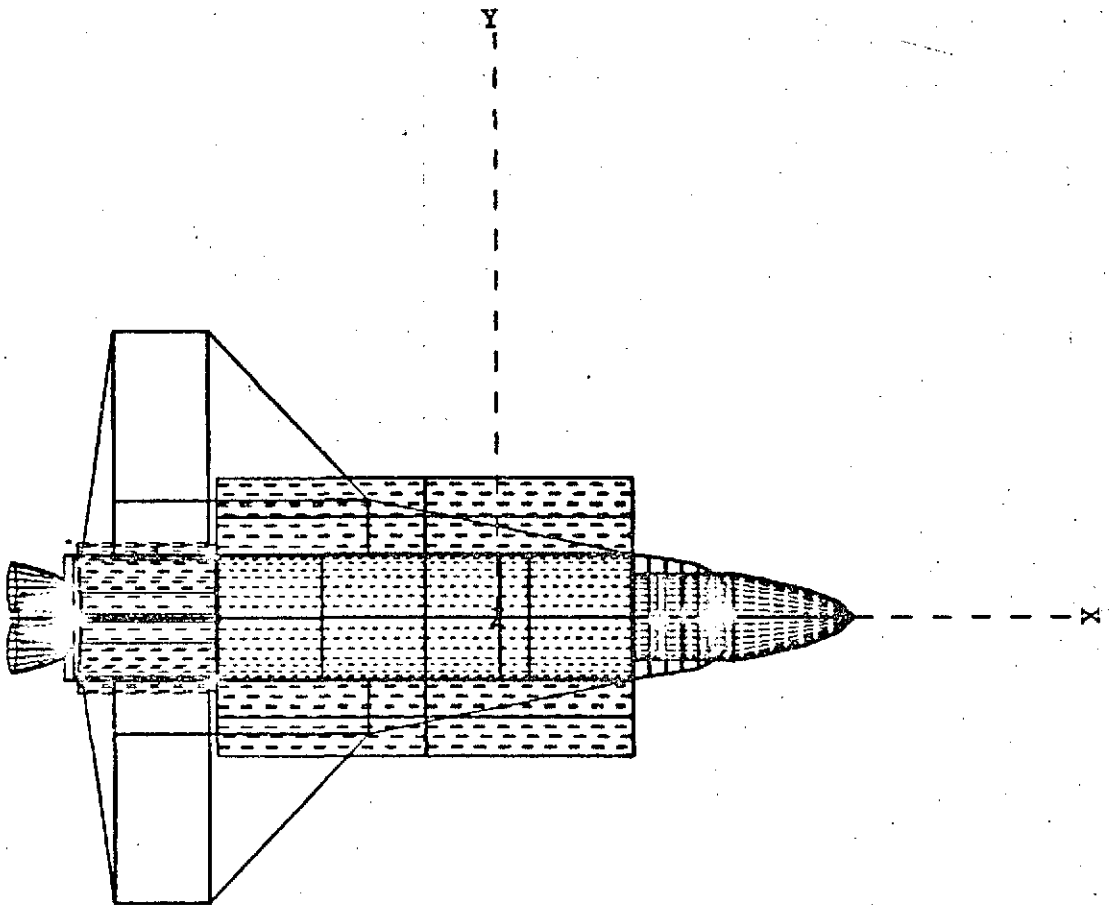

Figure 5 . Graphic Display of Top View of the Current Modeled Orbiter

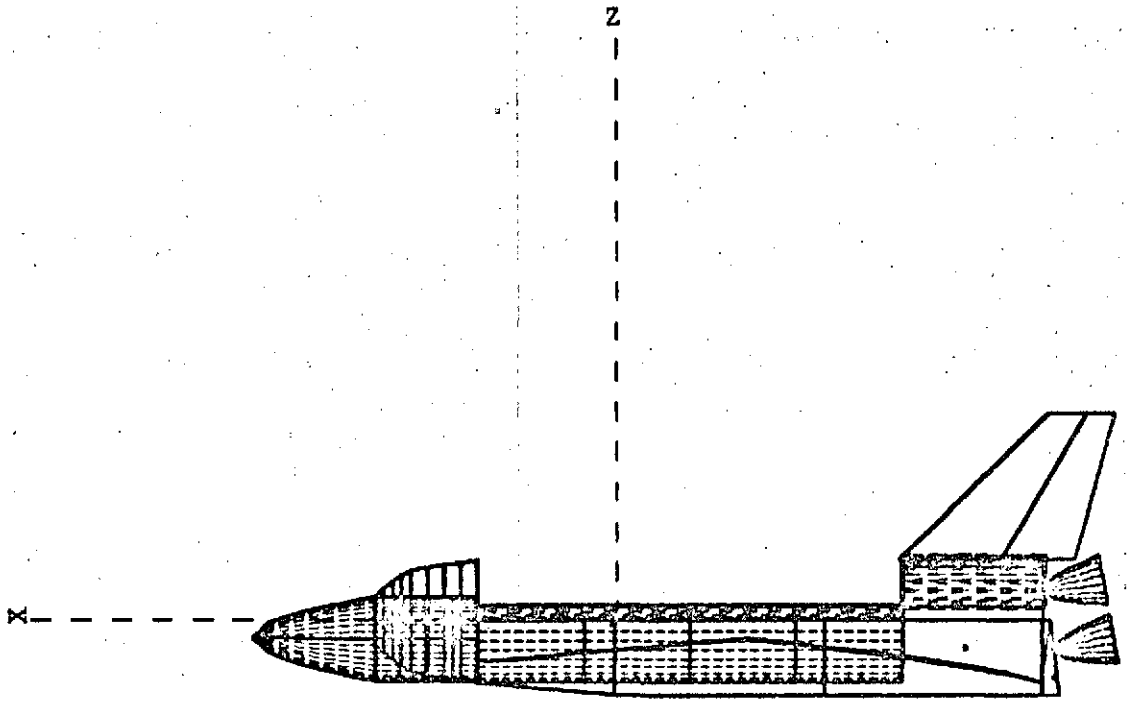

Figure 6 . Graphic Display of a Side View of the Current Modeled Orbiter

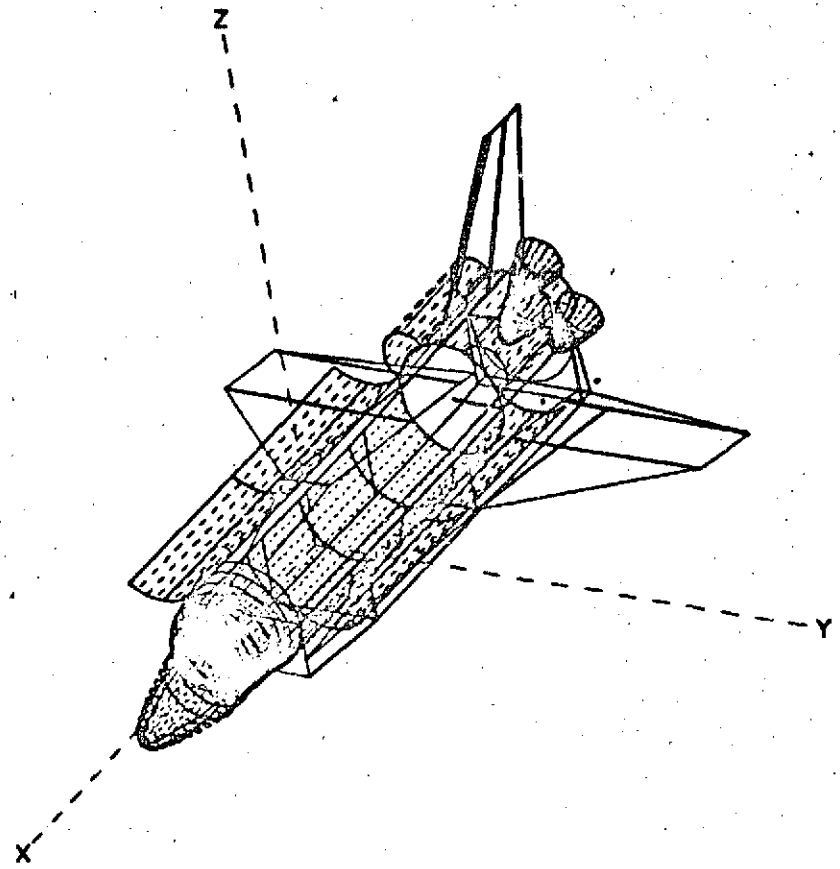

Figure 7. Graphic Display of a Three Dimensional View of the Current Modeled Orbiter

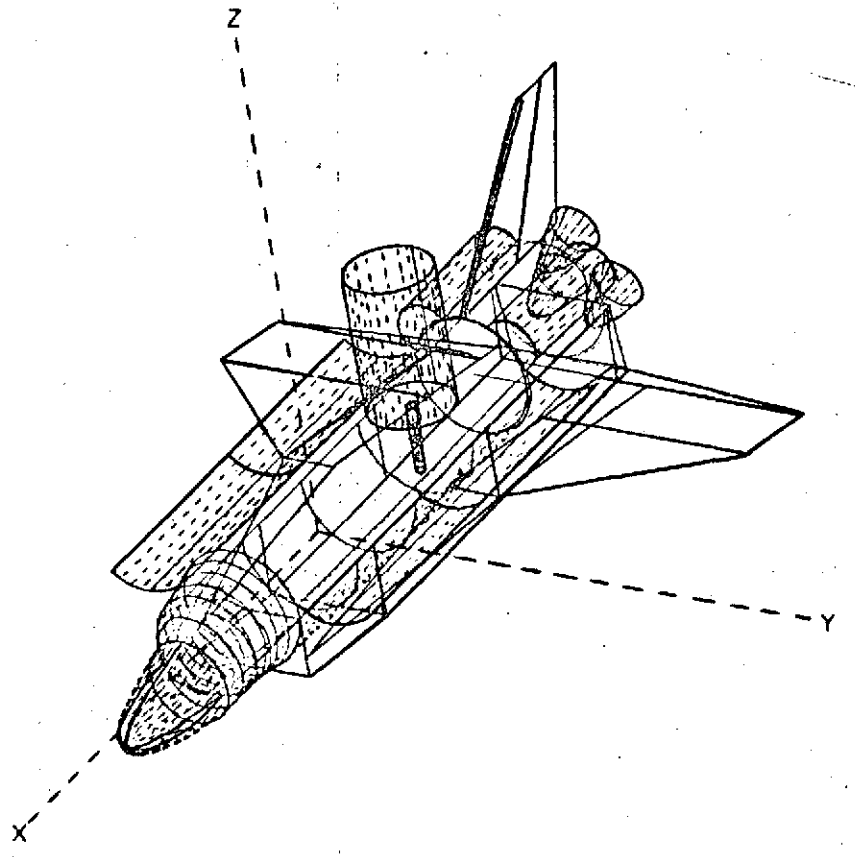

Figure 8 . Graphic Display of Shuttle Orbiter with Representative Payload

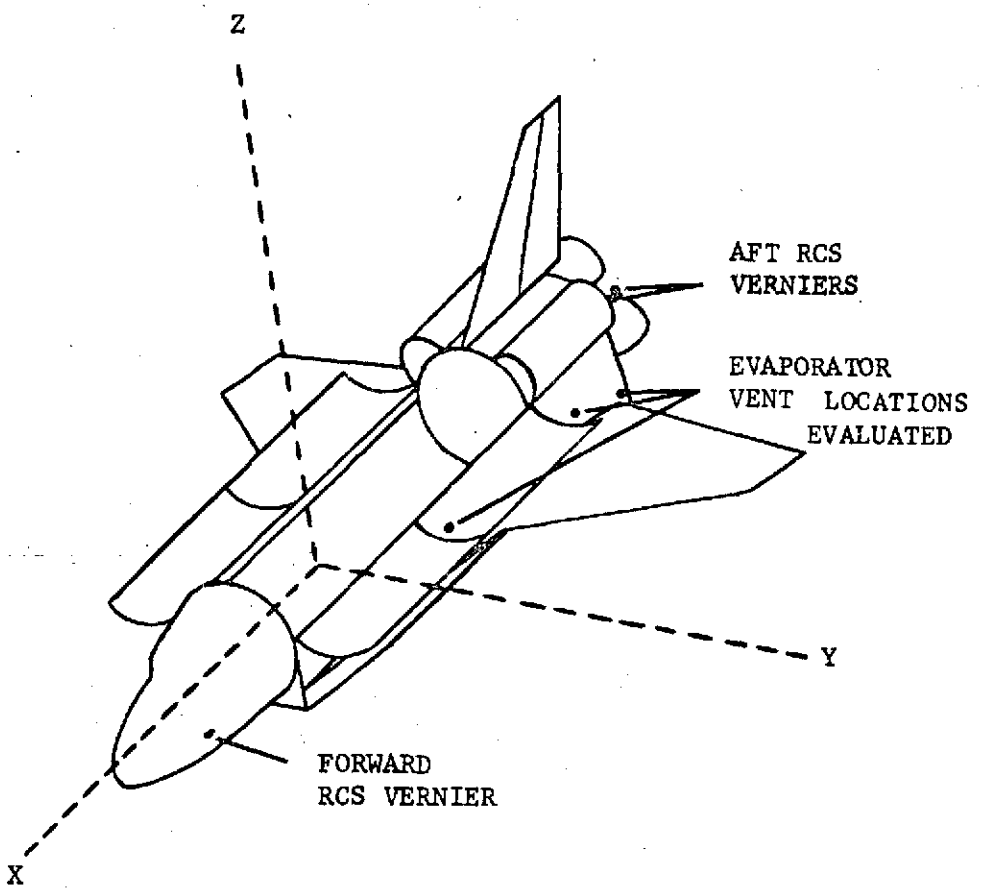

Figure 9 . Graphic Display of Engine and Vent Surfaces

of the payloads in question. In addition, lines-of-sight were established only with respect to this representative Payload and its position in the experiment bay. With the sources modeled and the relative symmetry of the sources considered, the mass and number densities and the returned fluxes calculated along any line-of-sight with respect to a normal (+Z) direction and to the position in the experiment bay will only vary slightly. As more sources are added to the model and those sources which may have more directional influence are added, the contaminants along any given line-of-sight with respect to location in the Orbiter experiment bay can be expected to show larger spatial variations. Those payloads whose pointing requirements include large deviations from pointing along the +Z axis will see larger spatial variations in the contaminant environment. Until more definitive information is available concerning operational requirements of the various payloads, the nature and extent of the sources are better defined, and the geometries associated with the Orbiter are better known, Payload lines-of-sight for one representative Payload position are considered.

Nine lines-of-sight were established with respect to the +Z axis. These lines-of-sight are:

a. zero degree line-of-sight (in the +Z direction),
b. fifty degree lines-of-sight (4 directions; forward in the (+Z,+X), aft in the (+Z,-X), port in the (+Z,+Y), and starboard in the (+Z,-Y) directions),
c. twenty-five degree lines-of-sight (2 directions; port in the (+Z,+Y) and starboard in the (+Z,-Y) directions),
d. forty-five degrees to the aft (2 directions both port and starboard and fifty degrees from the normal or +Z direction).

These basic lines-of-sight are graphically depicted in Figures 10 through 15 along with the line-of-sight designation number.

In order to develop mass and number column densities and the returned flux along a given line-of-sight, a series of interaction spheres are placed along the line-of-sight in

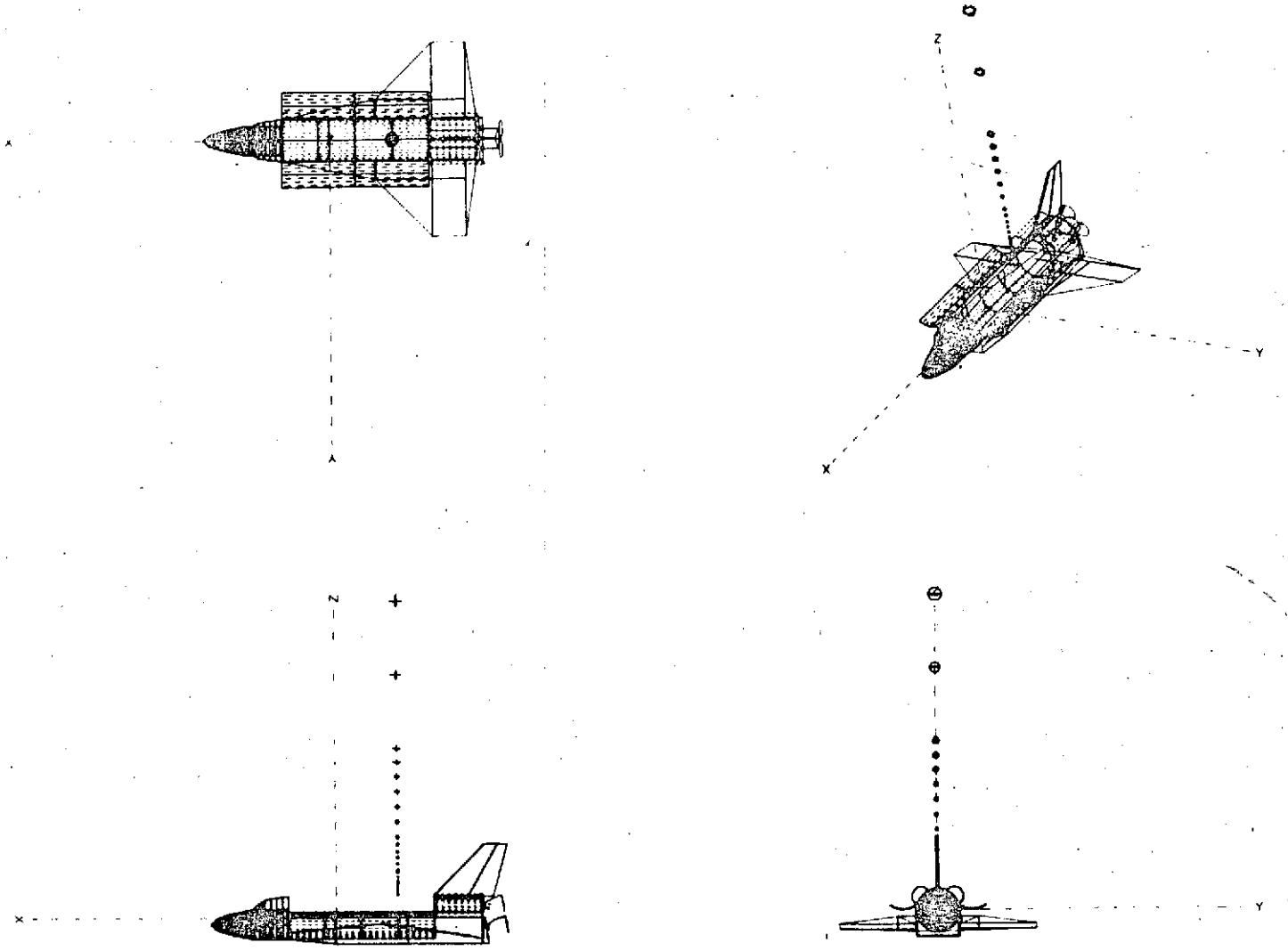

Figure 10. Zero Degree Line-of-Sight - LOS 00

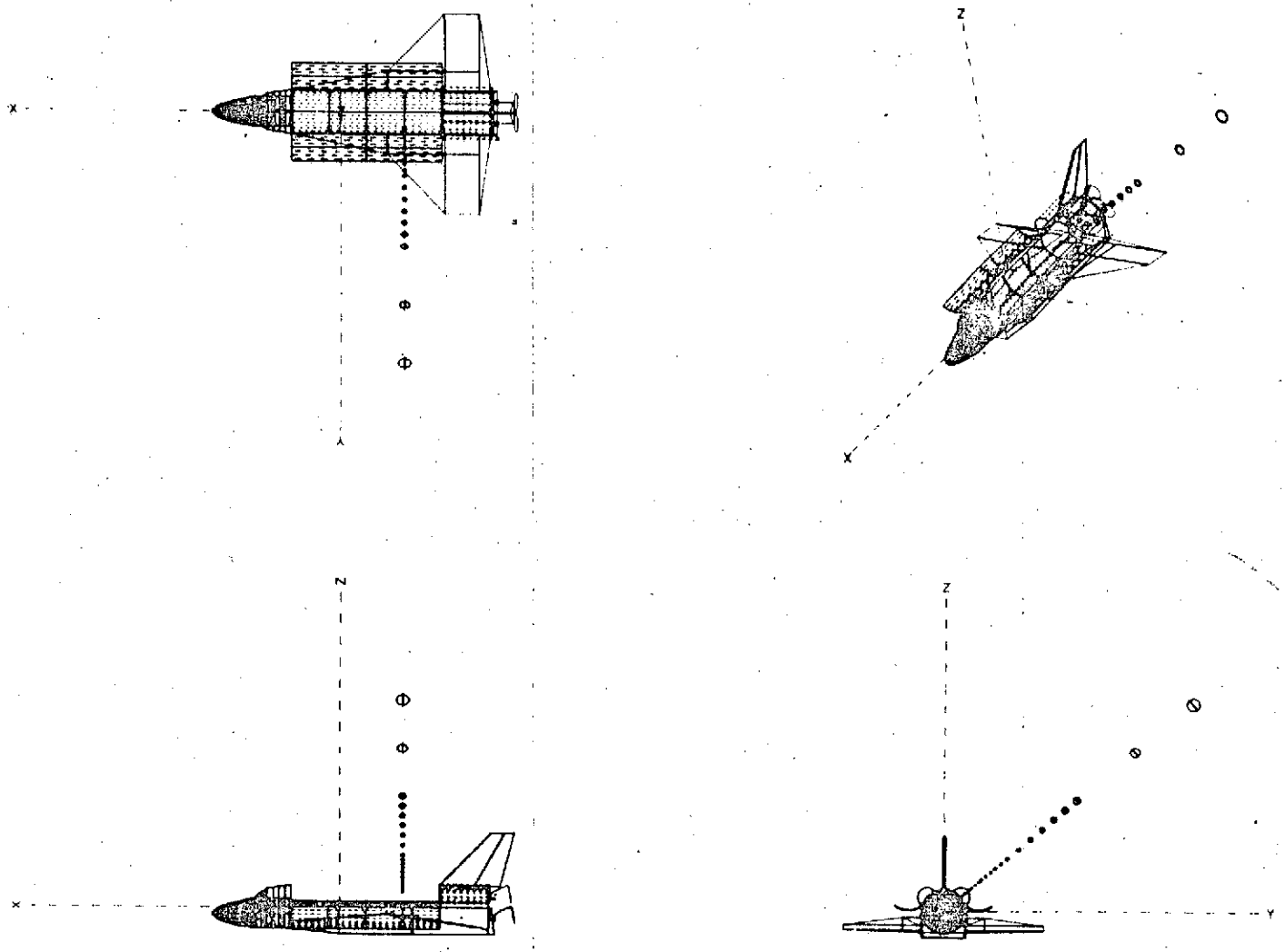

Figure 11. Fifty Degree +Y Line-of-Sight - LOS 02

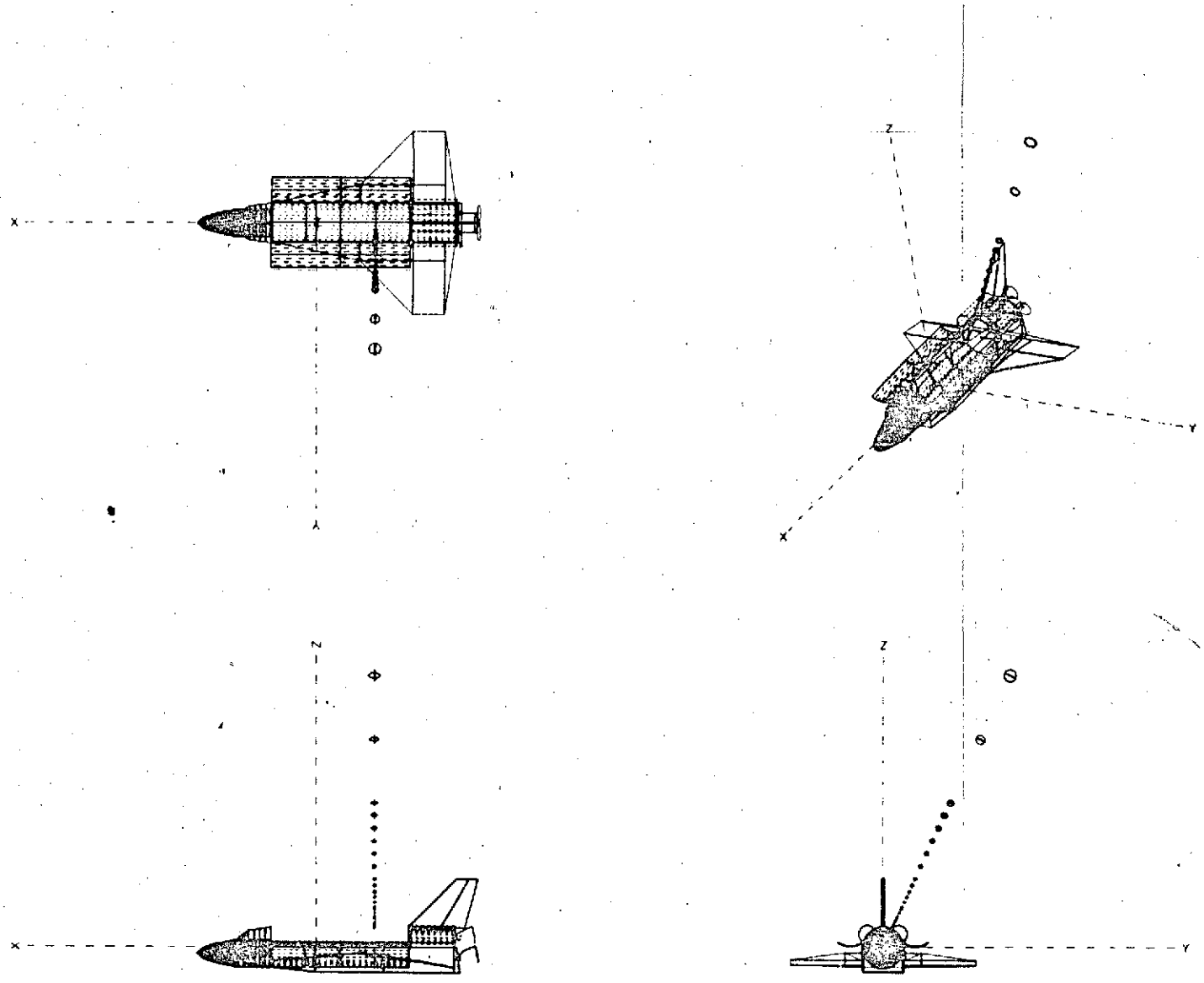

Figure 12. Twenty-five Degree +Y Line-of-Sight - LOS 03

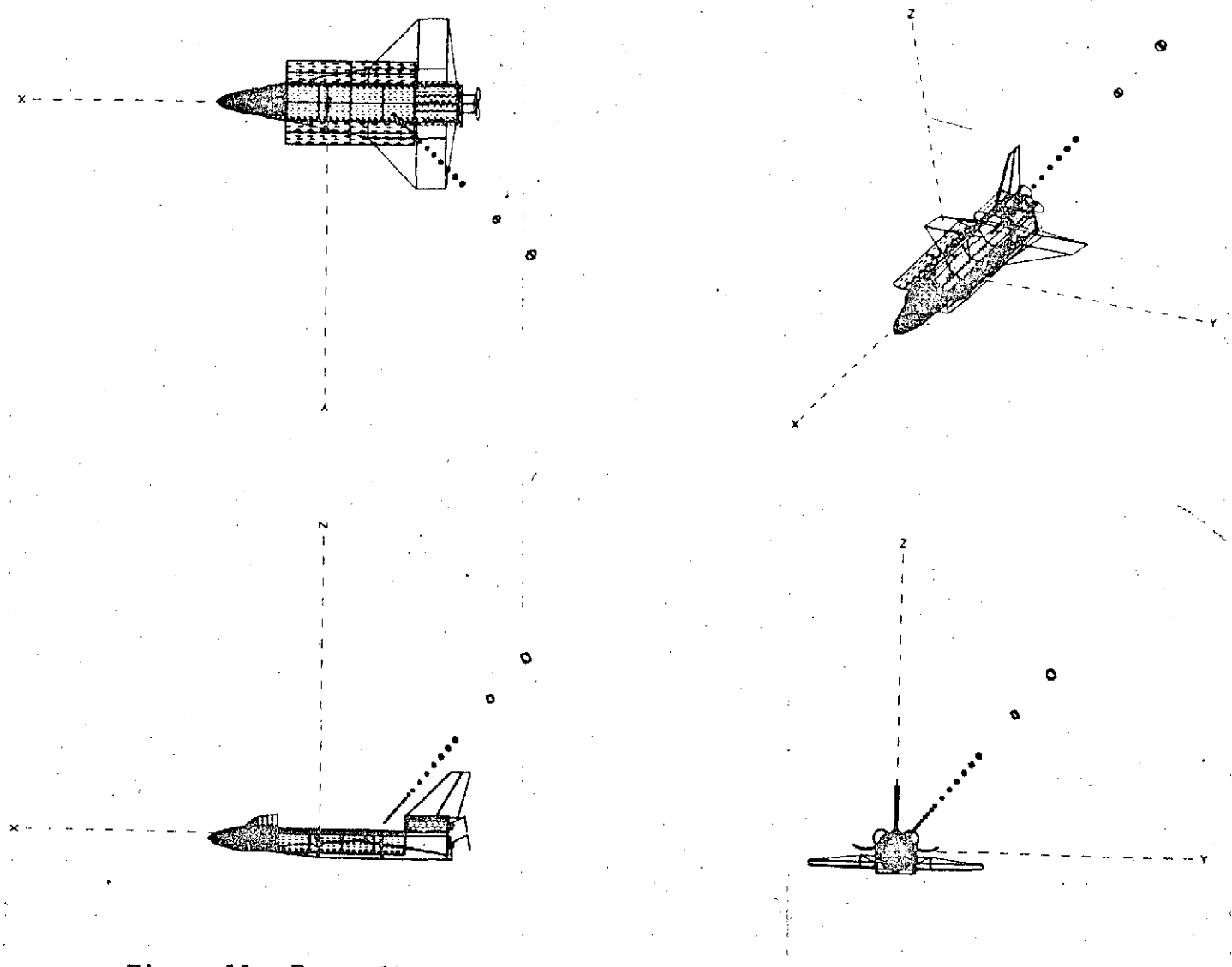

Figure 13. Forty-five Degrees off +Y Towards -X and Fifty Degrees off +Z Line-of-Sight - LOS 04

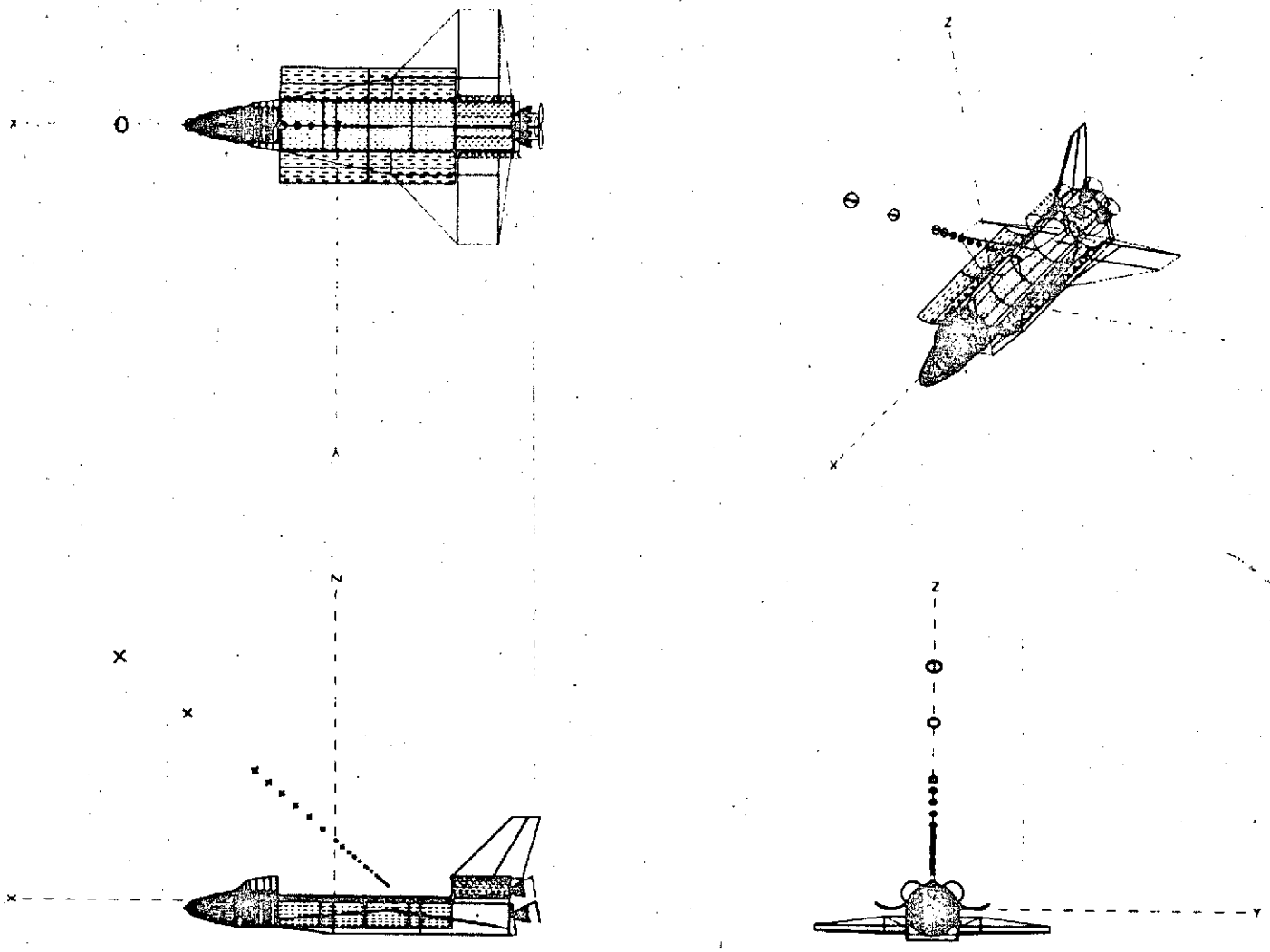

Figure 14. Fifty Degree +X Line-of-Sight - LOS 05

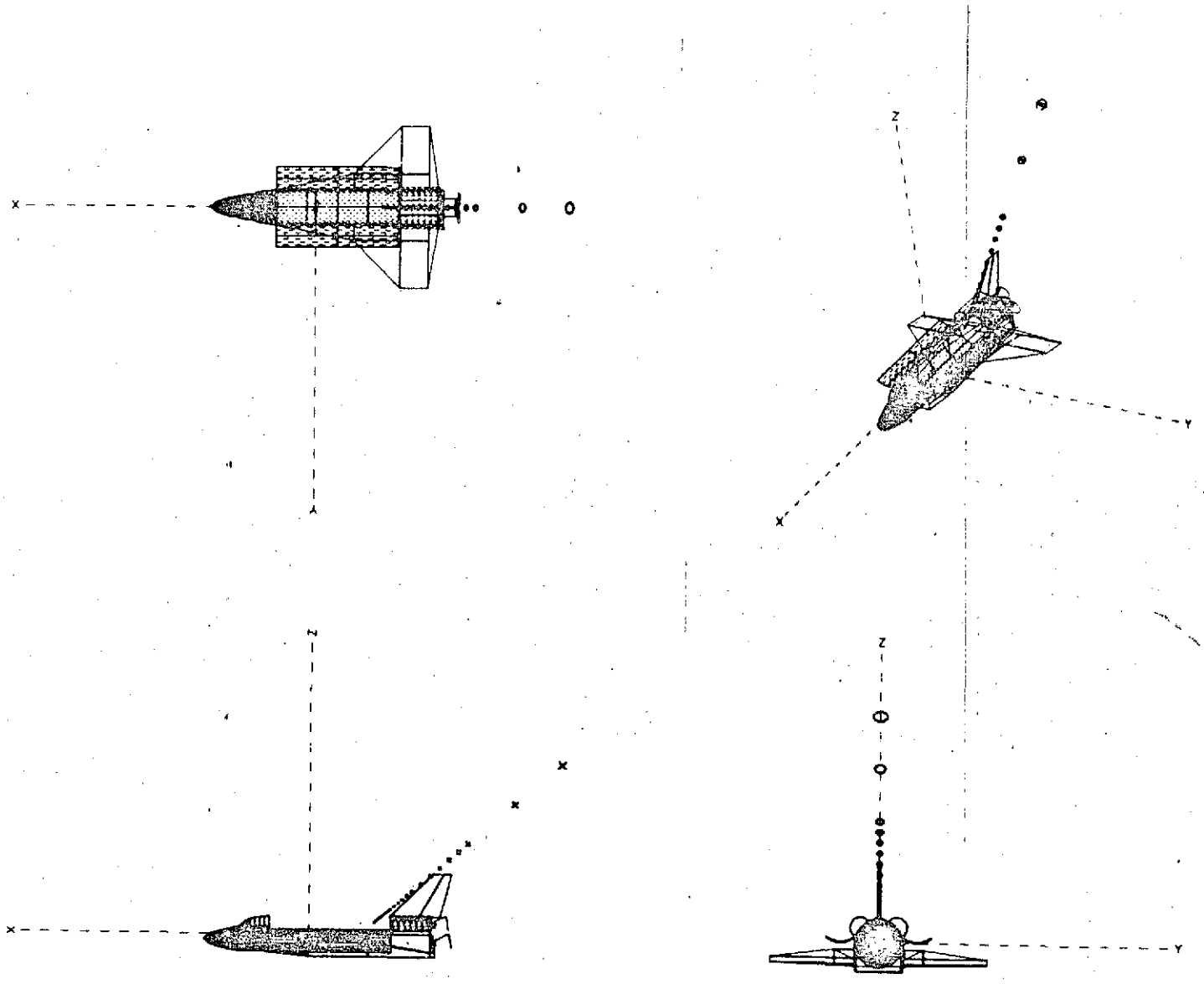

Figure 15. Fifty Degree -X Line-of-Sight - LOS 06

question such that the spheres' diameters fall within the field-of-view of the Payload or sensitive surface in question. These spheres are extended out from the Orbiter until the induced atmosphere density falls approximately to that of the ambient atmosphere. Each sphere is treated as a surface just like that previously described for geometrical modeling of the Orbiter and representative Payload surfaces. View factors are calculated for each sphere with respect to the surfaces the spheres see on the Orbiter and Payload.

The flux arriving and subsequently the density of the induced atmosphere is calculated for each sphere (Figure 16). An interaction plane is developed at the center of each sphere which is representative of the field-of-view of the surface in question. This interaction plane acts as a source representing the returned flux of contaminants colliding with the ambient atmosphere. As resolution is required (depending upon the field-of-view of the surface in question, directional influence of the source, and the interaction function with the ambient atmosphere), the interaction spheres and planes are subdivided.

The integration along the line-of-sight for all the spheres results in the definition of the mass column densities of contaminants. By knowing the physical makeup of the contaminants (e.g. H_2O, O_2, N_2, N_2O_4, CO_2, etc.) in these mass column densities, the number column densities^2 can be defined for each constituent of the induced atmosphere. This is also true for defining the returned flux of the contaminants as they interact with the ambient atmosphere.

In the same manner, surface-to-surface deposition rates of contaminants can be established as a function of surface temperature, lines-of-sight, and orbital altitude.

In many instances, the density of the induced environment does not decrease uniformly with distance along a line-of-sight because of point sources and shadowing considerations. This rules out simple analytical approaches to the return flux calculation and requires geometrical relations to be established by a computer model to accurately assess the induced contaminant environment.

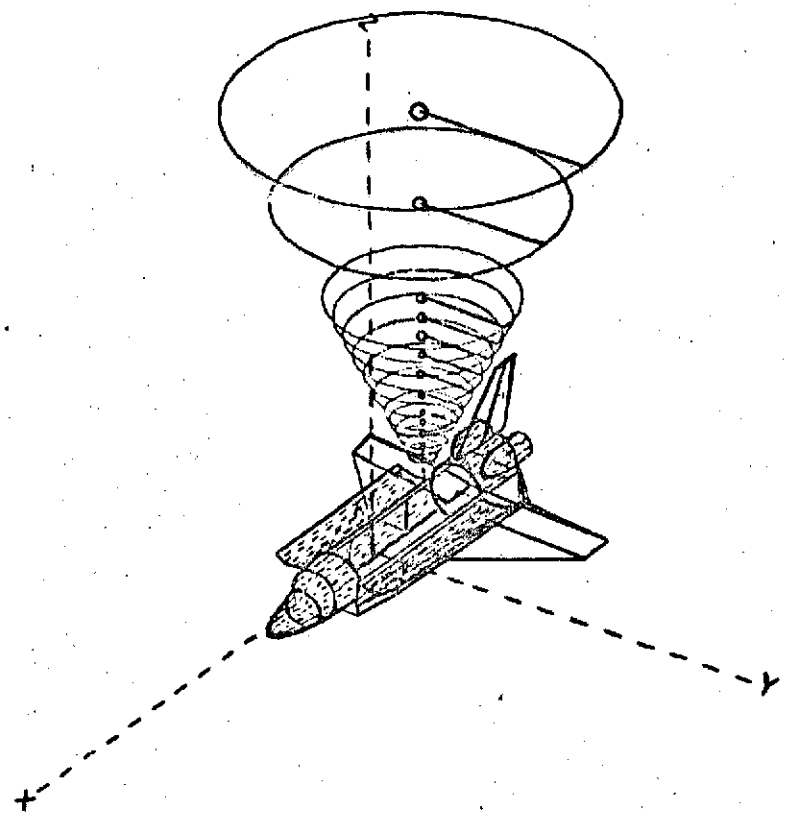

GENERAL CONFIGURATION

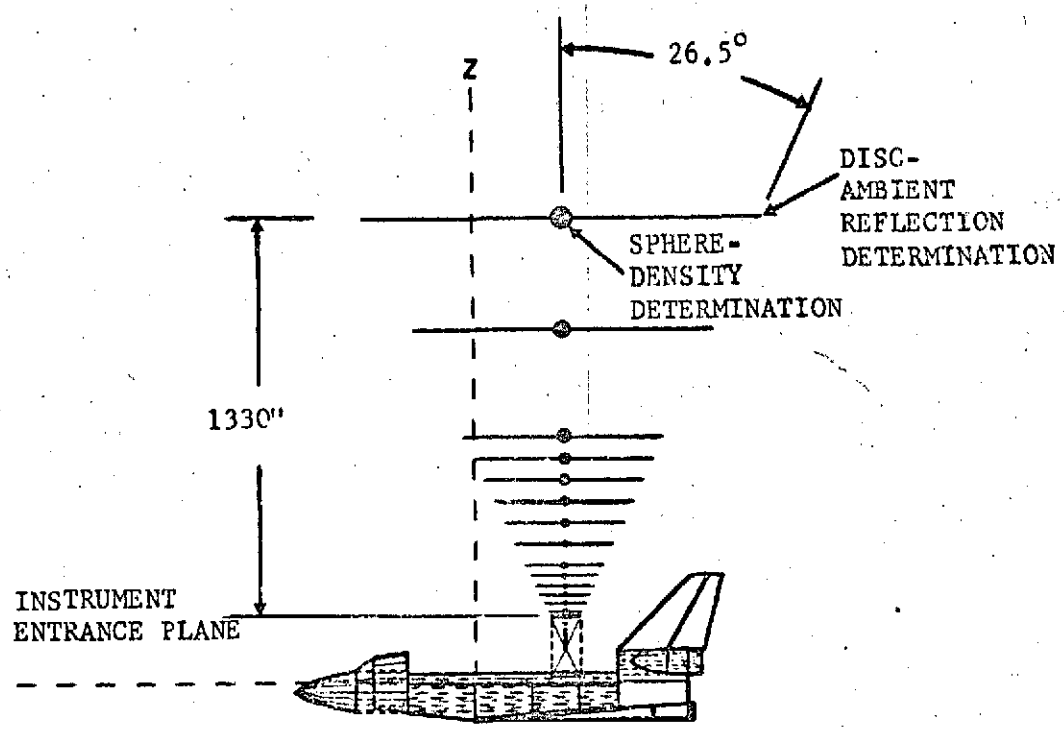

DISC AND SPHERE MODELING GEOMETRY
0° LINE-OF-SIGHT

Figure 16. Graphic Display of Orbiter, Payload, and Interaction Spheres and Planes Used to Calculate Contaminant Levels Along Given Lines-of-Sight

As mentioned previously, the interaction spheres were established to basically encompass the fields-of-view of the majority of the Payloads. By using this technique, the mass and number column densities can be calculated along a given line-of-sight with sufficient fidelity to be representative. However, for the case of deposition from the returned flux, the phenomena is not necessarily a point source response and deposition over an entire optic or in fact over the internal walls of a telescope such as the infrared telescope can equally degrade the performance of the system. Therefore, interaction planes are established at each interaction sphere which are extended to encompass the entire field of a typical limiting system such as an f/2 telescope. By using this technique, not only that mass capable of being directly in the field-of-view can be accounted for but that which is off axis and can intercept the entire optic or the internal walls of a typical telescope can also be accounted for. As the f number of a telescope or system increases (e.g., f/16, f/20, etc.), the percentage of mass capable of impinging internal to the telescope decreases proportional to the f number.

In addition, this technique allows the mass or flux arriving not only at the bottom of the telescope to be established but that reaching the aperture of the system to be equally assessed. This latter point is important in assessing the effectiveness of aperture windows, doors, and sun shields. This is graphically represented in Figure 16.

4. SOURCES

4.1 General Discussion - A review was conducted of all available documentation for identification of potential Orbiter contamination sources. As a result of this review, the potential contaminant sources were broken up into four categories. These categories are major sources, other Orbiter sources, reflections and resublimation from Orbiter surfaces, and boost and reentry sources. These categories were chosen to represent basically different levels of contamination, unique geometric influences, and different phases of operational activities.

In many instances, the available information was insufficient in detail to uniquely model or define specifically. However, based upon Skylab experience and results, those sources where detailed information was not available were treated in a similar manner as on the Skylab program.

The following sections discuss each of the above potential sources considered and presents where applicable the physical relationships modeled.

4.2 Major Sources - The major sources considered for this study were:

a. outgassing,
b. offgassing,
c. leakage,
d. evaporator,
e. Reaction Control Subsystem (RCS) 25 lb vernier engines,
f. the returned flux reflecting from the ambient environment.

These sources represent the largest contributors to the induced environment either steady state or transient in nature. The contaminant quantities, source locations, emission rates, chemical composition, and emission patterns are detailed for these sources.

For this study, the difference between outgassing and offgassing is defined as: outgassing is that contribution which comes

from the material bulk characteristics and is long term in nature. Offgassing is related to the volatiles which are either adsorbed to the material and/or carried in the preparation of a material and boil off very rapidly when exposed to vacuum.

The other contaminant sources mentioned later in this section must eventually be quantitatively analyzed and considered in a total Payload/Orbiter contamination analyses. At present, their impact has been assessed to be less significant than the major sources or design and test data is insufficient at this time to perform more than a qualitative analysis.

4.2.1 Outgassing - The molecular emission from non-metallic materials exposed to the vacuum environment of space will be one of the most significant contributors to the contaminant environment of the Shuttle Orbiter and Payloads whether the Payloads are free flyers or flown in the sortie mode. The majority of deposition observed on Skylab was the result of outgassing from non-metallic materials. Even though these materials were basically controlled to specifications contained in the NASA 50M02442 document, the long term nature of this bulk outgassing rate contributes significantly to the deposition on spacecraft surfaces. For the majority of Shuttle Orbiter and Payload surfaces, their temperatures will essentially be the same as on Skylab for similar attitudes and will see approximately the same deposition rates for comparable source characteristics.

Although the majority of the Orbiter surfaces will be covered with carbon and/or ceramic coated silica tiles, the adhesive covering required to bond these materials may represent a significant outgassing source. In addition, when a Payload becomes operational, the experiment bay doors will have to be open exposing a significant area of the Orbiter which will not be ceramic tiles and exposing typical non-metallic materials. During on orbit operations this potential outgassing source consists of approximately 3300 ft^2 out of approximately 7200 ft^2 of exposed surface area to the vertical or +Z direction of the Orbiter. In addition, a Payload can contribute up to 1200 ft^2 of exposed external surface area to the total exposed non-metallic surface area of the Orbiter/Payload.

The Orbiter Thermal Protection Subsystem (TPS) consists of materials applied externally to the primary structural shell of the Orbiter covering approximately 11,600 ft^2 out of a total of 12,961 ft^2. In addition to relatively small areas such as thermal pane windows and thermal seals, the major portion consists of three separate types of material coverings including Low Temperature Reusable Surface Insulation (LRSI), High Temperature Reusable Surface Insulation (HRSI), and Reinforced Carbon-Carbon (RCC) (see Figure 17). The LRSI and HRSI are very similar in composition, differing only in thickness and thermal barrier characteristics. Both consist of silica tiles coated with RSI ceramic coating (hydrophobic treatment with silicone resin) bonded to the Orbiter structural shell with RTV 560 adhesive .01" to .015" in thickness. Joint gaps between each individual tile of 0.050 ± 0.015" allow for tile expansion during periods of high temperature extremes and provide "escape routes" for outgassed material to the external environment. These tile expansion gaps can also trap or adsorb material as a result of ground handling, trap material from the Solid Rocket Booster Motor (SRBM) staging, and provide a geometry where trapped material may slowly diffuse. This latter condition is important in assessing the short term offgassing characteristics and the long term outgassing of the bonding material.

RSI tiles ≥ 0.75" thick in addition incorporate tile gap thermal barrier strips running along each joint partially sealing the outgassant escape routes. HRSI is used basically on the Orbiter lower surfaces, the nose cone area, and vertical stabilizer leading edge (4555 ft^2) while LRSI covers essentially all of the Orbiter upper surfaces (6482 ft^2). RCC is used only in areas of very high temperature extremes ($>2300^{\circ}F$) such as the nose cone and leading edges of the Orbiter Wings (563 ft^2). By far, the largest outgassant source from the TPS will be the RTV 560 adhesive used with the RSI tiles. RTVs characteristically demonstrate an initial steady-state outgassing rate (OGR) of approximately 1×10^{-8} g/cm^2/second at $100^{\circ}C$. This rate will be attenuated due to tile geometry and adhesive location, consequently a uniform OGR of 5×10^{-10} g/cm^2/second at $100^{\circ}C$ was assumed for all TPS surfaces in the modeling effort. Depending upon the bonding nature of the RTV compound used, the geometries associated with the tiles, and the repeated variety of thermal

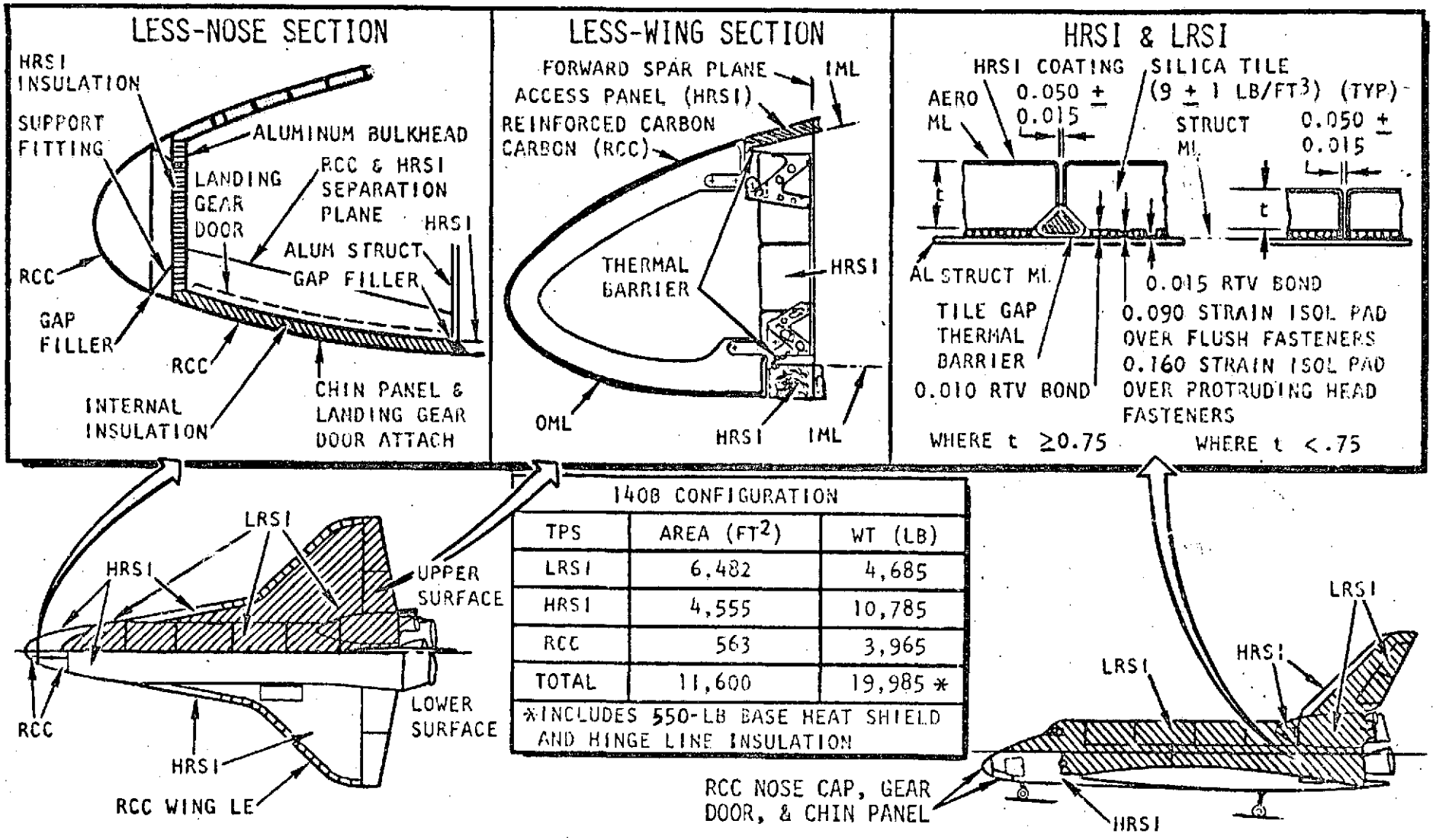

140B CONFIGURATION		
TPS	AREA (FT^2)	WT (LB)
LRSI	6,482	4,685
HRSI	4,555	10,785
RCC	563	3,965
TOTAL	11,600	19,985 *
*INCLUDES 550-LB BASE HEAT SHIELD AND HINGE LINE INSULATION		

Ref. SD 72-SH-0071B Orbiter Definition Handbook, R.I., 2/4/74

Figure 17. Orbiter Thermal Protection Subsystem Configuration

environments seen by the Orbiter, this outgassing rate may be high but it is within the range generally specified for materials which have been considered as space qualified. RTV 568 is currently being considered to replace the RTV 560. RTV 568 demonstrates a much lower outgassing rate and should reduce the levels of contamination due to outgassing significantly.

Molecular emission patterns will closely follow a cosine law distribution and emission velocities have been considered the "most probable" thermal velocities as detailed later in this section.

During nearly all Shuttle Orbital operations, the experiment bay doors are in an open position allowing the active thermal control system space radiators to be constantly exposed to space vacuum (see Figure 18). These radiators have a total surface area of 2040 ft^2 (1440 ft^2 effective area) of which 1360 ft^2 (1030 ft^2 effective) faces in a +Z direction and 680 ft^2 (410 ft^2 effective) radiates essentially in a -Z direction. These surfaces most likely will be coated with a bonded silvered Teflon. Since the bonding mechanisms and overall outgassing characteristics are as yet unknown for the silvered Teflon, for modeling purposes a white thermal control paint was assumed. Either Z93 which is a potassium silicate bonded zinc oxide and has a characteristic initial steady state outgassing rate of 9×10^{-11} g/cm^2/second at 100°C or S13G which is a silicone (RTV 602) with zinc oxide pigment having a rate of 1×10^{-8} g/cm^2/second at 100°C might be used. In either case, the radiators will be potential contaminant sources not only while the experiment bay doors are open but also with the doors closed and the bay evacuated.

In modeling these surfaces, an initial steady state outgassing rate of 5×10^{-10} g/cm^2/second at 100°C was also assumed as with previously mentioned parameters characteristic to outgassing sources of the Orbiter surface.

For specific payloads, the experiment bay inboard cavity lower half will be enclosed with an experiment bay liner for contamination control and insulation. For this study, the liner is assumed to be a multi-layered, polyester adhesive bonded fabric which covers an approximate area of 1413 ft^2. Listed below are the various laminations and their respective thicknesses for the experiment bay liner considered.

Material	Thickness (MILS)
Teflon Film	1.0
Vacuum Deposited Aluminum	0.05
Polyester Adhesive	0.3

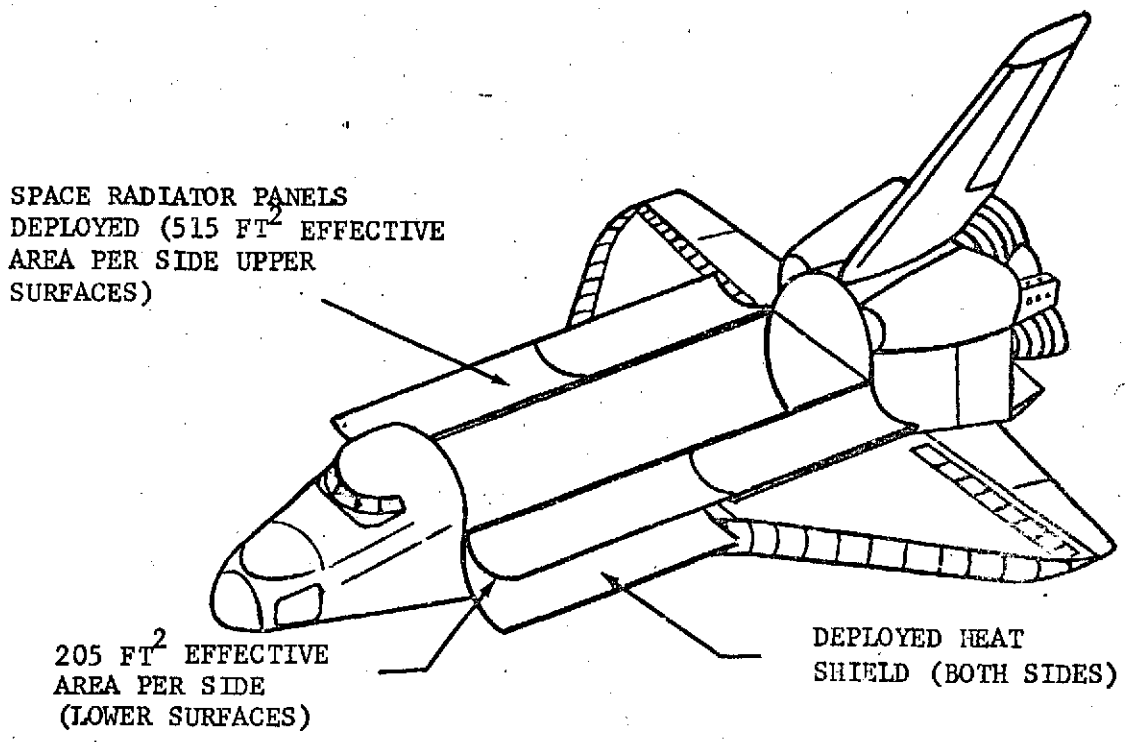

Figure 18. Active Thermal Control System Radiator Configuration

Kapton Polyimide Film	1.0
Polyester Adhesive	0.6
PRD49-IV Plain Weave Cloth	4.3
Polyester Adhesive	0.6
Kapton Polyimide Film	1.0
TOTAL	8.85

The forward half of the experiment bay liner is backed by 20 layers of multilayered insulation and the aft half is backed by 2.5 inches of bulk insulation. Although Teflon and Kapton characteristically have very low outgassing rates, the adhesives and insulations will outgas and escape through seams and joints as well as any adsorbed material which will be trapped in the experiment bay liner from ground handling and as a result of the launch and reentry phases. Considering the configuration and composition of the experiment bay liner, an initial steady-state outgassing rate of 1×10^{-11} g/cm^2/second appears valid for temperatures of $100^{\circ}C$.

The forward and aft ends of the experiment bay (X_o = 576 and 1307 respectively) are covered with 2 inches of TG 15000 bulk insulation packaged in a manner unknown at this time. The area of each bulkhead is approximately 177 ft^2. The inboard surfaces of the TG 15000 are covered with Orcon aluminized fabric which contains numerous air breathing holes covered with filter cloth and will allow contaminants trapped behind the liner (i.e. outgassants and cabin atmosphere leakage) to pass through the liner and eventually be emitted to space through the joints in the bulkhead and past the window and hatch seals on the forward bulkhead. Outgassing from the bulkhead liners will also be relatively low on the order of 1×10^{-11} g/cm^2/second for the surfaces at $100^{\circ}C$.

The outgassing rates of the aforementioned Shuttle nonmetallic materials exposed to space vacuum are inherently dependent upon several factors including surface temperature variations and extremes, accumulative exposure times to space environment, physical and chemical characteristics of the individual materials, and precure procedures employed. To accurately describe the source characteristics of an outgassing surface, specific tests must be

conducted and where possible specific surface geometries must be included as in the case of the RSI tiles and their respective gaps exposing the RTV bonding material.

For the purposes of this study, the integrated initial steady state outgassing rate of 5×10^{-10} g/cm^2/second for all surfaces at 100°C was assumed to be representative of outgassing as a contaminant source. This incorporates an estimate that 10% of the total Orbiter exterior surface will outgas.

Skylab contamination modeling demonstrated that the outgassing rate of a vacuum exposed non-metallic material varies exponentially with surface temperature and exposure time described by the relationship:

$$OGR = OGR_{100} \quad (e^{-t/\tau})(e^{\frac{T-100}{29}})$$

where; OGR = Outgassing rate in g/cm^2/second,

OGR_{100} = Initial steady-state OGR at 100°C,

t = Time in hours of vacuum exposure,

τ = Time in hours for OGR to decay to 1/e (.368) of its initial value for space vehicles having orbits similar to Skylab $\tau \simeq 4100$ hours,

T = Temperature of the outgassing surface in degrees centigrade.

Outgassing molecules demonstrate a distribution representative of the Lambert cosine law ($\cos \theta / r^2$, where θ is the angle from the surface normal and r is the distance from the surface to the point of interest within the distribution). Outgassing will be a continuous source of contamination throughout the entire on orbit periods of Shuttle missions varying with the previously mentioned parameters. The velocity at which the outgassants will leave a surface will depend upon the surface temperature and the molecular

weight of the outgassed species. The most probable velocity for outgassed molecules will be:

$$V = \left(\frac{2R_oT}{M}\right)^{\frac{1}{2}} = 129\sqrt{\frac{T}{M}}$$

where;

V = Velocity of the outgassants in meters/second,

T = Temperature of the outgassants in degrees Kelvin,

M = Molecular weight of the outgassants (M=100).

The major constituents and molecular weights of the outgassants are of course dependent upon the materials used on the Shuttle Orbiter and the Payloads. These include RTVs from binders, paints, and sealants, and breakdown of long hydrocarbon organic chains. Because of the wide variety of potential outgassants, an average molecular weight of 100 was assumed for this study.

4.2.2 Offgassing - Most non-metallic materials such as RTVs demonstrate a period of relatively high weight loss upon initial exposure to vacuum before reaching a characteristic steady state outgassing rate. During manufacture, assembly, ground handling, and launch facility and refurbishment; operations liquids such as solvents, chemicals for special processing, and water vapor (atmospheric or otherwise) will become entrapped or absorbed into the external cavities of non-metallic materials and in some cases metal surfaces (e.g. TPS tile joints and porous surface materials). In addition, adsorbed light gases and high vapor pressure materials used in application processes will also be present on externally exposed surfaces. These in addition to others are treated as a single source, offgassing, uniformly distributed over all Orbiter surfaces. These entrapped and adsorbed substances are considered to offgas for only the first 100 hours of vacuum exposure with an exponentially decreasing rate. An Orbiter material used extensively over the vehicle which demonstrates this offgassing

phenomena quite vividly is the RTV 560 adhesive used on the TPS. Vacuum chamber weight loss tests (see Figure 19) for this material held at 24°C indicates a time dependent relationship at a constant temperature for the offgassing rate to be:

$$OFR_{24^oC} = 2.62e^{-0.0714t} + 3.0e^{-0.0105t}$$

where;

OFR_{24^oC} = Offgassing rate at 24°C in g/cm^2/second X 10^{-8},

t = Time in hours of exposure.

As with outgassing, the offgassing rate is a function of the surface temperature. Therefore, the offgassing rate at any temperature will be:

$$OFR_T = \left[32.5e^{-0.0714t} + 37.2\,e^{-0.0105t}\right] e^{\frac{T-100}{29}}$$

where;

OFR_T = Offgassing rate as a function of surface temperature in g/cm^2/second X 10^{-10}, (One percent of all surfaces are assumed to be capable of offgassing so the above exponent is 10^{-10}.)

Other parameters of offgassing will be similar to those of outgassing: e.g., the plume distribution from the source surface will be a $\cos\theta/r^2$ function and the molecules will be emitted with a velocity of:

$$v = 129\sqrt{\frac{T}{M}}$$

where;

v = Velocity of the offgassing molecules in meter/second,

T = Temperature in degrees Kelvin,

M = Molecular weight (M=18 assumed).

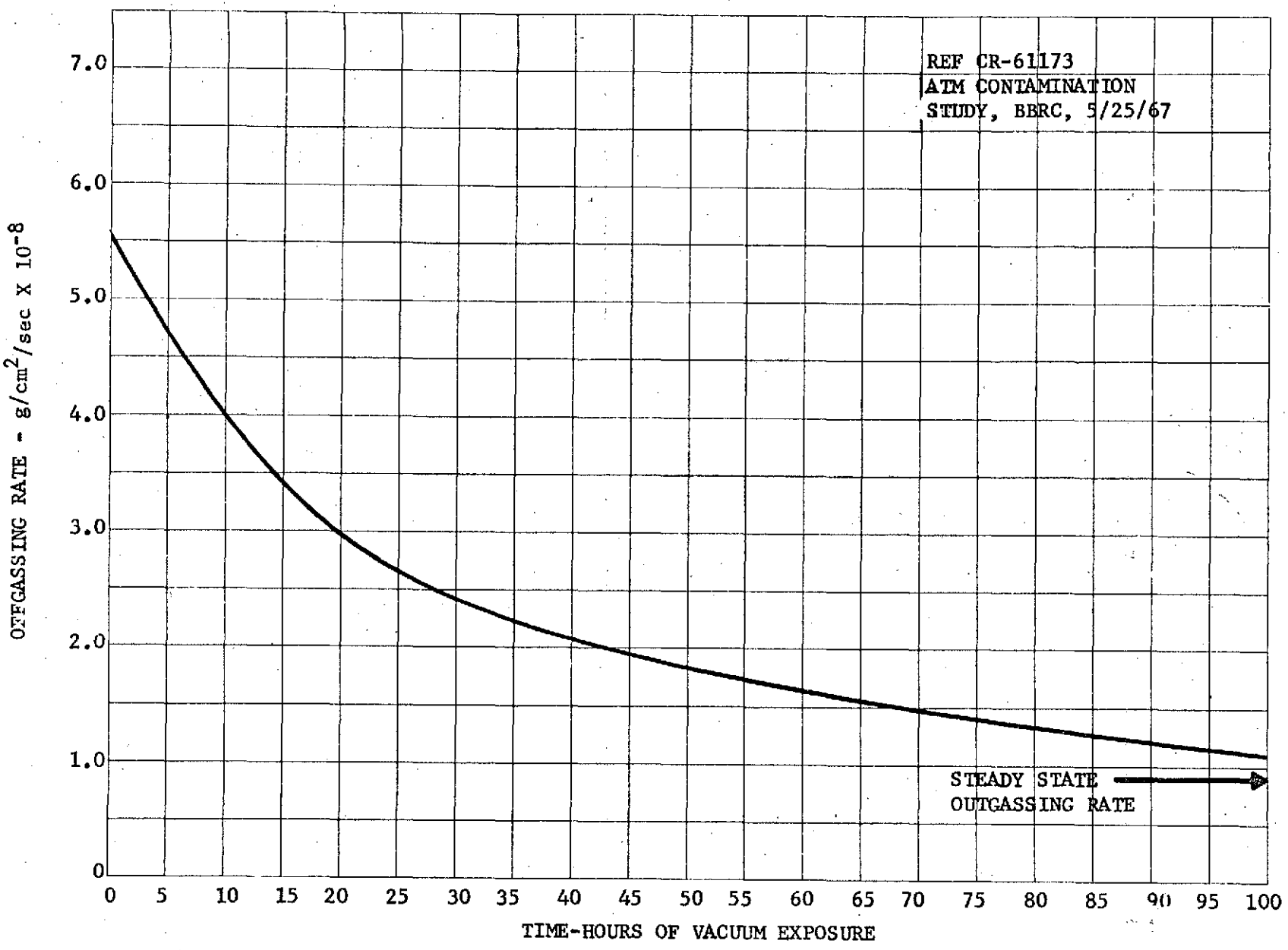

Figure 19. Offgassing Rate as a Function of Exposure Time to Vacuum for RTV 560 Binder

4.2.3 Leakage - Leakage from the crew compartments of the Shuttle Orbiter will continuously emerge from structural seams, hatches, microscopic cracks, and seals around support hardware such as instrumentation feed-throughs. The crew compartments will be pressurized to 14.7 psia with O_2/N_2 and the nominal leakage rate is estimated to be approximately 7 lbs/day. The Skylab leak rate was specified to 14 lbs/day and the measured value during the mission was approximately 3.75 lb/day. However, the Skylab internal environment pressure was approximately 5 psia. The factor of 3 higher in environment pressure for the Orbiter plus the continued relaunching and reentry of the Orbiter may create a larger leak rate than that already stated.

Leakage contaminants from these compartments will consist primarily of: 1) normal atmospheric gases; 2) internal materials and black box outgassing products; 3) astronaut by-products; 4) frictional erosion creating particles from materials subject to abrasion; and 5) evaporation from liquid sources.

The normal cabin atmosphere will not condense on most of the Orbiter and Orbiter/Payload surfaces since these gases have triple points which are considerably lower than the lowest surface temperature of the Orbiter. However, the potential of condensation will exist for such cryogenically cooled surfaces as employed in the infrared telescope Payloads and associated subsystems. The second source of leakage products is from outgassed materials in the crew compartment interior. Although most internal materials will outgas at a much lower rate than those external to the spacecraft, some of the electronic components which operate at elevated temperatures will outgas at significant rates. In any case, total contribution from this source to the contaminant environment will be negligible. The third source, astronaut by-products, are elements and compounds such as CO_2 emitted orally and dermally plus flatus and some fecal and urine products which escape their containers. The fourth source, frictional erosion particles, will in the majority of cases be too large to pass through microscopic leakage orifices and will be removed from the cabin atmosphere through the Environmental Control Life Support System (ECLSS) debris filters. The last source identified is water vapor evaporated from liquid sources. Much of this moisture

will be collected by the ECLSS condensate system along with various condensable and water soluble products in the atmosphere (although approximately 0.076 lb/day of water vapor will be allowed to leak overboard).

Since the bulkhead between the cabin area and the experiment bay area represents a probable area for cabin leakage, the leakage was modeled assuming that the total 7 lbs/day leakage from the forward experiment bay bulkhead which includes a 40" diameter EVA hatch, a 16" diameter window, and numerous instrumentation feedthroughs. The effluents were assumed to be emitted in a $\cos \theta / r^2$ distribution in an aft direction from that surface. The actual amount that will leak from this area will require a further analysis of the cabin structure for most probable leakage points. Of the 7 lb/day leakage, the following constituents and fraction of mass flow rate were modeled:

Constituent	Mass Flow Rate
O_2	1.625 lb/day
N_2	5.229 lb/day
H_2O	0.076 lb/day
CO_2	0.070 lb/day

Leakage will be emitted in molecular form having a most probable velocity based on the molecular weight (M) of the individual constituents and assuming a cabin environment temperature of 25°C where:

$$v = \left(\frac{2R_o T}{M}\right)^{\frac{1}{2}} = 2220 \sqrt{\frac{1}{M}}$$

v = 413 meters/second (assuming average M = 29)

4.2.4 Evaporator - During the normal Orbiter fuel cell operation, the fuel cell will generate approximately 158 lbs of excess H_2O/day which will be expelled overboard through the evaporator vent system. The evaporator system will flash evaporate this excess water and will eject the resulting vapor to space through two non-propulsive supersonic nozzles. The exact

locations of these nozzles are as yet to be determined. Therefore, three of the prime option locations were investigated in this study. Figure 20 depicts the candidate locations of the supersonic nozzles along with the Orbiter station number designators for each evaporator nozzle location. The vent system will be in operation on the average of 60% of all on orbit time during which it will flow at a rate of approximately 11 lbs H_2O/hour (5.5 lbs/hr/vent). Through vacuum chamber testing of the evaporator vent system at Johnson Space Center (JSC) and from a semi-empirical analysis[1], the plume distribution from any one of the supersonic nozzles was determined to be:

$$F(r, \theta) = \frac{N_c (\cos \theta)^{\eta}}{r^2} \quad ; \; -\frac{\pi}{2} < \theta < \frac{\pi}{2}$$

where; $N_c = \left(\frac{\eta + 1}{2\pi}\right) \dot{M}$

$\eta = 6.272$,

θ = Angle between nozzle centerline and point of interest within the plume,

r = Distance between nozzle and point of interest within the plume,

$\dot{M}$ = Molecular flowrate = 5.5 lb/hr = 6.95×10^{-1} g/second.

therefore; $F(r, \theta) = \frac{0.812 \; (\cos \theta)^{6.272}}{r^2}$

The plume distribution as determined during the Supersonic Nozzle/Plume Test in Chamber A at JSC in June 1973 is depicted in Figure 21 for a nominal flowrate of 16 lbs H_2O/hr. This flowrate is nearly 3 times higher than the per nozzle rates now anticipated from the evaporator vent system, but the resulting distribution should be representative. In addition, this test indicated that

(1) Naumann, R.J., "Column Densities Resulting from Shuttle Sublimator/Evaporator Operation," NAS-TM-X-64794, October 1973.

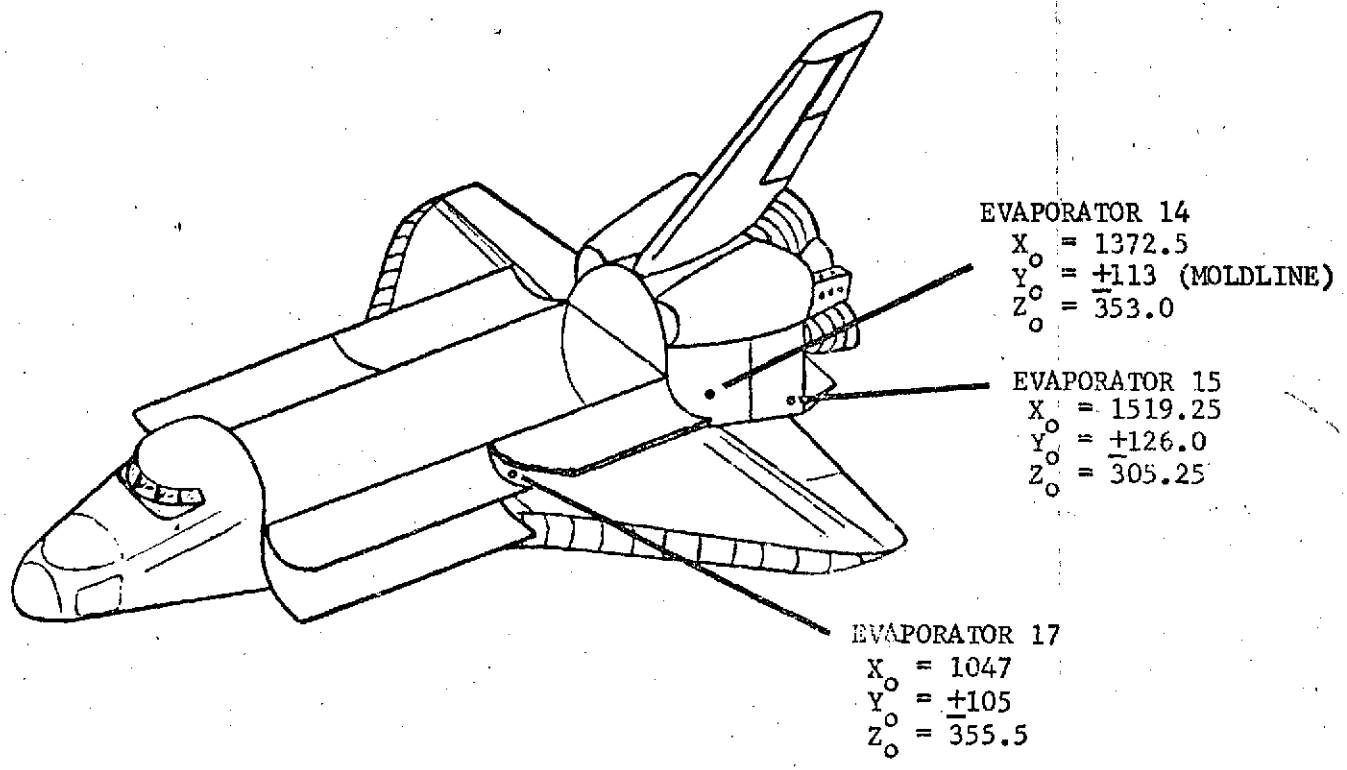

Figure 20. Candidate Evaporator Locations

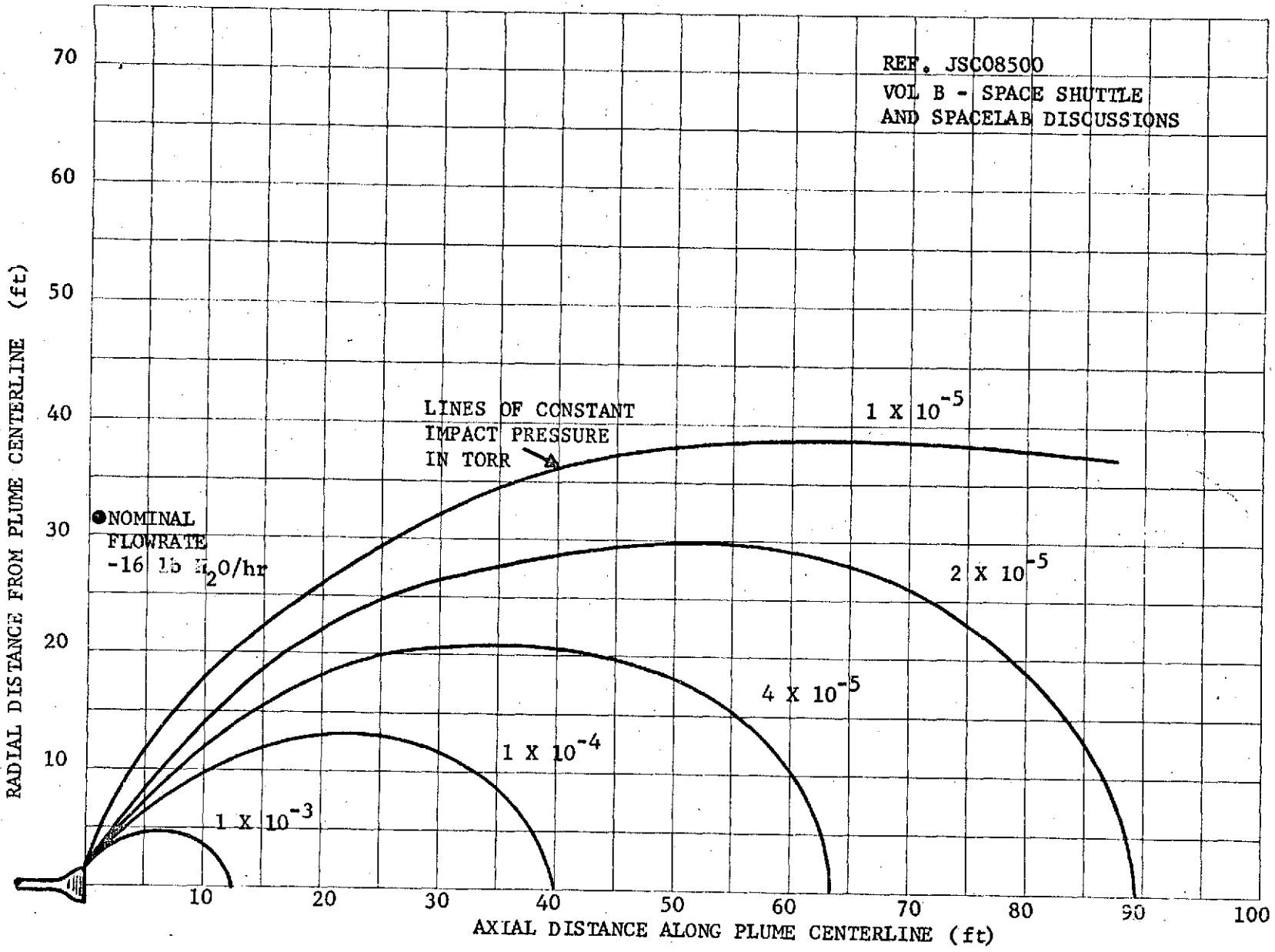

Figure 21. Impact Pressure Data - Supersonic Evaporator Nozzle

the fraction of mass expanding to angles $>90^{o}$ varies between 0.001 and 0.002 for differing nozzle lengths.

Molecular velocities of the expelled water vapor were modeled using the mean radial velocity relationship:

$$v = \sqrt{\frac{2\gamma RT}{(\gamma-1)M}}$$

where: $\gamma = c_{p/c_v} = 1.4$,

R = Universal Gas Constant,

T = 273 degrees, Kelvin,

M = Molecular weight = 18 g/mole water

therefore; $v_{273^{o}K} = 1003$ meters/second

4.2.5 Reaction Control Subsystem (RCS) Vernier Engines - The RCS engines considered for this study were the six 25 lb thrust vernier engines. The forty 900 lb thrust thrusters were not modeled or considered. These engines will mainly be used for major orbital station keeping and will not be used operationally for day-to-day on orbit station keeping. However, the 900 lb thrusters could contribute significantly to deposition on the Orbiter external surfaces and on Free Flying Payload surfaces during deployment which in turn will desorb over a period of time and may contribute to establishing on orbit constraints with respect to the operational measuring time of particular Payloads. Figure 22 shows the location and orientation of the Orbiter Reaction Control Subsystem engines.

Figure 23 shows the location and schematically the forward flow fields for the 25 lb vernier RCS engines. Two 25 lb thrust verniers are located forward of the Orbiter cabin one on each side of the Orbiter. These engines exhaust down (-Z direction) from the Orbiter. There are no Orbiter surfaces in the direct field-of-view of these engines. However in side and back flow, these engines can contribute to mass column densities and deposit on some Orbiter surfaces.

Four 25 lb thrust verniers are located aft near the Orbital Manuevering Subsystem (OMS) with two engines on each side of the Orbiter. Each set of these verniers are positioned such that one engine on both sides thrusts in the downward direction (-Z direction) as the forward verniers. The remaining two verniers each thrust away from the Orbiter in the port (+Y) and the starboard (-Y) direction. These rear vernier engines have the capability of directly impinging upon principal Orbiter surfaces. In particular, the aft downward firing (-Z) thrusters can impinge upon a considerable amount of the Orbiter Wing area thus presenting an additional contaminant source in reflection and deposition from these vernier engines.

At present there is insufficient information available regarding the specific design of these engines to justify a detailed analysis of the exhaust flow fields beyond that used in

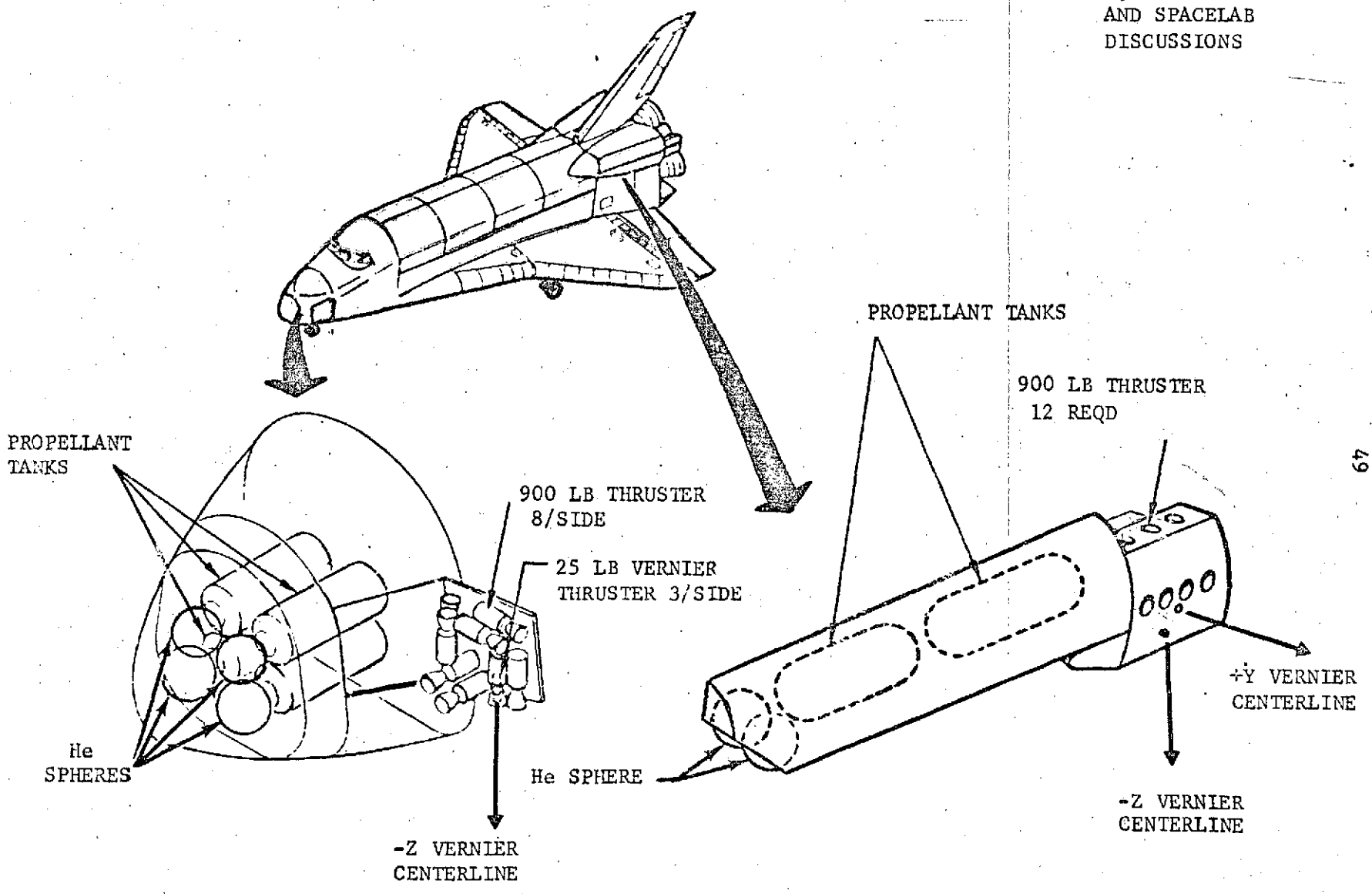

Figure 22. Orbiter Reaction Control Subsystem

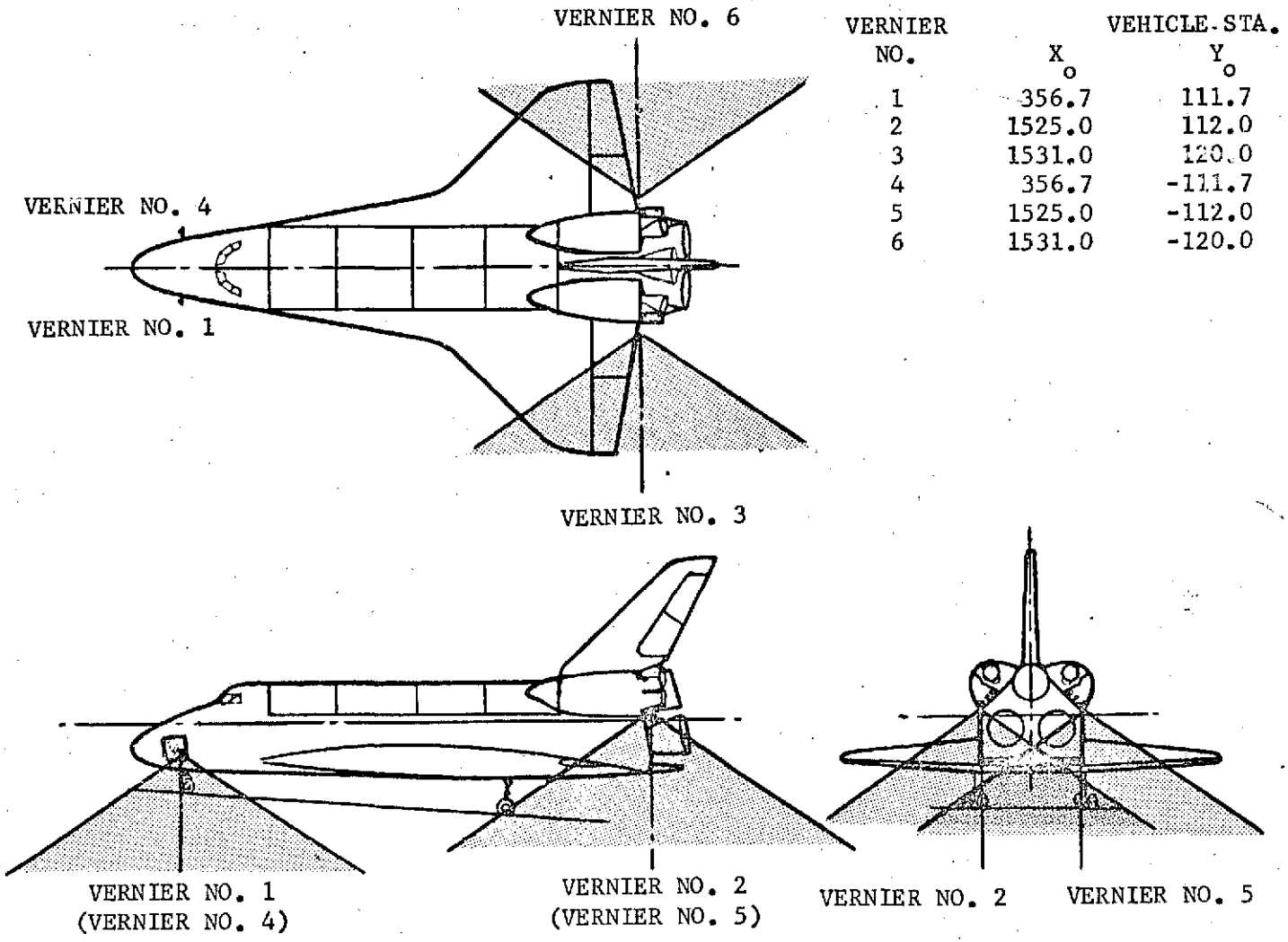

VERNIER NO.	VEHICLE-STA. NO. X_o	Y_o	Z_o
1	356.7	111.7	351.1
2	1525.0	112.0	442.0
3	1531.0	120.0	461.0
4	356.7	-111.7	351.1
5	1525.0	-112.0	442.0
6	1531.0	-120.0	461.0

Figure 23. Reaction Control Subsystem 25 lb Thrust Vernier Locations

this study. Modeling of the flow fields was based upon a scaled down version of the Skylab Marquardt R-4D N_2O_4/MMH 100 lb engine. An approach developed by Simons[1] was modified to establish a closed form analytical representation for the mass contained in the engine flow field for angles from 0° to 140° from the engine centerline. These angles encompass the major portion of the vernier engine flow field mass which can either reflect or deposit on Orbiter surfaces and contribute significantly to the induced environment. Beyond 140°, the experimental data of Chirivella and Simon[2] indicate the mass flux may approach a constant value becoming independent of θ. This observation was injected into the present study by modifying the model of Simons[1] so that it predicted a constant mass flux in the plume for angles greater than 140° up to 180°.

From the modified approach of Simons, the mass flux from the 25 lb vernier RCS engines using the R-4D similarity for angles between 0° and 40° and between 40° and 140° from the engine centerline becomes:

for $0^\circ \leq \theta \leq 40^\circ$

$$\dot{m} = 3.7/r^2 \left[\cos\left(\pi/2\, \theta/\theta_i\right)\right]^{8.65}$$

where;

$\dot{m}$ = Mass flux rate in $g/cm^2/second$,

r = Distance from the exit plane of the engine nozzle in inches,

$\theta_i = 115^\circ$,

θ = Angle in degrees between 0° and 40° from the engine centerline.

(1) Simons, G.A.: "Effect of Nozzle Boundry Layers on Rocket Exhaust Plumes," AIAA Journal, Vol. 10, No. 11, November 1972

(2) Chirivella, J.E. and Simon, E.: "Molecular Flux Measurements in the Back Flow Region of a Nozzle Plume," J.P.L., JANNAF 7th Plume Technology Meeting, April 1973

for $40^{\circ} < \theta \leq 140^{\circ}$

where;

$$\dot{m}^{o} = (0.9)/r^{2}\ e^{-0.0467\ (\theta - 40^{\circ})}$$

where;

$\dot{m}^{o}$ = Mass flux rate in g/cm^{2}/second,

r = Distance from the exit plane of the engine nozzle in inches,

θ = Angle from the centerline of the engine in degrees for $\theta > 40^{\circ}$.

For the back flow regions, the mass flux between 140° and 180° from the engine centerline becomes:

for $140^{\circ} < \theta \leq 180^{\circ}$

$$\dot{m}^{o} = 0.9/r^{2}\ e^{-4.67}$$

where;

$\dot{m}^{o}$ = Mass flux rate in g/cm^{2}/second,

r = Distance from the exit plane of the engine nozzle in inches.

A mean velocity of 3,505 m/second was assumed for this study.

An estimate of the species concentrations in the RCS vernier engine plumes is given below:

Constituent Mole Fractions for an O/F Ratio of 1.636 (1)

CO	0.12861
CO_2	0.04160
H	0.01163
H_2	0.16313

(1) Ratliff, A. W.; Auden, B. J. and Thornbill, D. D.: "Analysis of Exhaust Plumes from Skylab--Configuration R-4D Attitude Control Motors," LMSC/HREC D162171, March 1971.

H_2O	0.33876
NO	0.00062
N_2	0.30933
O	0.00027
OH	0.00582
O_2	0.0023

No consideration was given in this study to the potential of condensation in the flow fields of the vernier engines. As mentioned previously, these results are subject to the assumption that the Orbiter vernier engines are similar in design to the Skylab R-4D engines scaled down. Depending upon the Orbiter RCS engine injector design, the resulting flow fields will be subject to changes as a result of oxidizer to fuel striation thus providing unique flow fields which may not be adequately represented by the Skylab R-4D plumes. However, reasonably good contamination effects data from Skylab RCS engine in flight deposition measurements and correlation with pre-Skylab mission ground tests programs exists to base a preliminary RCS vernier contamination impact analysis on Shuttle Payloads.

4.2.6 Returned Flux - With some Shuttle Payloads operating at considerably lower orbital altitudes (200 km) than Skylab (435 km) and with cryogenically cooled Payloads, the returned contaminants as a result of interacting with the ambient orbital environment represents a potential significant source.

The returned flux of contaminants will be a function of a number of variables. These are:

a. the molecular size and weight of the contaminants leaving the Orbiter,

b. the velocity at which the contaminants leave the Orbiter,

c. the density and molecular size of the ambient atmosphere,

d. the orbital altitude,

e. the attitude of the Orbiter and the Payload with respect to the velocity vector of the ambient atmosphere,

f. the temperature of the surfaces of the Orbiter and the Payloads,

g. the source locations and flux rates which comprise the induced environment.

Figure 24 shows how the return flux rate varies as a function of orbital altitude. At Skylab altitudes (435 km), the return flux is a factor of 52.7 less than at a 200 km altitude for a given mass column density along an experiment line-of-sight. The return flux is directly related to the number density of the ambient atmosphere.

The medium density at a given altitude is used in the modeling. This value will vary between orbital daytime and high sunspot activity and for orbital nighttime and low sunspot activity. At 200 km, the ambient molecular density can vary between 10^9 and 10^{10} molecules/cm^3. At 435 km, the molecular density may vary between 10^7 and 10^8 molecules/cm^3. A medium density of 1.3 X 10^8 molecules/cm^3 at 435 km and 6.85 X 10^9 molecules/cm^3 at 200 km has been used in return flux calculations.

As discussed in Section 3.3, the returned flux is computed from the interaction planes positioned at the collecting sphere locations. The density calculated at each location is allowed to interact with the ambient atmosphere so that a collision frequency for a specific contaminant molecule is established. The scattered molecules are emitted in a cos θ distribution that is aligned along the velocity vector or equivalently, with respect to the ambient molecule direction. Through geometry consideration, the fraction of the scattered contaminant molecules that can reach the representative payload is determined.

For any given line-of-sight, the returned flux of contaminants for that line-of-sight will vary sinusoidally. Solar oriented Payloads in attitudes similar to Skylab will see the returned flux in the mode as the Orbiter comes from orbital midnight to orbital noon. The point of orbital sunrise will be the point of maximum returned flux of the ram condition as the velocity vector is aligned along the line-of-sight towards the Payload. This would also be the period of maximum flux since the Orbiter/Payload surfaces are warming due to solar exposure and are outgassing at a higher rate.

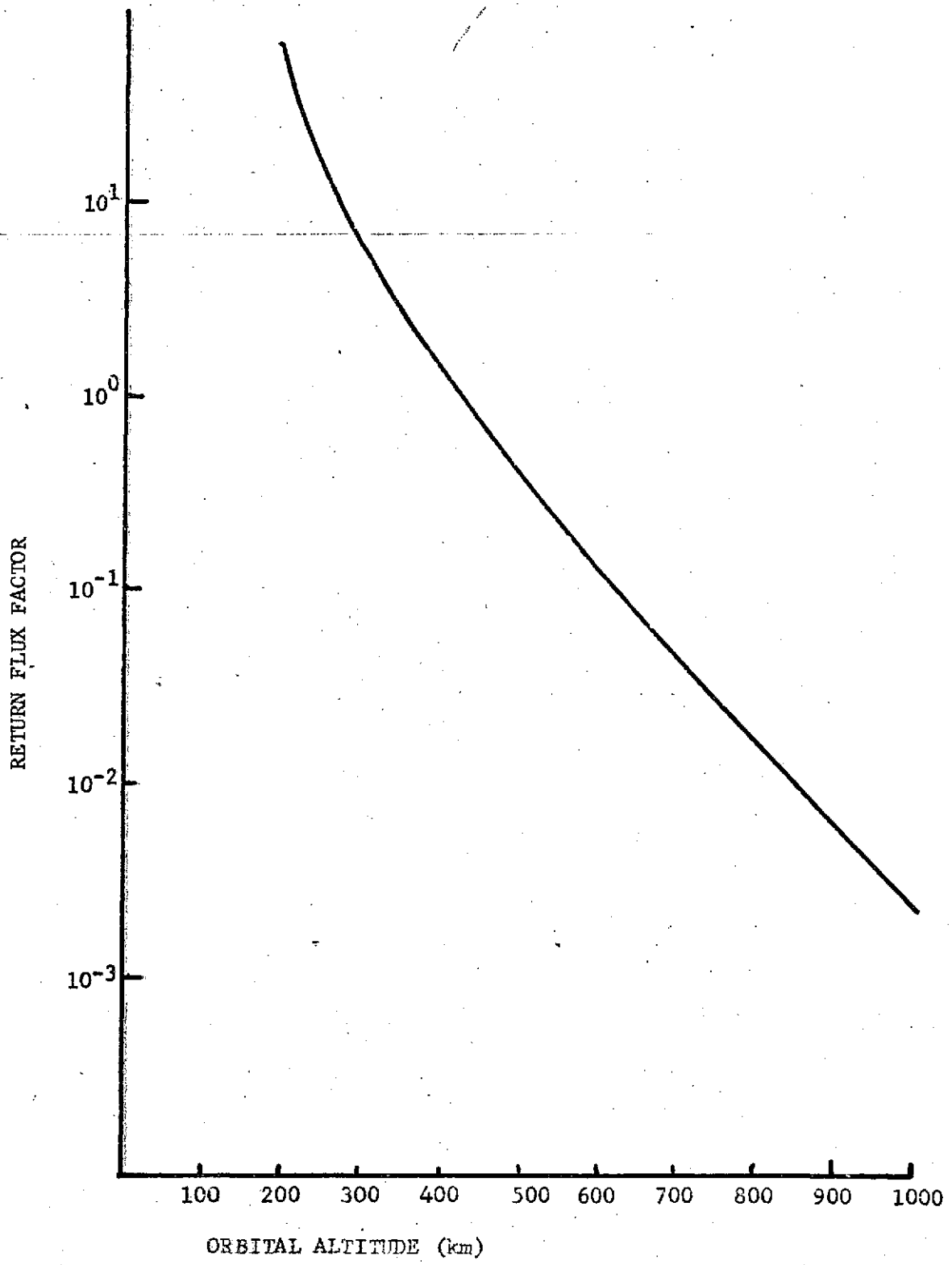

Figure 24. Return Flux as a Function of Orbital Altitude Normalized to 435 Kilometers

Just the opposite will be true for those Payloads whose viewing requirements require anti-solar lines-of-sight. In this case, maximum ram will occur at orbital sunset with the fluxes at a minimum since the Orbiter/Payload surfaces will be cooling and not outgassing as heavily. However sources not dependent on vehicle surface temperatures will have the same impact as the solar oriented case mentioned above.

Before a more detailed analysis can be performed, the pointing requirements for an experiment with respect to the velocity vector and the vehicle must be accurately determined.

4.2.7 Summary of Major Sources - Presented in Table I is a summary of the major sources modeled. This summary presents the duration/frequency, constituents, plume shape function, velocity, and size parameter for each of the sources modeled.

Those secondary sources such as reflections and resublimation from the Orbiter surfaces are a function of the model geometry, a $\cos \theta / r^2$ distribution in reflection, the flowrate defined by the particular source, and a corresponding plume shape function as given in Table I. These sources are not defined discretely since the geometrical relationship of the model preclude listing all the surface interactions in this report to define this type source.

Table I Major Sources Summary

Major Sources	Duration/ Frequency	Flowrate	Constituents	Plume Shapa Function	Velocity	Size Parameter
Outgassing	Continuous	$5\times10^{-10}\, e^{-t/4100}\, e^{(T-100)/29}$ g/cm^2/sec (10%)	Hydrocarbon chain fragments, RTV's, etc.	$\cos\theta/r^2$	12.9 $\sqrt{T}$ m/sec	Molecular Avg. M = 100
Offgassing	Continuous for first 100 hours on-orbit	$[.325e^{-.0714t} + .372e^{-.0105t}]\, e^{(T-100)/29}$ g/cm^2/sec x 10^{-8}	Water light gases Volatiles	$\cos\theta/r^2$	30.4 $\sqrt{T}$ m/sec	Molecular Avg. M = 18
Evaporator (2) *	~60% of on-orbit Time	5.5 lb/hr/vent	Water	$(\cos\theta)^{6.272}/r^2$	1003 m/sec	Molecular M = 18
Cabin Atmos Leakage	Continuous	7 lb/day	O_2 N_2 CO_2 H_2O	$\cos\theta/r^2$	2220 $\sqrt{\frac{T}{M}}$ m/sec	Molecular Avg. M = 29
RCS Vernier Engines**	As Reqd.	3.0 lb/orbit Y-POP attitude @ 200 km	H_2O N_2 H_2 CO CO_2 H	$\frac{(\cos\frac{\pi\cdot\theta}{2\theta_j})^{8.65}}{r^2}$ $0^\circ\le\theta\le40^\circ$; $\frac{e_2}{r^2}$ $.0467(\theta-40^\circ)$ $40^\circ<\theta\le140^\circ$; $\frac{e_2}{r^2}$ -4.67 $140^\circ<\theta\le180^\circ$	3505 m/sec	Molecular
Ambient Reflection	~10 min per orbit	Varies with above sources & orbital attitude	Any of the above sources	$\cos\theta/r^2$ from collision points	7.65×10^3 m/sec	Varies with all above sources

* Plume reflections off of structural surfaces (e.g. wings, experiment bay doors) are equivalent to a source equal to the plume impingement rate with a $\cos\theta/r^2$ distribution and a velocity of $30.4\sqrt{T}$ m/sec from the surface where T = surface temp.

** RCS plume reflections off of structural surfaces are assumed to have a rate equal to the plume impingement rate with a $\cos\theta/r^2$ distribution and a velocity equal to $129\sqrt{\frac{T}{M}}$ where T = surface temperature.

4.3 Other Orbiter Sources - Although the intent of this study was to address the known major Orbiter contamination sources as discussed in Section 4.2, a general sources review was conducted to establish the nature and potential impact of these other sources to the Orbiter induced environment. Some 40 sources have been identified and are presented in Tables II through IV. These sources have been broken up into 3 basic phases. These phases are launch sources, on orbit sources, and reentry sources.

The majority of these sources are associated with other than the on orbit phase which was addressed in this study. However their identification and tracking becomes important as the requirements for contamination control begins to be established for the Orbiter and the Orbiter/Payload interface.

Those on orbit sources identified in Table II were not modeled since the source rate is either small or these sources have limited duty cycles. As higher fidelity is required and developed with respect to the Orbiter and Orbiter/Payload modeling, some of these sources could become significant in that they may have a directional influence upon either a Payload or a Payload/Orbiter critical surface.

Where available, the source duration (or frequency), mass flow rate, and constituents have been identified. No doubt as the overall program develops more rigorous definitions of requirements for operational controls on the Orbiter and the Payloads, these sources will change in number and definition.

Table II. Other Shuttle Sources - On Orbit

Operational Phase	Source	Duration/ Frequency	Mass Flow Rate	Constituents
On Orbit:	Fecal Canister Vent	TBD/ As req'd	0.058 lb/day 0.187 lb/day 0.803 lb/day 0.003 lb/day Trace	O_2 N_2 H_2O CO_2 Volatiles
	Airlock	TBD/ As req'd	3.8 lb/oper 12.0 lb/oper 0.18 lb/oper 0.16 lb/oper	O_2 N_2 H_2O CO_2
	Waste Fuel Cell Water Vent	TBD/ As req'd	0 to 23 lb/dump Max	H_2O
	Fuel Cell O_2 Purge Vent	60 sec/one ea. 3600 Amp-hrs	5 lb/hr/fuel Cell	0.0835 lb O_2/Purge 0.0075 lb H_2O/Purge
	Fuel Cell H_2 Purge Vent	60 sec/one ea. 6480 Amp-hrs	0.6 lb/hr/fuel Cell	0.0101 lb H_2/Purge 0.0149 lb H_2O/Purge
	Supplemental Radiator Heat Rejector - (Conceptual)	Continuous - fuel cell H_2O	0 to 6 lb/hr	H_2O
	OMS Cargo Bay Kit He Tank Leakage	Continuous/48 hours prior to launch to end of mission	158×10^{-5} scc/min	He

Table II . Other Shuttle Sources - On Orbit (Concluded)

Operational Phase	Source	Duration/ Frequency	Mass Flow Rate	Constituents
On Orbit:	OMS Cargo Bay Kit N_2O_4 Tank Leakage	Continuous/48 hours prior to launch to end of mission	110 X 10^{-5} scc/min	He and N_2O_4
	OMS Cargo Bay Kit MMH Tank Leakage	Continuous/48 hours prior to launch to end of mission	110 X 10^{-5} scc/min	He and $N_2H_3CH_3$
	900 lb Thrust Reaction Control System Engines - (40)	As req'd/ As req'd.	~3.24 lb/sec/engine during steady-state firing	N_2, H_2O, CO, CO_2, H_2 HNO_3, plus trace contam.
	EVA Suit	As req'd/ continuous during EVA	1.72054 lb/hr 0.0158 lb/hr 9.5 X 10^{-6} lb/hr TBD	H_2O O_2, N_2, CO_2 Organics Particles
	Orbital Maneuvering Subsystem 6000 lb Thrust Engines - (2)	As req'd/ As req'd for Major Orbit Maneuvers	TBD - (~20 lb/sec/ engine)	H_2, H_2O, CO, CO_2, H_2, HNO3, plus trace contam.
	Hydraulic Leakage	Continuous	TBD	Hydraulic Fluid

Table III. Other Shuttle Sources - Launch

Operational Phase	Source	Duration/ Frequency	Mass Flow Rate	Constituents
Launch:	Nose Sphere Vent	120 sec/once - at launch	3.848 lb	Air
	Right Hand Chine Vent	120 sec/once - at launch	4.884 lb	Air
	Left Hand Chine Vent	120 sec/once - at launch	4.884 lb	Air
	Right Hand RCS Thruster Cavity Forward Vent	120 sec/once - at launch	3.552 lb	Air
	Left Hand RCS Thruster Cavity Forward Vent	120 sec/once - at launch	3.552 lb	Air
	Right Hand RCS Oxidizer Cavity Forward Vent	120 sec/once - at launch	11.248 lb	Air
	Left Hand RCS Oxidizer Cavity Forward Vent	120 sec/once - At launch	11.248 lb	Air
	Volume Around Crew Module Vent - (2 plc)	120 sec/once - At launch	89.281 lb	Air
	Payload Bay Vent - (8 plc)	120 sec/once - At launch	1139.6 lb (empty bay)	Air/N_2
	Right Hand RCS Thruster Cavity Aft Vent	120 sec/once - At launch	5.92 lb	Air

Table III. Other Shuttle Sources - Launch (Continued)

Operational Phase	Source	Duration/ Frequency	Mass Flow Rate	Constituents
Launch:	Left Hand RCS Thruster Cavity Aft Vent	120 sec/once - At launch	5.92 lb	Air
	Right Hand OMS Engine Cavity Vent	120 sec/once - At launch	10.952 lb	Air
	Left Hand OMS Engine Cavity Vent	120 sec/once - At launch	10.952 lb	Air
	Vertical Stabilizer Vent	120 sec/once - At launch	29.23 lb	Air
	Aft Fuselage Vent - (2 plc)	120 sec/once - At launch	377.178 lb	Air
	Right Hand Aft Wing Vent	120 sec/once - At launch	18.8508 lb	Air
	Left Hand Aft Wing Vent	120 sec/once - At launch	18.8508 lb	Air
	Aft Fuel Tenk Cavity Vent - LH	120 sec/once - At launch	33.744 lb	Air
	Aft Oxidizer Tank Cavity Vent - RH	120 sec/once - At launch	28.12 lb	Air
	Aft Lower Mid Fuselage Vent - (4 plc)	120 sec/once - At launch	600.14 lb	Air
	Forward Lower Mid Fuselage Vent - (2 plc)	120 sec/once -	188.7 lb	Air

Table III. Other Shuttle Sources - Launch (Continued)

Operational Phase	Source	Duration/ Frequency	Mass Flow Rate	Constituents
Launch:	Right Hand Wing Leading Edge Vent	120 sec/once - At launch	TBD	Air
	Left Hand Wing Leading Edge Vent	120 sec/once - At launch	TBD	Air
	Auxiliary Power Unit System Exhaust Outlets - (4)	10 min/prelaunch phase	0.2 lb/sec N_2H_4 consumed for all phases	H_2 - 8.4 lb N_2 - 78.0 lb NH_3 - 31.2 lb H_2O - 2.4 lb
		9 min/Boost phase		H_2 - 7.56 lb N_2 - 70.2 lb NH_3 - 28.08 lb H_2O - 2.16 lb
	Evaporator Vent	Continuous/Ascent Phase	50 lb/hr	H_2O
		Continuous/Coast Phase	38 lb/hr	H_2O
	Solid Rocket Booster Separation Motors - (16)	TBD/at SRB Separation (43 Km)	TBD - 23,000 lb thrust per engine	Combustion Products
	APU Steam Generator	13.25 min/ Ascent Phase	3 lb/min	H_2O
	Space Shuttle Main Engines - (3)	490 sec/ Ascent Phase	TBD - 470,000 lb thrust per engine	H_2O, O_2, H_2, scorched surface emissions
	Solid Rocket Motors - (2)	Launch up to 43 Km/Ascent Phase	TBD	Combustion Products
	Hydraulic Leakage	13.25 min/ Ascent phase	4 ml/hr/actuator (6 TCV Actuators)	Hydraulic Fluid

Table III. Other Shuttle Sources - Launch (Concluded)

Operational Phase	Source	Duration/ Frequency	Mass Flow Rate	Constituents
Launch:	Thrust Termination Motors - (4)	TBD/ Ascent Phase	TBD	Combustion Products
	Deorbit Motor	TBD/ Ascent Phase	TBD	Combustion Products

Table IV . Other Shuttle Sources - Reentry

Operational Phase	Source	Duration/ Frequency	Mass Flow Rate	Constituents
Reentry:	Auxiliary Power Unit System Exhaust Outlets - (4)	5 min/Post expt. data acq. phase	0.2 lb/sec N_2H_4 Consumed for all phases	H_2 - 4.2 lb N_2 - 39 lb NH_3 - 15.6 lb H_2O - 1.2 lb
		2 min/pre-deorbit phase		H_2 - 1.68 lb N_2 - 15.6 lb NH_3 - 6.24 lb H_2O - 0.48 lb
		46 min/entry to touchdown phase		H_2 - 38.64 lb N_2 - 358.8 lb NH_3 - 143.52 lb H_2O - 11.04 lb
		2 min/touchdown to rollout phase		H_2 - 1.68 lb N_2 - 15.6 lb
		2 min/touchdown	0.2 lb/sec N_2H_4 consumed for all phases	NH_3 - 6.24 lb H_2O - 0.48 lb plus .005 mas fraction aniline, ($C_6H_5NH_2$) and trace metals
	TF33-P-7A Air Breathing Propulsion System Engines - (6)	Ferry flight duration/ As req'd depending on landing site	TBD	JP Fuel Combustion Products

Table IV . Other Shuttle Sources - Reentry (Concluded)

Operational Phase	Source	Duration/ Frequency	Mass Flow Rate	Constituents
Reentry:	ABPS JP Fuel Vent	Ferry flight duration/ As req'd depending on landing site	TBD	JP Fuel
	Ammonia Evaporator Vent	Continuous - subsequent to reentry starting at 100,000 ft until GSE hookup	0 to 130 lb/hr Max	NH_3 - 42 lb
	Evaporator Vent	Continuous/ Deorbit Phase	38 lb/hr	H_2O
		Continuous/ Entry Phase	44 lb/hr	H_2O
	APU Steam Generator	45 min/Reentry & Landing Phase	3 lb/min	H_2O
	Hydraulic Leakage	45 min/Reentry & Landing Phase	4 ml/hr/actuator (4 elevon actuators)	Hydraulic Fluid

4.4 Reflection and Resublimation from Orbiter Surfaces - The Shuttle Orbiter configuration geometrically presents a source that Skylab essentially did not have. The Orbiter Wings and the Orbiter experiment bay doors present surfaces where contamination sources can be reflected from or deposit and resublimate. The operational nature of the Orbiter essentially precludes any vents being located on the bottom side. Therefore, the majority of active sources are all located on the Orbiter top side where the Payloads are also positioned. The Orbiter Wings and experiment doors will act as secondary contamination sources for general surface outgassing, offgassing, evaporator venting, and RCS vernier engine firings.

Although these surfaces will be warm on orbit and deposition from sources which produce H_2O, CO_2, O_2, N_2, etc. will not occur on these surfaces, they are capable of reflecting contaminants into Payload lines-of-sight. In particular, the cryogenically cooled Payloads may under certain conditions condense these light contaminants on their external operational surfaces and change their properties.

Of particular significance are the RCS verniers. All of the four rear position 25 lb thruster forward flow fields are capable of impinging upon the Orbiter Wings and experiment bay doors when opened. Experience from Skylab has shown that bipropellant engines such as currently planned for the Orbiter will deposit contaminants that will resublimate with time. On Skylab 0.2% of the mass flux arriving at Quartz Crystal Microbalance (QCM) surfaces at approximately $10^{o}C$ condensed. The condensed engine contaminates desorbed to 1/e of the deposited material in 72 hours and the resulting deposition that did not sublime was approximately 20% of the original deposit.

Based upon anticipated RCS 25 lb thrust propellant usage requirements, (Table V) up to 48 lbs (Y-POP attitude at a 200 kilometer orbit) could be expended per day of operation. The nominal duty cycle of these engines is on the order of 0.070 seconds. If these engines were fired at a uniform rate per day, the resulting firing frequency would be once every 15

Table V . Effect of Orbital Altitude on RCS Vernier Fuel Usage for Payload Pointing with Various Orbiter Orientations*

Orientation	Fuel Usage, lbs/orbit		
	100 n.mi. Orbit	200 n.mi. Orbit	500 n.mi. Orbit
Y-POP, Z-Local Vertical	0.3	0.3	0.3
Y-POP Inertial	3.4	2.3	2.1
Z-POP Inertial	12.8	3.0	2.6
X-POP Inertial	11.0	.6	.5

* (JSC 07700 Vol. XIV, Revision B)

seconds. With the desorption characteristics observed from Skylab RCS engines and the potential firing frequency of the Orbiter 25 lb thrust RCS engines, the reflection and subsequent deposition and desorption from the Orbiter surfaces will be a potential significant contamination source.

An even larger problem potentially exists with the forty 900 lb RCS vernier engines which are used for large on orbit operational activities.

For this study, additional care was given to increasing the number of nodes representing the Orbiter Wings and experiment bay doors to obtain better resolution in defining these secondary sources. Observed Skylab RCS deposition and sublimation data was used to assess the potential impact. Although operationally the Orbiter surface temperatures will probably be higher than those that saw RCS deposition on Skylab, the Skylab values used are felt representative for this study.

The reflection of plume impingment from both the evaporation system and the RCS were considered a $\cos \theta / r^2$ distribution with respect to the normal of the surface at a rate equal to the plume impingement rate. The reemission velocities were modeled as the most probable velocity based upon the temperature of the emitting surface:

where;

$$v = \left(\frac{2R_o T}{M}\right)^{\frac{1}{2}}$$

$$v = 30.4 \sqrt{T} \quad \text{for molecular weight of 18.}$$

where: v = Velocity in meters/second,

T = Temperature in degrees Kelvin.

These assumptions are considered valid for exhaust vapor when considering that the surface characteristics of most of the Orbiter surfaces will be non-uniform such that the impinging contaminants will reside there for a short period of time, acquire essentially the temperature of the surface and be re-emitted with the same characteristic distribution and temperature as outgassed molecules. Molecules such as H_2O, CO_2 and CO which have strong dipole moments reside for significant periods of time at a surface to be accommodated. Experiments have shown that for molecules less than leV incident on surfaces near 300 to 330^{o}K have a diffuse (cosine) scattering pattern.

An analogous situation exists for the reflection of the evaporator flow field off of the Orbiter Wings.

In summary, since all of the engines and vents must necessarily be above the Orbiter Wings, the capability of reflecting these effluents into experiment lines-of-sight exists. The net effect is a concentration of the overboard vent sources to the Payload side of the vehicle.

4.5 Boost and Reentry Contamination Sources - A qualitative assessment of the boost and reentry phases was made to establish the contamination potential during these phases. Little is known about the stowage requirements for individual Payloads during launch and reentry. Although the Orbiter has established some basic control measures to minimize the potential of Payloads being contaminated, the effectiveness will remain in doubt until test data and possibly first Shuttle Orbiter flights have been completed. Both the launch and reentry phases subject the Orbiter to considerable dynamic influences of heat, pressure overloads, and vibrations. To totally protect the Payloads during these phases may require complex or costly measures. The following sections briefly discuss the contamination potential of Payloads during launch and reentry.

During approximately 90 seconds of the boost period starting about 30 seconds prior to maximum dynamic pressure, atmospheric frictional heating will cause heavy offgassing and outgassing from the Orbiter and booster structures, coatings, and contaminant layers acquired during ground operations. These

emitted products will become trapped in cracks and corners and will condense on cooler surfaces of both the Orbiter and Payloads. If external pressures over the passive vent areas become greater than over others and the difference exceeds the normal internal to external pressure difference, then the hot emission products can be swept into the Orbiter to condense or otherwise be trapped on internal surfaces. Shock impingement and turbulent boundary layer action will generate pressure differences sufficient for this purpose. Also, such pressure differences can result from steering manuevers. Locations of the pressure difference points will vary with velocity and angle of attack during launch.

At the time of solid rocket booster separation, the experiment bay pressure will have reduced to approximately 0.04 psi. Pressures generated across passive vent areas by the separation rocket exhausts can be several times this amount. Highly contaminating solid rocket combustion products will enter the passively vented volumes and become temporarily trapped and be re-emitted at some later time. Exhaust products will also become trapped on external surfaces.

Instrumented Titan payloads have indicated deposits of 26 micrograms per square centimeter from separation rockets on surfaces over 17 feet away from and 90° off the separation rocket engine axis. White paint samples located in the same vicinity had their absorptivity values more than doubled as a result of discoloration from boost emissions and separation rocket exhaust product deposition.

Once the outgassing and exhaust products have been deposited, they will migrate as temperature conditions vary over the Orbiter structure. Particulate matter will become entrained with outgassing species. Paints and other coatings scorched, melted, and blistered by rocket exhaust will spall or slough off and become entrapped on other surfaces.

The same instrumented Titan flights mentioned previously have indicated that the contaminants deposited during boost were migrating from the solar heated side to cooler surfaces after orbit injection. In these instances, deposition buildup

on instruments mounted on the cool side was nearly equal to loss from instruments on the hot side. Loss from the hot side instruments was 10% to 15% per week initially. However, loss and buildup rates on the instruments were most likely influenced by special coatings on the instrument surfaces. Deposits on other hot surfaces were evidently being lost at a higher rate because all emissions from the hot surfaces cannot be expected to return to cold surfaces.

It can be seen that the threat from boost generated contaminants can be expected to continue for some time after the boost process is completed. Protection for contamination sensitive Payloads would require leaving them enclosed in the lined experiment bay and, perhaps, rotating the Orbiter to heat all surfaces for a few days. Pressure gages located in the lower experiment bay area would indicate when the early, heavy offgassing pulse has subsided.

During the extremely high heating conditions of reentry, surface temperatures far above those generated during boost and orbit will be experienced. Frictional heating and erosion will occur on leading surfaces and the hot plasma surrounding the Shuttle will radiate heat into areas that do not experience frictional heating. As this heat pulse soaks into the vehicle, materials will start outgassing at much higher rates. The heat soak and high temperature condition will last much longer than the reentry blackout period. Heavy outgassing can be expected to continue to below the 40,000 foot altitude level where atmospheric pressure will exceed 3.5 psi. Erosion and outgassing products will be forced into all passive vents. Active vents will normally be closed during the severe blackout period but it is doubtful that they could be left closed all the way down to the 40,000 foot altitude level. Opening them prior to this altitude would permit the heavy contaminant sheath around the vehicle to be forced into the lined experiment bay volume. Of course, contamination of the Payload at this time is not so critical because the data taking mission will have been completed and experiments can be cleaned before reuse. However, investigators may be interested in maintaining orbit condition

cleanliness of their experiments as a check point and contamination at this time would invalidate the check. This would certainly be true for contamination instruments or samples. In addition, these conditions may require unanticipated refurbishing requirements and increase payload turn around times.

The external pressure during reentry would force contaminants into cracks and crannies that are inaccessible for cleaning. From these locations, the contaminants can migrate onto more critical surfaces during subsequent missions. One solution to this problem would be to pressurize the liner volume from an onboard clean gas supply during the reentry period, at least down to the 40,000 ft. altitude level. Small instruments could be enclosed in either vacuum canisters or hermetically sealed canisters pressurized from a clean supply prior to reentry.

Some of the more contamination sensitive payloads to be carried are the ultraviolet and the cryogenically cooled infrared telescopes and the grazing incidence telescopes for XUV and X-Ray. The cryogenically cooled detectors will be especially susceptible to contaminant condensation. Ultraviolet telescopes have a much lower tolerance to contaminant deposits on optical elements than do the longer wavelength instruments. Thin layers deposited on grazing incidence optics will present a much greater effective thickness along the actual grazing path. The resultant scatter and/or adsorption could become intolerable if special precautionary measures are not taken to limit contaminant deposits.

The first steps in protecting the sensitive Payloads will be the use of a properly designed and attached experiment bay liner. In addition, properly located and operated active vents and effective cargo door seals will be important first steps towards prevention of contaminants impacting the stowed Payloads. The following additional precautionary measures are suggested:

a. the development of a purge/protective bag which can be used during ground operations to protect the Payload and will break away on Orbit upon command,

b. insure that all sensitive Payloads have aperture doors and that they provide an integral seal for the Payload during boost and reentry and can be used as on orbit protective covers to minimize compromising the Payload in the advent of an anomalous high contamination period,

c. maintain a positive purge on all sensitive Payloads during boost and reentry so that no backfilling of ingested contaminants would occur,

d. design into the stowage pallet sufficient capability to protect the apertures of sensitive Payloads,

e. carry contaminant deposition indicators and witness samples with the experiments (Deposition indicators will indicate when the environment deposition characteristics are within acceptable limits. Witness samples, located near the contamination sensitive elements and operated at the same temperature, will indicate the amount of deposition that has occurred or when tolerance limits have been reached so that the required refurbishing can be initiated.),

f. delay cooling of sensitive elements until the environment is acceptable (as indicated by deposition monitors).

5. RESULTS AND EVALUATION

5.1 General Discussion - Presented in this section is a summary of results and evaluations. The results are principally presented as summary tables indicating the induced molecular environment as a function of sources and the lines-of-sights considered. An assessment of the particulate environment and the contribution from molecular scattering is presented. An accumulative effects profile for typical missions is also presented for the molecular environment.

The evaluation of effects of the induced environment is developed through a series of susceptibility matrices. These matrices present:

a. Payload description matrix for each Payload,
b. Skylab correlation matrix,
c. summary of effects matrix,
d. an evaluation matrix.

The evaluation matrix establishes a risk factor associated with each Payload configuration evaluated based upon Woods' Hole standards, Goddard Space Flight Center Astronomy Workshop contamination requirements, and Skylab results. Comments and value judgements are established from the above criteria for classes of Payloads which represent what is considered as typical phases of operational activities.

5.2 Summary of Column Densities, Molecular Column Densities, and Returned Flux Calculations - The results of the modeling are represented by three basic parameters. These are: 1) the mass column density along a line-of-sight, 2) the corresponding molecular column density, and 3) the maximum possible return flux at representative orbital altitudes of 200 km and 435 km. These orbital altitudes were selected since they essentially encompass the majority of identified desired and minimum orbital altitudes for the sortie Payloads. For all intent and purpose, the returned flux is the most significant variable as a function of orbital altitude and can be determined for other altitudes by ratioing ambient densities with respect to those presented in this study. For those Payloads

where deposition is a concern, the returned flux is used as the basis of this calculation.

The variations for each source considered for each line-of-sight are presented in Tables VI through XI. Each source and its contribution to the lines-of-sight are discussed individually in the following sections. Table XII shows the maximum and minimum values that can be expected for combinations of sources considered. The maximum predictions include outgassing and offgassing at a beta angle of 73 degrees while the minimum predictions include outgassing at the coldest orbit temperature at a zero degree beta angle.

5.2.1 Outgassing - The surface temperatures of the Orbiter surfaces as a function of beta angle have been approximated from existing Skylab black surface temperature analysis for a solar inertial attitude. These temperatures have been used to establish the impact of beta angle on the outgassing rate. Because the Orbiter will have many different possible attitudes on orbit, an exact thermal analysis would be required to determine the surface temperatures that would apply to any one specific mission.

From Table VI, the molecular number column density from outgassing varies from 2.6×10^{11} to 6.3×10^{11} molecules/cm^2 between the lines-of-sight considered for a 73 degree beta angle maximum period. In general, lines-of-sight along +Z(1), 50 degrees off of +Z towards $\pm$Y(2), 25 degrees off of +Z towards $\pm$Y(3), and 50 degrees off of +Z towards +X(5) have lower predicted values. Lines-of-sight 45 degrees off of $\pm$Y towards -X(4), and 50 degrees off of +Z towards -X(6) have the highest values predicted for outgassing contributions.

Under the assumptions for outgassing outlined in Section 4.2.1, all lines-of-sight at all beta angles have values in excess of 10^{11} molecules/cm^2 during any one orbit. If the effective outgassing rate of 5×10^{-10} g/cm^2/second used in this study was an order of magnitude less (5×10^{-10} g/cm^2/second which is characteristic of black velvet paints and very low outgassing rates), the number column densities associated with a mass column density of 10^{-11} g/cm^2/second would still be on the order of 10^{10} molecules/cm^2. However, the use of lower outgassing adhesives (RTV 568) and incorporation of test data on the RSI tiles could decrease these values even further.

Table VI. Mass Column Density (M.C.D.) and Molecular Number Column Density (N.C.D.) Predictions

SOURCE / LINE-OF-SIGHT & BETA ANGLE		OUTGASSING (ALL POLAR MOLECULES) M.C.D. g/cm^2	N.C.D. $_2$ $mol./cm^2 sec$	OFFGASSING @ 10 Hrs. (ALL POLAR MOLECULES) M.C.D. g/cm^2	N.C.D. $_2$ $mol./cm^2 sec$	LEAKAGE M.C.D. g/cm^2	N.C.D. $_2$ $mol./cm^2 sec$
(1) 0+Z						1.0(-9)	2.2(+13)
0°	MAX	*1.4(-11)	8.8(+10)	6.1(-11)	2.0(+12)	**2.0(-11)	4.7(+11)
	MIN	8.8(-13)	5.5(+9)	3.7(-12)	1.2(+11)		
60°	MAX	3.0(-11)	1.9(+11)	1.3(-10)	4.3(+12)		
	MIN	1.6(-11)	1.0(+11)	6.6(-11)	2.2(+12)		
73°	MAX	5.8(-11)	3.6(+11)	2.5(-10)	8.3(+12)		
	MIN	4.4(-11)	2.8(+11)	1.9(-10)	6.3(+12)		
(2) 50±Y°						9.9(-10)	2.2(+13)
0°	MAX	1.0(-11)	6.3(+10)	4.3(-11)	1.4(+12)	2.0(-11)	4.7(+11)
	MIN	8.6(-13)	5.4(+9)	3.6(-12)	1.2(+11)		
60°	MAX	2.1(-11)	1.3(+11)	9.0(-11)	3.0(+12)		
	MIN	1.1(-11)	6.9(+10)	4.8(-11)	1.6(+12)		
73°	MAX	4.2(-11)	2.6(+11)	1.8(-10)	6.0(+12)		
	MIN	3.2(-11)	2.0(+11)	1.3(-10)	4.3(+12)		
(3) 25±Y°						1.1(-9)	2.3(+13)
0°	MAX	1.3(-11)	8.1(+10)	5.4(-11)	1.8(+12)	2.2(-11)	4.9(+11)
	MIN	8.9(-13)	5.6(+9)	3.8(-12)	1.3(+11)		
60°	MAX	2.6(-11)	1.6(+11)	1.1(-10)	3.7(+12)		
	MIN	1.4(-11)	8.8(+10)	5.9(-11)	2.0(+12)		
73°	MAX	5.2(-11)	3.3(+11)	2.2(-10)	7.3(+12)		
	MIN	3.9(-11)	2.4(+11)	1.7(-10)	5.7(+12)		
(4) 50±Y° 45-X						8.8(-10)	1.9(+13)
0°	MAX	1.7(-11)	1.1(+11)	7.4(-11)	2.5(+12)	1.8(-11)	4.2(+11)
	MIN	8.4(-13)	5.3(+9)	3.6(-12)	1.2(+11)		
60°	MAX	3.5(-11)	2.2(+11)	1.5(-10)	5.0(+12)		
	MIN	1.9(-11)	1.2(+11)	7.9(-11)	2.6(+12)		
73°	MAX	7.0(-11)	4.4(+11)	3.0(-10)	1.0(+13)		
	MIN	5.3(-11)	3.3(+11)	2.2(-10)	7.3(+12)		
(5) 50+X°						1.6(-9)	3.5(+13)
0°	MAX	1.3(-11)	8.1(+10)	5.4(-11)	1.8(+12)	3.2(-11)	7.5(+11)
	MIN	1.1(-12)	6.9(+9)	4.7(-12)	1.6(+11)		
60°	MAX	2.7(-11)	1.7(+11)	1.1(-10)	3.7(+12)		
	MIN	1.4(-11)	8.8(+10)	6.1(-11)	2.0(+12)		
73°	MAX	5.4(-11)	3.4(+11)	2.3(-10)	7.7(+12)		
	MIN	4.0(-11)	2.5(+11)	1.7(-10)	5.7(+12)		
(6) 50-X°						8.6(-10)	1.9(+13)
0°	MAX	2.6(-11)	1.6(+11)	1.1(-10)	3.7(+12)	1.7(-11)	1.9(+13)
	MIN	7.4(-13)	4.6(+9)	3.2(-12)	1.1(+11)		
60°	MAX	5.2(-11)	3.3(+11)	2.2(-10)	7.3(+12)		
	MIN	2.7(-11)	1.7(+11)	1.1(-10)	3.7(+12)		
73°	MAX	1.0(-10)	6.3(+11)	4.4(-10)	1.5(+13)		
	MIN	7.8(-11)	4.9(+11)	3.3(-10)	1.1(+13)		

* 10^{-11} = (-11)

**_____ = polar constituents

Table VII. Maximum Return Flux Predictions to Representative Payload

SOURCE / LINE-OF-SIGHT & BETA ANGLE		OUTGASSING (ALL POLAR MOLECULES) RETURN FLUX (MAX.) 200 Km g/cm²sec	435 Km g/cm²sec	OFFGASSING @ 10 Hrs. (ALL POLAR MOLECULES) RETURN FLUX (MAX.) 200 Km g/cm²sec	435 Km g/cm²sec	LEAKAGE RETURN FLUX (MAX.) 200 Km g/cm²sec	435 Km g/cm²sec
(1) 0+Z							
0°	MAX	0	*5.5(-12)	5.5(-11)	1.0(-12)	9.0(-10)	1.7(-11)
	MIN	0	3.4(-13)	3.3(-12)	6.3(-14)	** 1.8(-11)	3.4(-13)
60°	MAX	0	1.2(-11)	1.2(-10)	2.2(-12)		
	MIN	0	6.2(-12)	5.9(-11)	1.1(-12)		
73°	MAX	0	2.3(-11)	2.2(-10)	4.3(-12)		
	MIN	0	1.7(-11)	1.7(-10)	3.2(-12)		
(2) 50+Y						8.9(-10)	1.7(-11)
0°	MAX	0	3.9(-12)	3.9(-11)	7.3(-13)	1.8(-11)	3.4(-13)
	MIN	0	3.4(-13)	3.2(-12)	6.1(-14)		
60°	MAX	0	8.2(-12)	8.1(-11)	1.5(-12)		
	MIN	0	4.3(-12)	4.3(-11)	8.2(-13)		
73°	MAX	0	1.6(-11)	1.7(-10)	3.1(-12)		
	MIN	0	12.(-11)	1.2(-10)	2.2(-12)		
(3) 25+Y						9.9(-10)	1.9(-11)
0°	MAX	0	5.1(-12)	4.8(-11)	9.2(-13)	2.0(-11)	3.7(-13)
	MIN	0	3.5(-13)	3.4(-12)	6.5(-14)		
60°	MAX	0	1.0(-11)	9.9(-11)	1.9(-12)		
	MIN	0	5.5(-12)	5.3(-11)	1.0(-12)		
73°	MAX	0	2.0(-11)	2.4(-10)	3.7(-12)		
	MIN	0	1.5(-11)	1.5(-10)	2.9(-12)		
(4) 50+Y, 45-X						7.9(-10)	1.5(-11)
0°	MAX	0	6.6(-12)	6.6(-11)	1.3(-12)	1.6(-11)	3.1(-13)
	MIN	0	3.3(-13)	3.2(-12)	6.1(-14)		
60°	MAX	0	1.4(-11)	1.3(-10)	2.6(-12)		
	MIN	0	7.4(-12)	7.1(-11)	1.3(-12)		
73°	MAX	0	2.7(-11)	2.7(-10)	5.1(-12)		
	MIN	0	2.1(-11)	2.0(-10)	3.7(-12)		
(5) 50+X						1.4(-9)	2.7(-11)
0°	MAX	0	5.1(-12)	4.8(-11)	9.2(-13)	2.9(-11)	5.4(-13)
	MIN	0	4.3(-13)	4.2(-12)	8.0(-14)		
60°	MAX	0	1.1(-11)	9.9(-11)	1.9(-12)		
	MIN	0	5.5(-12)	5.5(-11)	1.0(-12)		
73°	MAX	0	2.1(-11)	2.1(-10)	3.9(-12)		
	MIN	0	1.6(-11)	1.5(-10)	2.9(-12)		
(6) 50-X						7.7(-10)	1.5(-11)
0°	MAX	0	1.0(-11)	9.9(-11)	1.9(-12)	1.5(-11)	2.9(-13)
	MIN	0	2.9(-13)	2.9(-12)	5.4(-14)		
60°	MAX	0	2.0(-11)	2.0(-10)	3.7(-12)		
	MIN	0	1.1(-11)	9.9(-11)	1.9(-12)		
73°	MAX	0	3.9(-11)	3.9(-10)	7.5(-12)		
	MIN	0	3.0(-11)	3.0(-10)	5.6(-12)		

* 10^{-12} = (-12)

** _____ = polar constituents

Table VIII. Mass Column Density (M.C.D.) and Molecular Number Column Density (N.C.D.) Predictions For Lines-of-Sight for Evaporators as Sources

SOURCE	EVAPORATOR 14 (ALL POLAR MOLECULES)		EVAPORATOR 15 (ALL POLAR MOLECULES)		EVAPORATOR 17 (ALL POLAR MOLECULES)	
LINE-OF-SIGHT	M.C.D. g/cm^2	N.C.D. $mol./cm^2$	M.C.D. g/cm^2	N.C.D. $mol./cm^2$	M.C.D. g/cm^2	N.C.D. $mol./cm^2$
(1) 0+Z	*1.9(-9)	6.2(+13)	2.9(-11)	9.5(+11)	9.4(-11)	3.1(+12)
(2) 50±Y	2.7(-9)	9.1(+13)	1.3(-10)	4.2(+12)	1.9(-10)	6.3(+12)
(3) 25±Y	2.9(-9)	9.7(+13)	2.9(-11)	9.7(+11)	1.2(-10)	4.0(+12)
(4) 50±Y,45-X	6.2(-9)	2.0(+14)	7.8(-11)	2.6(+12)	1.9(-10)	6.3(+12)
(5) 50+X	4.8(-10)	1.6(+13)	5.5(-12)	1.8(+11)	2.5(-11)	8.3(+11)
(6) 50-X	1.4(-9)	4.7(+13)	3.9(-11)	1.3(+12)	1.0(-10)	3.3(+12)

* $10^{-9} = (-9)$

Table IX. Maximum Return Flux Predictions to Representative Payload For Prime Evaporator Locations as Sources

SOURCE / LINE-OF-SIGHT	EVAPORATOR 14 RETURN FLUX (MAX.) 200 Km $g/cm^2 sec$	EVAPORATOR 14 RETURN FLUX (MAX.) 435 Km $g/cm^2 sec$	EVAPORATOR 15 RETURN FLUX (MAX.) 200 Km $g/cm^2 sec$	EVAPORATOR 15 RETURN FLUX (MAX.) 435 Km $g/cm^2 sec$	EVAPORATOR 17 RETURN FLUX (MAX.) 200 Km $g/cm^2 sec$	EVAPORATOR 17 RETURN FLUX (MAX.) 435 Km $g/cm^2 sec$
(1) 0±Z	*1.7(-9)	3.2(-11)	2.6(-11)	4.9(-13)	8.4(-11)	1.6(-12)
(2) 50±Y	2.4(-9)	4.6(-11)	1.2(-10)	2.2(-10)	1.7(-10)	3.2(-12)
(3) 25±Y	2.6(-9)	4.9(-11)	2.6(-11)	4.9(-13)	1.1(-10)	2.0(-12)
(4) 50±Y,45-X	5.6(-9)	1.1(-10)	7.0(-11)	1.3(-12)	1.7(-10)	3.2(-12)
(5) 50+X	4.3(-10)	8.2(-12)	4.9(-12)	9.4(-14)	2.2(-11)	4.3(-13)
(6) 50-X	1.3(-9)	2.4(-11)	3.5(-11)	6.6(-13)	9.0(-11)	1.7(-12)

* $10^{-9} = (-9)$

Table X. Mass Column Density (M.C.D.) and Molecular Number Column Density (N.C.D.) Predictions for Lines-of-Sight for RCS 25 lb Thrust Vernier Engines as Sources

SOURCE LINE-OF-SIGHT	RCS VERNIER ENGINE #3 M.C.D. g/cm^2	RCS VERNIER ENGINE #3 N.C.D. $mol./cm^2$	RCS VERNIER ENGINE #2 M.C.D. g/cm^2	RCS VERNIER ENGINE #2 N.C.D. $mol./cm^2$	RCS VERNIER ENGINE #1 M.C.D. g/cm^2	RCS VERNIER ENGINE #1 N.C.D. $mol./cm^2$
(1) 0+Z	*4.7(-9)	1.1(+14)	1.2(-8)	3.0(+14)	8.0(-11)	1.9(+12)
	** 2.6(-9)	6.9(+13)	6.8(-9)	1.9(+14)	4.4(-11)	1.2(+12)
(2) 50±Y	1.5(-8)	3.7(+14)	2.9(-8)	7.2(+14)	2.1(-10)	5.1(+12)
	8.6(-9)	2.3(+14)	1.6(-8)	4.4(+14)	1.2(-10)	3.1(+12)
(3) 25±Y	9.1(-9)	2.2(+14)	3.0(-8)	7.3(+14)	1.4(-10)	3.5(+12)
	5.1(-9)	1.4(+14)	1.7(-8)	4.5(+14)	7.9(-11)	2.1(+12)
(4) 50±Y,45-X	2.6(-8)	6.5(+14)	1.2(-8)	3.2(+14)	1.6(-10)	3.9(+12)
	1.5(-8)	4.0(+14)	6.9(-9)	2.1(+14)	9.0(-11)	2.4(+12)
(5) 50+X	9.3(-10)	2.3(+13)	6.2(-10)	1.5(+13)	1.8(-10)	4.3(+12)
	5.2(-10)	1.4(+13)	3.5(-10)	9.3(+12)	1.0(-10)	2.7(+12)
(6) 50-X	6.9(-9)	1.7(+14)	2.8(-9)	6.8(+13)	6.3(-11)	1.5(+12)
	2.8(-9)	6.8(+13)	1.6(-9)	4.1(+13)	3.5(-11)	9.4(+11)

* 10^{-9} = (-9)

** _____ = polar constituents

Table XI. Maximum Return Flux Predictions to Representative Payload For RCS 25 lb Thrust Vernier Engines as Sources

SOURCE / LINE-OF-SIGHT	VERNIER ENGINE 3 RETURN FLUX (MAX.) 200_2Km g/cm^{2}sec	VERNIER ENGINE 3 RETURN FLUX (MAX.) 435_2Km g/cm^{2}sec	VERNIER ENGINE 2 RETURN FLUX (MAX.) 200_2Km g/cm^{2}sec	VERNIER ENGINE 2 RETURN FLUX (MAX.) 435_2Km g/cm^{2}sec	VERNIER ENGINE 1 RETURN FLUX (MAX.) 200_2Km g/cm^{2}sec	VERNIER ENGINE 1 RETURN FLUX (MAX.) 435_2Km g/cm^{2}sec
(1) 0+Z	*4.2(-9)	8.0(-11)	1.1(-8)	2.0(-10)	7.2(-11)	1.4(-12)
	** 2.3(-9)	4.4(-11)	6.2(-9)	1.2(-10)	3.9(-11)	7.5(-13)
(2) 50±Y	1.4(-9)	2.6(-10)	2.6(-8)	4.9(-10)	1.9(-10)	3.6(-12)
	7.9(-9)	1.5(-10)	1.4(-8)	2.7(-10)	1.1(-10)	2.0(-12)
(3) 25±Y	7.9(-9)	1.5(-10)	2.7(-8)	5.1(-10)	1.3(-10)	2.4(-12)
	4.6(-9)	8.7(-11)	1.5(-8)	2.9(-10)	7.1(-11)	1.3(-12)
(4) 50±Y,45-X	2.3(-8)	4.4(-10)	1.1(-8)	2.0(-10)	1.4(-10)	2.7(-12)
	1.4(-8)	2.6(-10)	6.2(-9)	1.2(-10)	8.1(-11)	1.5(-12)
(5) 50+X	8.4(-10)	1.6(-11)	5.6(-10)	1.1(-11)	1.6(-10)	3.1(-12)
	4.6(-10)	8.8(-12)	3.1(-10)	6.0(-12)	9.0(-11)	1.7(-12)
(6) 50-X	6.3(-9)	1.2(-10)	2.5(-9)	4.7(-11)	5.6(-11)	1.1(-12)
	2.5(-9)	4.8(-11)	1.43(-9)	2.7(-11)	3.1(-11)	6.0(-13)

* 10^{-9} = (-9)

**_____= polar constituents

Table XII. Range of Mass Column Density (M.C.D.) and Molecular Number Column Density (N.C.D.)

SOURCE CONDITION* / LINE-OF-SIGHT	*MAX-WITH MAX VERNIER AND EVAP.		*MAX-WITH MAX EVAP. AND NO VERNIER		*MAX-WITH NO VERNIER OR EVAP.		**MIN-WITH MIN EVAP. AND MAX VERNIER		**MIN-WITH MIN EVAP. AND NO VERNIER		**MIN-WITH NO EVAP. OR VERNIER	
	M.C.D. g/cm^2	N.C.D. $mol./cm^2$	M.C.D. g/cm^2	N.C.D. $mol./cm^2$	M.C.D. g/cm^2	N.C.D. $mol./cm^2$	M.C.D. $g.cm^2$	N.C.D. $mol./cm^2$	M.C.D. g/cm^2	N.C.D. $mol./cm^2$	M.C.D. g/cm^2	N.C.D $mol./cm^2$
(1) 0	***1.5(-8)	3.9(+14)	3.2(-9)	9.3(+13)	1.3(-9)	3.1(+13)	1.3(-8)	3.2(+14)	1.0(-9)	2.3(+13)	1.0(-9)	2.2(+13)
	9.0(-9)	2.6(+14)	2.2(-9)	7.1(+13)	3.3(-10)	9.1(+12)	6.8(-9)	1.9(+14)	5.0(-11)	1.4(+12)	2.1(-11)	4.8(+11)
(2) 50+Y	3.3(-8)	8.4(+14)	3.9(-9)	1.2(+14)	1.2(-9)	2.8(+13)	3.0(-8)	7.5(+14)	1.1(-9)	2.6(+13)	9.9(-10)	2.2(+13)
	1.9(-8)	5.4(+14)	2.9(-9)	9.8(+13)	2.4(-10)	6.7(+12)	1.6(-8)	4.4(+14)	1.5(-10)	4.7(+12)	2.1(-11)	4.8(+11)
(3) 25+Y	3.4(-8)	8.6(+14)	4.3(-9)	1.3(+14)	1.4(-9)	3.1(+13)	3.1(-8)	7.5(+14)	1.1(-9)	2.4(+13)	1.1(-9)	2.3(+13)
	2.0(-8)	5.6(+14)	3.2(-9)	1.1(+14)	2.9(-10)	8.1(+12)	1.7(-8)	4.5(+14)	5.2(-11)	1.5(+12)	2.3(-11)	5.0(+11)
(4) 50+Y 45-X	3.3(-8)	8.8(+14)	7.5(-9)	2.3(+14)	1.3(-9)	2.9(+13)	2.7(-8)	6.7(+14)	9.6(-10)	2.2(+13)	8.8(-10)	1.9(+13)
	2.2(-8)	6.1(+14)	6.6(-9)	2.1(+14)	3.9(-10)	1.1(+13)	1.5(-8)	4.0(+14)	1.0(-10)	3.0(+12)	1.9(-11)	4.2(+11)
(5) 50+X	3.3(-9)	8.2(+13)	2.4(-9)	5.9(+13)	1.0(-9)	4.3(+13)	2.5(-9)	5.8(+13)	1.6(-9)	3.5(+13)	1.6(-9)	3.5(+13)
	1.3(-9)	3.9(+13)	8.0(-10)	2.5(+13)	3.2(-10)	8.8(+12)	5.6(-10)	1.5(+13)	3.9(-11)	9.4(+11)	3.3(-11)	7.6(+11)
(6) 50-X	9.7(-9)	2.5(+14)	2.8(-9)	8.2(+13)	1.4(-9)	3.5(+13)	7.8(-9)	1.9(+14)	9.0(-10)	2.0(+13)	8.6(-10)	1.9(+13)
	4.8(-9)	1.3(+14)	2.0(-9)	6.3(+13)	5.6(-10)	1.6(+13)	2.9(-9)	7.0(+13)	5.7(-11)	1.7(+12)	1.8(-11)	4.1(+11)

* Includes offgassing rate after 10 hrs. exposure, 73° beta angle, solar inertial attitude

** Includes zero degree beta angle, no offgassing

*** ——— = Polar Constituents

*** 10^{-8} = (-8)

The return flux of outgassing molecules (Table VII) at 200 km was determined to be zero. The outgassant molecules (M=100) have a mean free path at this altitude of less than a few meters and would not travel into the field-of-view when the velocity vector of the ambient is such that a return flux is possible. The mass column density numbers predicted will exist, however, when the ambient atmosphere is capable of carrying outgassing molecules along a line-of-sight away from the vehicle but will not allow a return flux contribution.

5.2.2 Offgassing - The offgassing rates of volatile surface components as a function of beta angle varies with the temperature between beta angles as does outgassing. Table VI shows the molecular column density varies between 6.0×10^{12} and 1.5×10^{13} molecules/cm^2 for a 73 degree beta angle (maximum temperature) periods for all lines-of-sight. Since offgassing is physically similar to outgassing, the lowest values are predicted for lines-of-sight (1), (2), (3), and (5) while the highest values are predicted for the (4) and (6) lines-of-sight.

Under the assumptions outlined in Section 4.2.2, all lines-of-sight at all beta angles have in excess of 10^{12} molecules/cm^2 during an orbit. As defined, offgassing is a time dependent function as shown in Figure 19. The values presented in Table VI are for the 10 hour point into a mission when typically Payload activation activities might be expected to begin. However, for all intent and purposes, offgassing will remain at approximately the 10^{12} molecule/cm^2 level for the first 50 hours.

Although the offgassing modeled with this study was based upon the Orbiter, some consideration must be eventually given to the Payload itself. Internal Payload offgassing will probably restrict early on orbit measurement activities from 3 days to possibly 10 days.

On Skylab, two ATM related anomalies could be correlated to offgassing. On DOY 134 which was SL-1 launch day, activation of the number one ATM data transmitter antenna failed. Failure was traced to the number one coaxial switch which was thought to have failed from corona. Also, it took approximately 10 days for the internal pressure within the ATM canister to reach a pressure of 10^{-5} Torr so that high voltage power supplies could be turned on.

The returned flux values presented in Table VII are maximum possible during an orbit and will only occur for that period in the orbit when the velocity vector is aligned along the representative Payload optical axis. Unlike outgassing, the average molecular weight of the volatiles in the offgassing is low (M=18) and will have sufficient mean free paths for the orbital altitudes considered to react with the ambient atmosphere and be returned.

5.2.3 Leakage - The leakage rates will be constant for any beta angle since leakage is not dependent upon the Orbiter surface temperature. The constituents of leakage are identified so that polar species can be specified. Table VI presents a summary of the mass and number column densities for the polar molecules and the total molecular constituents of the leakage.

The CO_2 and H_2O molecular number column densities are all in the 10^{11} molecules/cm^2 range for all lines-of-sight. Line-of-sight (5) has a slightly higher value because it is in the +X direction off of the +Z direction over the Orbiter cabin which makes it closer to the cabin leak source. The total leakage molecular column density is on the order of 10^{13} molecules/cm^2 for all lines-of-sight.

Table VII presents the returned flux for the leakage.

5.2.4 Evaporators - Three evaporator locations were analyzed which were considered prime locations at the time of this analysis. Referring to Figure 20 they are; evaporator 15 (X location 1519), evaporator 14 (X location 1372) and evaporator 17 (X location 1047). Other evaporator locations being considered could significantly reduce mass column densities along specific lines-of-sight.

These evaporators can contribute mass along a line-of-sight by direct flow from the vent exit or by reflections from the Orbiter wing surfaces. It has been determined that reflections from the wings of the Orbiter are the major contributing contaminant source. Table VIII presents the mass and number column densities for the 3 evaporator locations considered.

From a molecular number column density standpoint, evaporator 14 has the largest contribution, evaporator 15 the least contribution and evaporator 17 an intermediate value. However, all evaporator locations contribute significantly to the induced environment.

The significance of the wing reflection problem is evident by considering that the contribution from evaporator 17 to all lines-of-sight results solely from wing reflections.

The least contribution case is for evaporator 17 to the line-of-sight (5) which falls below 10^{12} molecules/cm^2. All other evaporators for all lines-of-sight essentially exceed 10^{12} molecules/cm^2.

Any potential separation that may exist between the experiment bay doors and the side of the vehicle can become an effective path for evaporator effluents thus adding to the column density for specific lines-of-sight. In this analysis, no space was allowed to exist between the experiment bay doors and the Orbiter body.

The returned flux for the evaporator positions considered is presented in Table IX.

5.2.5 RCS 25 lb Thrust Vernier Engines - The RCS 25 lb thrust vernier engines can contribute to the column densities for a given line-of-sight by direct forward flow, reflection off of Orbiter surfaces, and backflow. The vernier engine locations and direction of thrust are schematically shown in Figure 23. Each of the vernier engines have been identified by a number for analysis considerations.

Each engine contribution mechanism was treated separately so that the impact from each mechanism can be evaluated. The backflow is included in this study since the exact configuration (specific shadowing and location) for the vernier engines was unknown. For lines-of-sight out of the (X,Z) plane, the values presented in Table X are for an engine firing on the same side of the vehicle as the line-of-sight in question.

For an engine firing on the opposite side of the Orbiter in relation to a line-of-sight out of the (X,Z) plane, the results are shown in Table XIII.

The forward vernier engines (1) and (4) firing in the -Z direction contributes only by the backflow mechanism. If backflow capability for these engines is eliminated, these engines would pose

Table XIII. RCS 25 lb Thrust Vernier Engines on -Y Side Contributions to Lines-of-Sight on the +Y Side

VERNIER ENGINE / LINES OF SIGHTS	VERNIER ENGINE RCS (6) MASS COLUMN DENSITY g/cm^2	NUMBER COLUMN DENSITY$_2$ mol./cm^2	RETURNED FLUX AT 200 Km g/cm^2 sec	RETURNED FLUX AT 435 Km g/cm^2 sec	VERNIER ENGINE RCS (5) MASS COLUMN DENSITY g/cm^2	NUMBER COLUMN DENSITY$_2$ mol./cm^2	RETURNED FLUX AT 200 Km g/cm^2 sec	RETURNED FLUX AT 435 Km g/cm^2 sec
50°+Y; LOS 02								
WING REFLECTION	4.0(-10)*	9.8(+12)	3.6(-10)	6.8(-12)	1.5(-10)	3.7(+12)	1.3(-10)	2.6(-12)
29% H_2O	1.2(-10)	3.9(+12)	1.1(-10)	2.0(-12)	4.4(-11)	1.5(+12)	3.9(-11)	7.5(-13)
18% CO	7.2(-11)	1.6(+12)	6.5(-11)	1.2(-12)	2.7(-11)	6.0(+11)	2.4(-11)	4.6(-13)
9% CO_2	3.6(-11)	5.1(+11)	3.2(-11)	6.1(-13)	1.4(-11)	1.9(+11)	1.3(-11)	2.4(-13)
25°+Y; LOS 03								
WING REFLECTION	2.0(-9)	4.8(+13)	1.8(-9)	3.4(-11)	7.5(-10)	2.7(+13)	6.7(-10)	1.3(-11)
29% H_2O	5.8(-10)	1.9(+13)	5.2(-10)	9.9(-12)	2.2(-10)	7.3(+12)	2.0(-10)	3.7(-12)
18% CO	3.6(-10)	8.0(+12)	3.2(-10)	6.1(-12)	1.4(-10)	3.0(+12)	1.3(-10)	2.4(-12)
9% CO_2	1.8(-10)	2.6(+12)	1.6(-10)	3.1(-12)	6.8(-11)	9.6(+11)	6.1(-11)	1.2(-12)
50°+Y, 45°-X; LOS 04								
WING REFLECTION	0	0	0	0	0	0	0	0
29% H_2O	0	0	0	0	0	0	0	0
18% CO	0	0	0	0	0	0	0	0
9% CO_2	0	0	0	0	0	0	0	0

* $10^{-10} = (-10)$

no problems. If backflow does exist, the contribution to all lines-of-sight is in the 10^{12} molecules/cm^2 range.

The aft vernier engines (2), (3), (5), and (6) contribute significantly to all lines-of-sight. The backflow contribution mechanism in this case is the smallest. The wing reflection as in the evaporator case is the most significant contamination source for all lines-of-sight for these aft vernier engines. If the CO, CO_2, and H_2O content of the engine exhaust gases are considered, the molecular number column densities as shown in Table X are in excess of 10^{12} molecules/cm^2 and reach 10^{14} molecules/cm^2 for some specific lines-of-sight.

As with the evaporator, the return flux from all the 25 lb thrust vernier engines exceeds 10^{-12}g/cm^2/second as shown in Table XI.

The RCS 25 lb thrust vernier engine contribution to the lines-of-sight analyzed are by far the highest of all of the sources considered in this study. The contribution to the mass column density and the deposition potential from these engines as a result of potential continuous firing requirements represents a near steady state source of contamination. It appears that this mode of maintaining attitude control is a significant contamination source and should be analyzed in detail when engine design information and specific mission attitude requirements become known.

5.3 Particulate and Molecular Scattering Environment - The induced environment in the vicinity of the Orbiter will be comprised of those molecular mass and number column densities presented in Section 5.2 and large random particles (larger than 5 to 10μ). Each of these contaminants are capable of raising the background levels to prevent faint or dim observations. Scattering of sun light from the molecular mass column densities will mostly impact Payloads which are measuring in the spectral region from the ultraviolet through the near infrared. Particulates will emit thermal energy received from the sun, earth, and the Orbiter/Payload and can be detected by Payloads which predominantly will be measuring in the mid to far infrared spectral regions. In each of these cases, there are some exceptions (e.g. very large particles which could scatter sufficient sun light in the ultraviolet or visible to be detected while high mass column densities could emit sufficient thermal energy to be detected in the infrared).

The molecular mass column densities can be more directly controlled through limiting overboard venting, placing tighter controls on material selection, and establishing tighter design controls. In addition, on orbit constraints can be developed to control operational activities so that particular sources will not impact the performance of a Payload. However, for the most part, the particulate environment on orbit can not be controlled as directly as that of the molecular environment. Basic ground cleanliness requirements can be established to minimize or limit what can not be directly controlled for the on orbit contribution of particulate contamination.

Control of particles generated on orbit will be very difficult despite ground handling precautions. The on orbit particulate environment will consist of dust and lint trapped on the Orbiter surfaces, experiment bay area, and the Payload surfaces. These particles will slowly work their way out and move away from the Orbiter under the influence of any nearby molecular flow fields from vents or under the influence of aerodynamic drag of the ambient atmosphere. In addition, paint flakes, meteoroid impact debris, ice crystals from any overboard dumps, material disintegration, and material and lubrication abrasion from moving parts will all add to the particulate environment.

The particulate environment for the Shuttle Orbiter will be a greater impact on Shuttle Payloads than that observed from Skylab. The infrared Payloads proposed will be very sensitive to particles and the level of particulates will most likely be considerably higher than that observed on Skylab.

The major contributors to the Orbiter particulate environment over that observed during the Skylab program will be:

a. abrasion of moving parts such as the experiment bay doors, Orbiter wing flaps, and gimbaling of individual Payloads,

b. solid rocket staging motor retrorocket firing deposition on the Orbiter external surfaces as well as ingestion of particulates into the experiment bay compartments during launch,

c. use of Reaction Control Subsystem vernier engines,

d. ground control re-servicing of the Payloads,

e. deterioration of Orbiter surfaces from multiple launchings and landings,

f. general construction of the surface tiles where expansion cracks between the tiles will trap particulates (nominally 0.050 of an inch wide which could trap particles on the order of 1200 microns).

As mentioned previously, the level of particulates contributing to the induced environment of a spacecraft can not be discretely predicted since there are so many factors involved which can not be controlled. For this study, a baseline was established for particulates as that observed on Skylab. The baseline is 1.2 particles/steradian second or approximately 16 particles/second (particles larger than 10 to 25 μ microns in size). The following sections discuss the impact the particulate and molecular environment have on representative Payloads from an electromagnetic interaction with the sun, earth, and the surfaces of the Orbiter/Payloads.

5.3.1 Particulate Environment - Particles in the vicinity of the Orbiter/Payload will contribute to the experiment noise background through scattering and thermal emission (black body). The major impact from particles ($r > 10\ \mu$) will be on the infrared Payloads and will be due to thermal emission. The scattering contribution will be much smaller and spectrally selective for these Payloads.

The noise background contribution from particles due to scattering and thermal emission is shown in Figure 25 as a function of particle temperature and size. The calculations were made for a basic 1.5m f/2 telescope with an assumed detector area of $10^{-7} m^2$ (0.3x0.3mm). The near field case is shown (radiation field completely covers the detector). For this case; the noise power is independent of the distance from the telescope to the particle, directly proportional to the detector area, and inversely proportional to the square of the telescope focal length. The near field

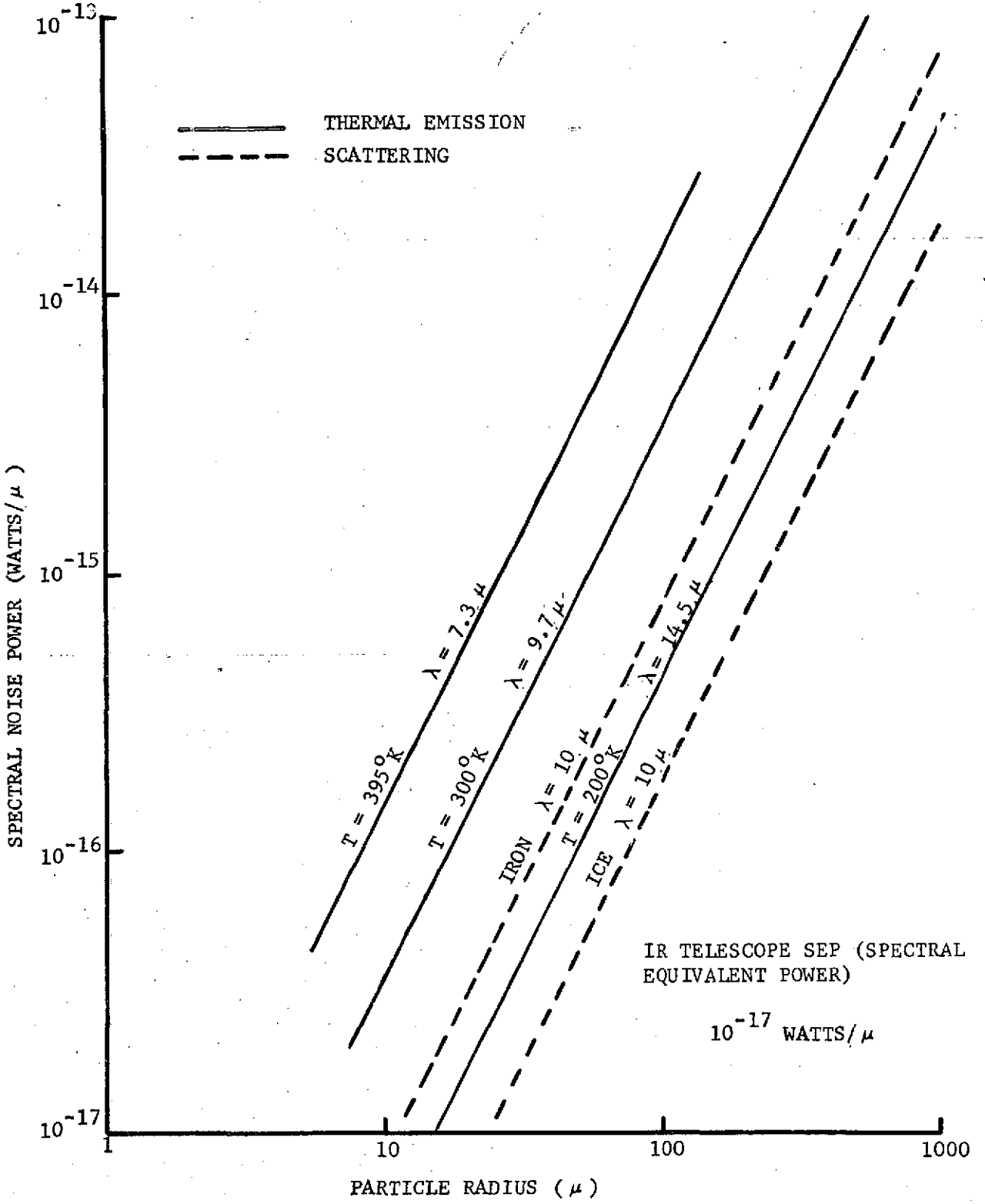

Figure 25. Particle Noise as a Function of Particle Radius and Temperature

analysis is valid for particles closer than approximately 15 km for the telescope described above. The near field boundary distance varies directly with the telescope focal length. It is recognized that typical Cassegrain systems have focal ratios between f/10 and f/20 and the values shown must be modified for specific systems as indicated above.

The NEP for the 1.5m infrared telescope was assumed to be 10^{-16} watts/$Hz^{\frac{1}{2}}$-10 μ or 10^{-17} watts/$Hz^{\frac{1}{2}}$-μ. Figure 25 shows that for the conditions stated particles with $r \geq 10\ \mu$ will potentially significantly contribute to the noise background of the infrared Payloads (whether they are paint flakes at 395°K warmed by the sun, at 300°K warmed by the earth or by the near vicinity of the Orbiter/ Payload, or an ice particle sublimating at 200°K). Also shown are the scattering influence from an iron particle and an ice particle which represent a wide range of influence from dielectric scatterers.

Skylab data indicated a particle sloughing rate of 16 particles/ second with $r > 25\ \mu$. It is expected that the Orbiter sloughing rate will be at least as high. The field-of-view of the infrared telescope was also assumed to be on the order of 0.5°. Therefore, on the average, a particle will appear in the infrared telescope field-of-view every 3.6 hours.

The dwell time of a particle in the field-of-view is a function of the particle trajectory, velocity, size, particle geometry, and orbital altitude. Figure 26 shows typical expected dwell times for 10 and 100 μ particles at 400 km altitude for a trajectory perpendicular to the optical axis of the telescope (cross axis) and at a 45 degree inclination to the optical axis. Figure 25 shows that the noise from a 100 μ particle is two orders of magnitude greater than a 10 μ particle. The 10 μ particle in itself approaches the NEP of the telescope. The response of the telescope as a function of field angle is a complex function which was approximated by a trapezoidal function and the flat portion corresponds to full particle noise input with the noise input decreasing in the wings. The 10 μ particle will approach the telescope NEP only on the flat portion of the function. The 100 μ particle will exceed the NEP across almost the entire angular response function. Therefore, the effective telescope field-of-view, and consequently the particle

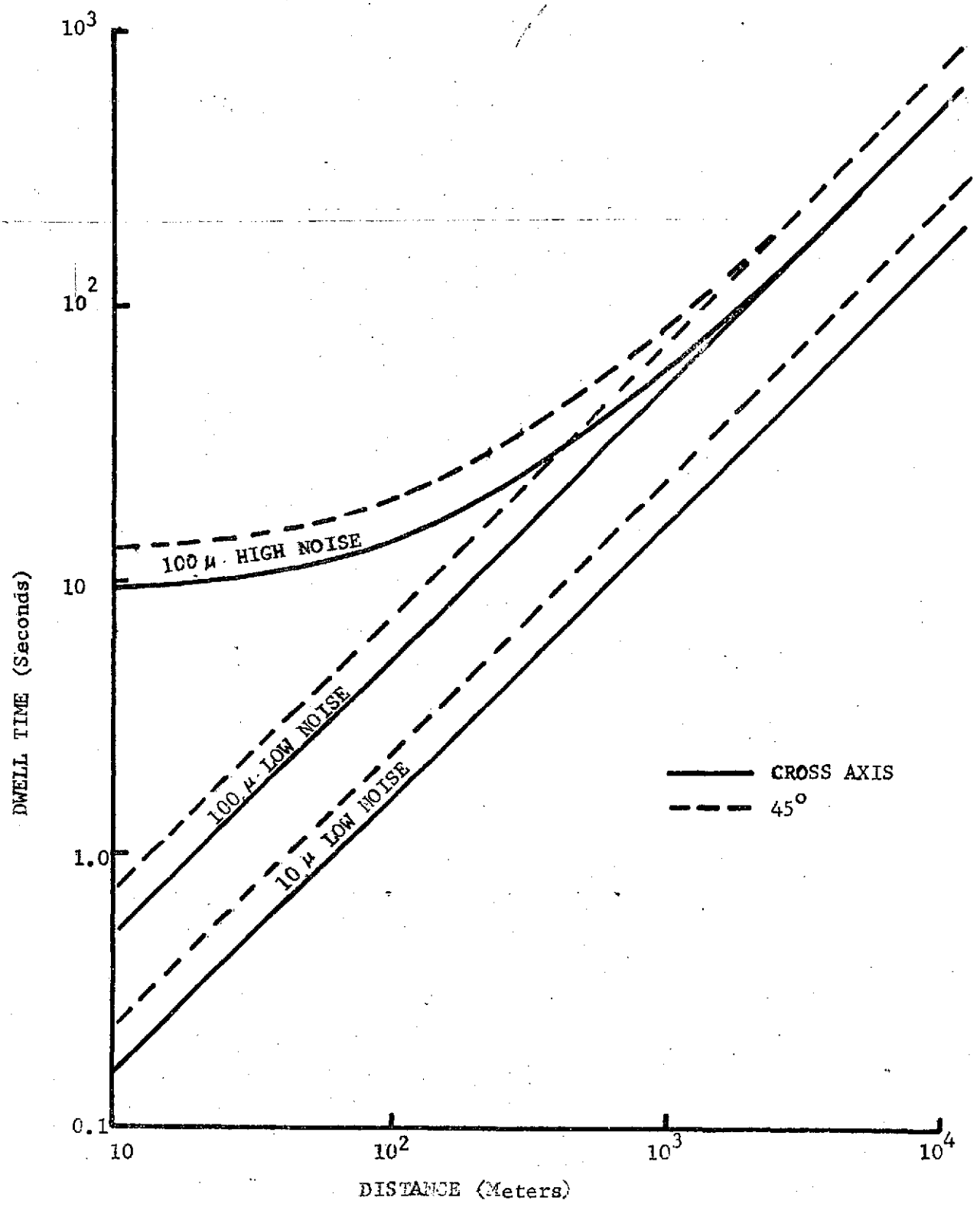

Figure 26. Particle Dwell Time vs Distance From Telescope For Flat Particles at 400 km

dwell time, will be greater for the 100 μ particle (assuming similar particle temperatures). This effect is shown in Figure 26.

Since the particle dwell time is also a function of particle velocity and the velocity is a function of the acceleration primarily due to atmospheric drag, the dwell time depends on the orbital altitude and is a function of the atmospheric density. Figure 27 shows the variations in particle acceleration as a function of atmospheric density for spherical and flat particles. Figure 28 shows the variation in atmospheric density as a function of orbital altitude for high, low, and average density conditions. At a nominal altitude of 400 km, the density can vary over two orders of magnitude depending on solar activity and orbital location (day/night). The curves in Figure 26 were developed for the 400 km average condition. If the low density case was assumed, the dwell times would increase by a factor of 30. If the altitude is increased to 700 km, the dwell times would increase by a factor of 40. Of course, lowering the altitude would decrease the dwell time.

The susceptibility of ultraviolet systems to thermal radiation from individual particles is negligible. The back scattered solar ultraviolet radiation from particles is also very small being equivalent to greater than 30th magnitude ultraviolet stars for optimum scattering sized particles ($r \sim \lambda$) at distances of 100 to 1000 meters. The scattering from individual particles in the visible region is equivalent to greater than 30th magnitude stars which can be seen by typical visible instrumented Payloads.

For individual particles from the ultraviolet through the visible, these particles will not affect specific data and will appear either momentary or transitory in the data. If the number of particles significantly increase, then a total scattering background could develop creating a signal condition which could affect the Payload in question. The level of particles at which this could occur is considered improbable unless there is a mission anomaly such as a major leak. Therefore, in the ultraviolet and the visible region, random particles are not considered a significant problem.

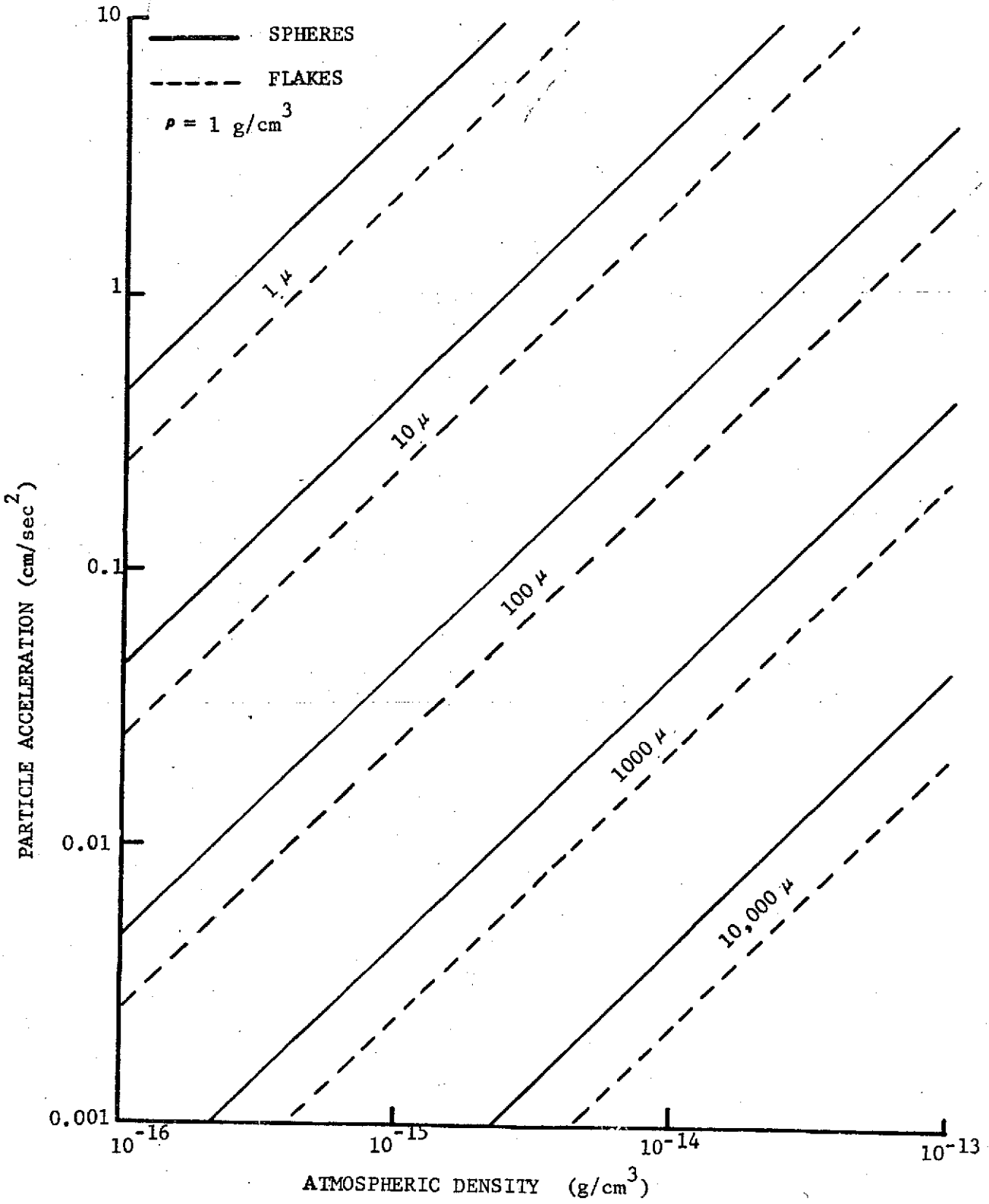

Figure 27. Particle Acceleration as a Function of Atmospheric Density and Particle Size

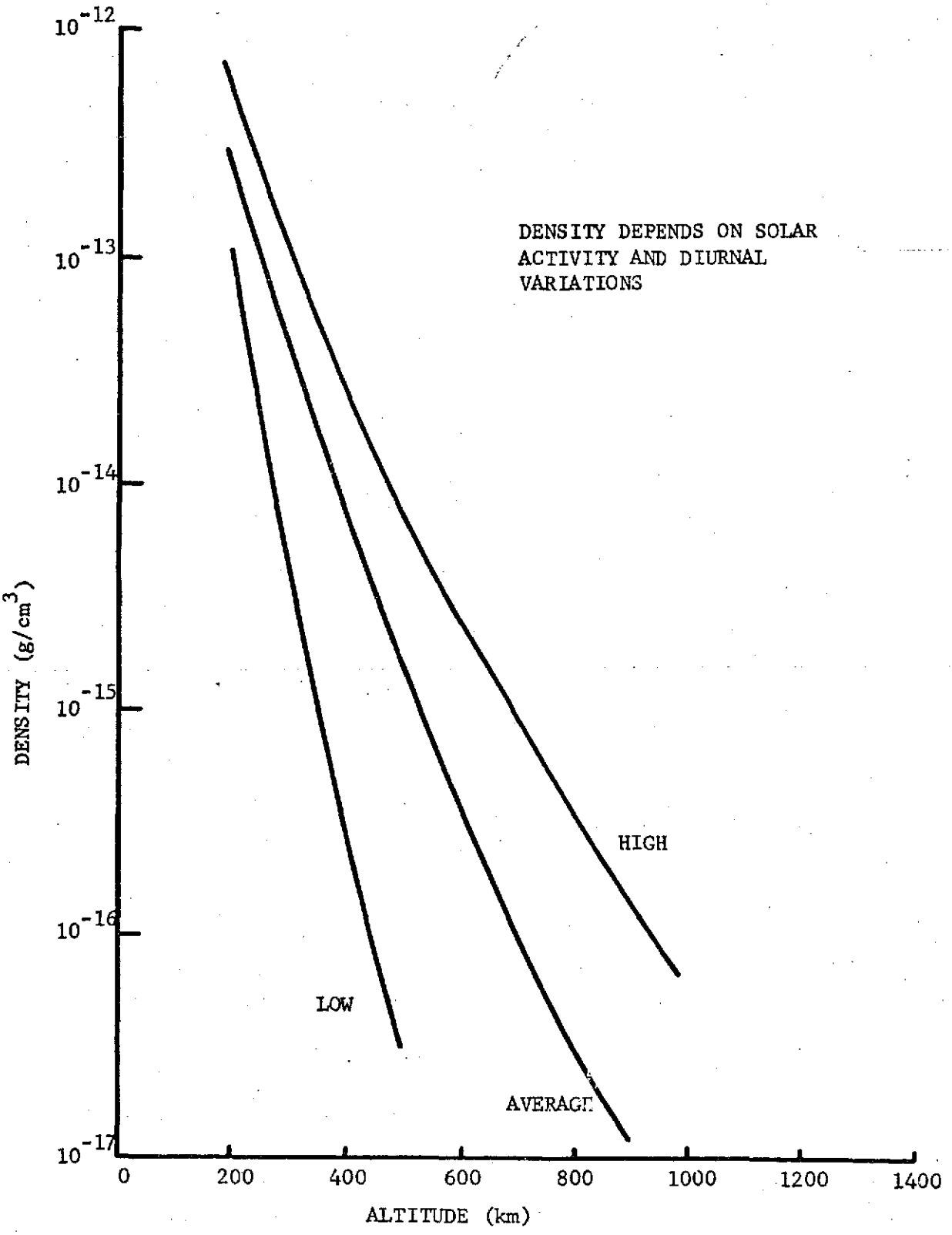

Figure 28. Ambient Atmosphere Density as a Function of Altitude

For Star Tracker systems, a technique similar to that used for Skylab will be required where the brightness of targeting stars should be considerably above the anticipated particulate brightnesses and Star Tracker updating frequency and duration be minimized to keep the probability of acquiring a false star very small.

5.3.2 Molecular Cloud Effects - The molecular cloud surrounding the Orbiter may result in experiment signal degradation from absorption and scattering. Molecular column densities presented in Section 5.2 ranged between 10^9 and 10^{13} molecules/cm^2 for the majority of sources and approximately 10^{15} molecules/cm^2 for the RCS 25 lb thrust vernier engines.

The baseline telescopes used for calculating image plane irradiance for the infrared Payloads and high resolution ultraviolet Payloads were respectively 1.5 and 1.0 meter f/20 system with a 0.5^o field-of-view. For the ultraviolet survey Payloads, a 0.75 meter f/2 system was assumed with a 5^o field-of-view.

Rayleigh theory was used to calculate the molecular scattering and a parametric analysis was performed using the following variables:

a. molecular diameters 3Å to 30Å,
b. spectral range 1000Å to 10μ,
c. column density 10^9-10^{13} molecules/cm^2,
d. low and high extremes for refractive indices simulating clear and opaque materials.

Worst case (peak) scattering occurred for large highly absorbing particles for large column densities.

In the ultraviolet region (1000 to 3000Å) for the majority of sources (column density 10^{13} molecules/cm^2), the focal plane irradiance, assuming no transmission losses, ranged between 6×10^{-14} to 4×10^{-12} watts/cm^2-μ for the high resolution 1 meter system and 6×10^{-12} to 4×10^{-10} watts/cm^2-μ for survey systems. For diffraction limited systems this corresponds to ultraviolet stars with magnitudes between 25 to 30. For non-diffraction limited systems (1 arc second blur corresponding to GSFC criteria), the noise equivalent magnitudes fall between 20 to 25.

For the RCS engine column density of 10^{15} molecules/cm^2 irradiances of $4x10^{-10}$ to $6x10^{-12}$ watts/cm^2-μ were determined for the high resolution/meter system and $6x10^{-10}$ to $4x10^{-8}$ watts/cm^2-μ for the survey system. This corresponds to ultraviolet stars with magnitudes between 20 to 25. For non-diffraction limited systems (1 arc second) the equivalent magnitudes are between 15 to 20.

Therefore, column densities of 10^{13} molecules/cm^2 are marginal when compared to the GSFC criteria (M_{uv} >20), and column densities of 10^{15} molecules/cm^2 cause a background noise which exceeds the criteria.

In the infrared region (1 to 10μ), the typical major source column density focal plane irradiance ranged between $1x10^{-13}$ to $1x10^{-7}$ watts/cm^2-μ. For an assumed 0.3x0.3mm detector, this corresponds to a noise input power of $1x10^{-20}$ to $1x10^{-14}$ watts/μ. This range exceeds the expected NEP of the 1.5 meter infrared Payload ($\sim 10^{-16}$ watts/$Hz^{\frac{1}{2}}$/μ for $\Delta\lambda/\lambda$ =0.5).

For the RCS 25 lb thrust vernier engine column density conditions, the focal plane irradiance is between $1x10^{-11}$ and $1x10^{-5}$ watts/cm^2/μ. This corresponds to $1x10^{-18}$ to $1x10^{-12}$ watts/μ for an assumed 0.3x0.3mm detector. This range also exceeds the expected NEP of the 1.5 meter infrared Payload.

Therefore, infrared scattering in the 1μ to 10μ range will impact the infrared systems in the shorter wavelengths.

Broadband absorption was investigated for a column density of 10^{15} molecules/cm^2 (maximum possible from the RCS 25 lb thrusters) for selective wavelengths between 0.1μ and 70μ. The absorption was evaluated at 0.15μ (for O_2) and at 6.3μ and at 70μ (for H_2O). For all wavelengths the transmission was > 99.9%.

5.4 Accumulative Effects - Typical Mission - The exact alignment of a Payload axis with the orbital plane and exposure times are required before accurate predictions of accumulative effects are possible. However, assumptions can be made so that accumulative effects can be ascertained for several realistic mission profiles.

Two cases are analyzed with the thought in mind that actual predictions for mission profiles other than these can vary both above and below either of these two cases.

5.4.1 Case 1 - Deep Space Payloads - Several assumptions are made and the validity of the results apply only to this specific case. These are: 1) the payload axis is such that the Z axis is in the orbital plane (Z-IOP) and 2) the vehicle (X,Z) plane is in the orbital plane (X-Z-IOP). Referring to Figure 29, the exposure time is assumed to exist midway between orbital noon and sunset and continue until midway between orbital midnight and sunrise.

A solar inertial type attitude was assumed so that the change in velocity vector orientation can be determined with respect to the Payload Z axis. For this analysis, a line-of-sight (1) along the vehicle +Z axis was assumed.

In this orientation, outgassing rates and offgassing rates are at their lowest since the Payload is on the coldest side of the vehicle. Outgassing and offgassing (at 10 hours) column densities for the minimum period in a zero beta angle configuration in Table VI were used.

The velocity vector angle change was calculated on the basis of a 4 degree per minute change for a 90 minute orbital period. The maximum evaporator contribution for the zero (1) line-of-sight was used for 60% of the time. The RCS 25 lb thrust vernier engine profile was based upon firing every 15 seconds at which time it would fire for a 0.070 seconds duration (nominal firing time pulse).

The results of this mission profile are shown in Table XIV. For 60% of the time, the molecular number column density will be 6.2×10^{13} molecules/cm^2 and every 15 seconds will be 1.9×10^{14} molecules cm^2/second. These values are for polar molecules. The return flux accumulation predicted is separated into polar and total impingement for 200 and 435 km orbital altitudes. The return flux values are based on a 53 degree view angle encompassing the representative Payload surface. The actual amount of return

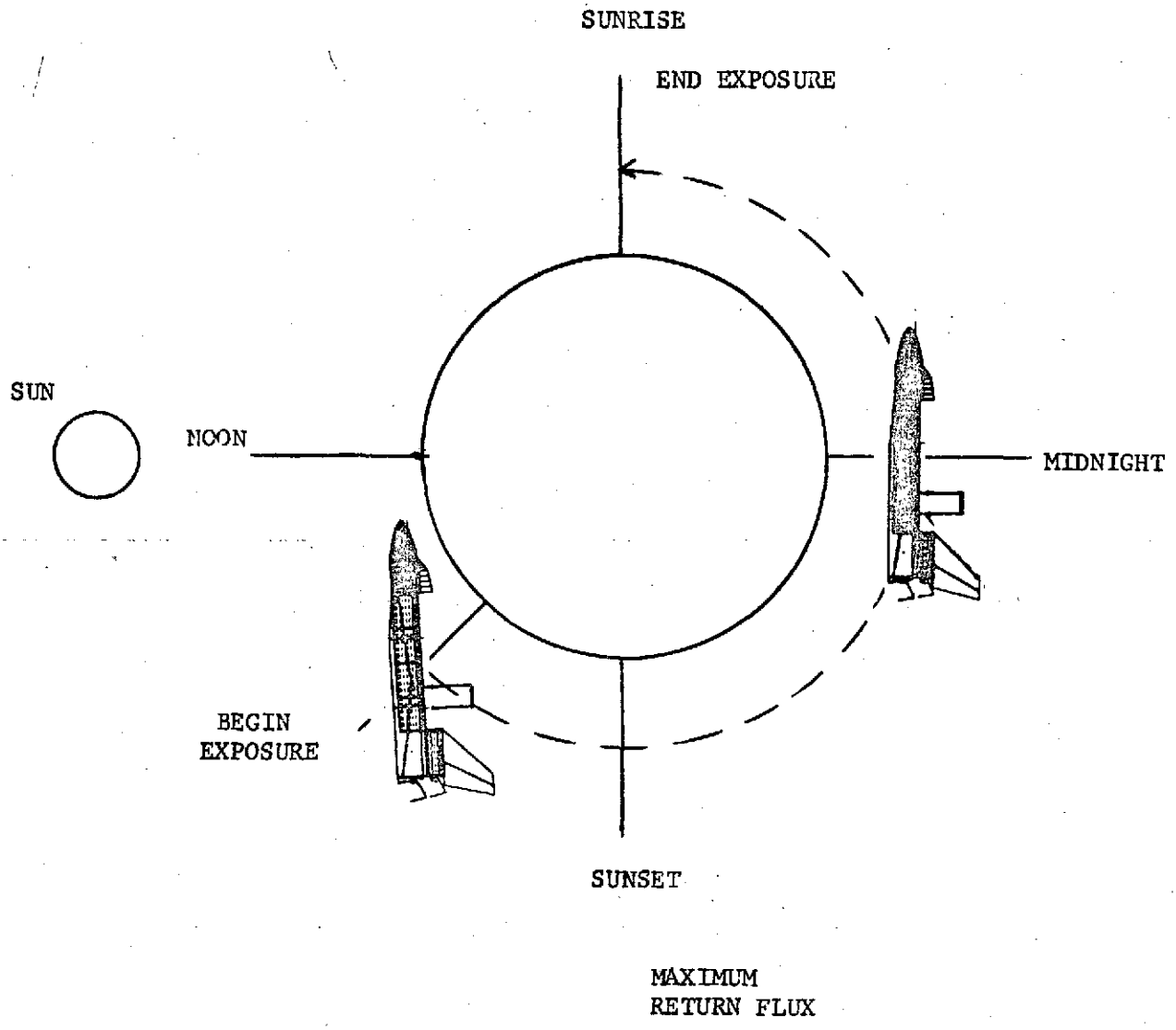

Figure 29. Orbiter Attitude for Deep Space Missions

Table XIV. Return Flux on Representative Payload Configuration Surface for a 53 Degree Field-of-View for Mission Profile in Figure 29

MISSION DURATIONS		ACCUMULATIVE RETURN FLUX (g/cm^2)	
		POLAR MOLECULES	TOTAL MOLECULES
435 Km	per orbit	3.2(-8)	5.8(-8)
	one day	5.1(-7)	9.3(-7)
	7 days	3.6(-6)	6.5(-6)
	14 days	7.1(-6)	1.3(-5)
	30 days	1.5(-5)	2.8(-5)
200 Km	per orbit	1.7(-6)	3.1(-6)
	one day	2.7(-5)	5.0(-5)
	7 days	1.9(-4)	3.5(-4)
	14 days	3.8(-4)	7.0(-4)
	30 days	8.1(-4)	1.5(-3)

Molecular Number Column Density

1) 60% of exposure time = 6.2×10^{13} polar molecule/cm^2

2) Every 15 seconds of exposure time = 1.9×10^{14} polar molecule/cm^2

flux reaching the experiment surfaces will depend strongly on the physical configuration. The return flux values presented here correspond to the bottom of a telescope tube 2.5 meters in diameter and 5 meters in length (Figure 16). This surface represents a primary mirror for a Cassegrain system. For other configurations, the return flux values will vary considerably, and may be acceptable for telescopes which have higher effective f numbers.

The total return flux values can be assumed to be the deposition values for a cryogenically cooled system since all contaminant molecules should deposit at the planned cryogenic temperatures.

5.4.2 Case 2 - Solar Experiment Payloads - For this case, the Payload +Z axis was assumed to be in the orbital plane (Z-IOP) and the vehicle (X,Z) plane in the orbital plane (X-Z-IOP). Referring to Figure 30, the exposure times were assumed to be from midway between orbital midnight and sunrise to orbital sunset. A solar inertial attitude was assumed and a line-of-sight (1) along the vehicle +Z axis was assumed as in Case 1.

In this orientation, outgassing rates and offgassing rates will be at their highest values since the Payload is on the warm side of the vehicle. Outgassing and offgassing (at 10 hours) number column densities for the maximum period in a 60 degree beta angle configuration in Table VI were used.

As for the previous case, the maximum evaporator contribution for the zero (1) line-of-sight was used. Maximum RCS 25 lb thrust vernier engines fluxes for every 15 seconds for a 0.070 second duration were also assumed.

The results of this mission profile are shown in Table XV. For 60% of the time, the total molecular column density is 8.9×10^{13} molecules/cm^2 and every 15 seconds it jumps to 3.3×10^{14} molecules/cm^2. The total number of molecules is presented rather than polar molecules since most solar type experiments are not necessarily susceptible to only polar molecules.

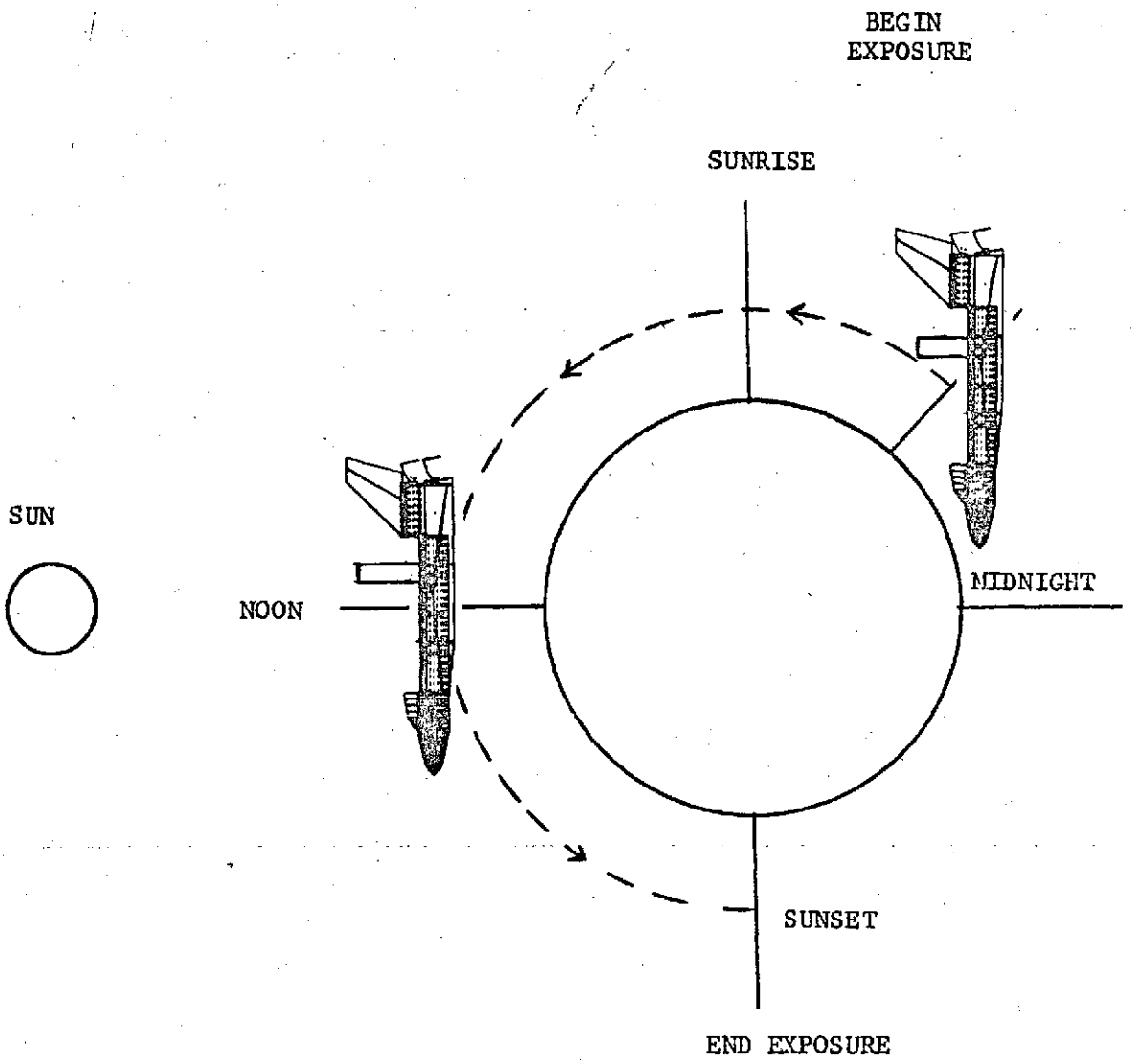

Figure 30. Orbiter Attitude for Solar Missions

Table XV. Return Flux on Representative Payload Configuration Surface for a 53 Degree Field-of-View for Mission Profile in Figure 30

MISSION DURATION		ACCUMULATIVE RETURN FLUX (g/cm^2)	
		POLAR MOLECULES	TOTAL MOLECULES
435 Km	per orbit	5.3(-8)	1.3(-7)
	one day	8.5(-7)	2.1(-6)
	7 days	5.9(-6)	1.5(-5)
	14 days	1.2(-5)	2.9(-5)
	30 days	2.5(-5)	6.2(-5)
200 Km	per orbit	1.8(-6)	5.8(-6)
	one day	2.9(-5)	9.3(-5)
	7 days	2.0(-4)	6.5(-4)
	14 days	4.0(-4)	1.3(-3)
	30 days	8.6(-4)	2.8(-3)

Molecular Number Column Density ($molecules/cm^2$)

1) 60% of exposure time = 6.7×10^{13} polar
   60% of exposure time = 8.9×10^{13} total

2) Every 15 seconds exposure time = 1.9×10^{14} polar
   Every 15 seconds exposure time = 3.3×10^{14} total

The return flux accumulation prediction is slightly higher than for Case 1 since the vehicle surfaces are warmer. However, not all of this material will deposit on solar experiments because of the relatively warm temperatures that will not allow adsorbtion of most simple gases.

Payload geometry will dictate the actual flux on a sensitive surface. The representative Payload surface modeled here corresponds to that shown in Figure 16.

5.5 Payload Susceptibilities - Payload susceptibility to contamination was developed from information presented in the Technical Letter ASD-PD-18743 identified in Applicable Documents, results from the Goddard Space Flight Center Astronomy Workshop criteria, comparison with similar experiment results gained from the Skylab Program, and from the definition of the induced environment as developed from this study. Although specific data is not available in many cases and the Woods' Hole standards are not applicable for all Payloads, the various category Payloads can be grouped and classified in general to specific affects of contamination.

The following sections present the susceptibility review developed for this study.

5.5.1 Identification of Payload Sensitive Experiments/Surfaces - Based upon the Technical Letter ASD-PD-18743, eleven Payload sensitive experiment/surfaces matrices were developed. These matrices address each of the eleven identified Payloads presented in the above Technical Letter and identifies the various instruments or experiments, location, contamination sensitivity, identification of sensitive element, and measurement objective/function of each experiment or experiment or critical surface. Tables XVI through XXVI present these matrices.

5.5.2 Correlation with Skylab Experiments - The eleven Payloads were treated as a class of Payloads (e.g. infrared, solar, ultraviolet, etc.) and were compared to similar Skylab experiments. The categorizing was based upon similar spectral range of operation.

Table XVI. Payload AS-01-S 1.5m Cryogenically Cooled IR Telescope

Instrument	Location	Contamination Sensitivity	Description	Measurement Objective/Function
1.5m IR Telescope	STA 951 (external)	Optics susceptible to particulates >20 μ m and vacuum condensible materials (VCM). No hot objects within 2π sterad of aperture unless covered by sunshade.	f/2 cryo cooled, 10 to 1000 μ. Internal temp ≈ 20°K.	Focuses 8.7 E-3 (0.5°) field on cassegrain image plane.
Broadband IR Filter Photometer	STA 951 (in telescope - external)	Optics susceptible to particulates >20 μ m.	Solid state, LHe cooled detector	Selected broadband photometry in 10 to 1000 μ range.
IR Photoconductor Array	STA 951	Optics susceptible to particulates >20 μ m and VCM.	LHe cooled, doped Ge detector array	Measures flux distribution with high NEP and spatial resolution in 5 to 100 μ region.
Fourier Interferometer-Spectrometer	STA 951 (in telescope - external)	Optics susceptible to particulates >20 μ m and VCM.	LHe cooled Interferometer	Line profiles and position with medium resolution (0.1/cm, 25 to 1000 μ).
Polarimeter	STA 951 (in telescope - external)	Optics susceptible to particulates >20 μ m and VCM.	LHe cooled polarization detectors	Measures amount of linear and circular polarization and angle.
Grating Spectrometer	STA 951 (in telescope - external)	Optics susceptible to VCM, possibly to particulates.	Multichannel detector LHe cooled	Moderate dispersion, intermediate band IR spectrophotometry, 50 to 100 μ.
Spectrophotometer	STA 951 (in telescope - external)	Optics susceptible to VCM, possibly to particulates.	24 channel, LHe cooled	Moderate dispersion spectrophotometer in the 10 to 50 μ band.
Instrument Selector Mechanisms	STA 951 (in telescope - external)	May be susceptible to VCM.	LHe cooled	
Aspect and Guide Star Tracker Optics and Sensors	STA 951 (outside telescope)	Sensitive to scattering from particles >1 μm; possibly to scattering from molecules.	0.3m Aspect Telescope & Star Guide Trackers	Provide error signals to gimbals with 0.485 E-6 rad (0.1 arc sec resolution).
Optional Equipment:				
Fine Pointed Gimbal/ Mount	STA 951 (external)	May be susceptible to particulates and VCM.		

Table XVII. Payload AS-03-S Deep Sky UV Survey Telescope

Instrument	Location	Contamination Sensitivity	Description	Measurement Objective/Function
(3) - 0.75m UV Survey Telescopes	STA 1246 (external)	Very sensitive to scattering from atoms and molecules around spacecraft and to material of any size deposited on optical surfaces.	Folded all reflective Schmidt f/2 $\bar{\omega}$ .087 rad. ($5^{o} \times 5^{o}$) field.	Direct imaging (M< 21) @ 210 nm, spectral surveys @ 0.1 nm resolution (M< 9) and 10 nm resolution (M< 15).
Camera/or Image Intensifier Camera	STA 1246 (external in telescope or airlock)	Very sensitive to scattering from atoms and molecules around spacecraft.	Reflective UV film camera/or electronographic camera.	Record images on UV sensitive film, wide field, high resolution images in reasonable exposure time.
Film Magazine	STA 1246 (added to objective grating)	Sensitive to radiation if not shielded; sensitivity depends on type of film.		
Objective Grating	STA 1246 (external - in telescope)	Susceptible to particles deposited on surface.		
Widefield Aspect Monitor & Tracker	STA 1246 (external)	Sensitive to scattering from particles > 1 μ m; possibly to scattering from molecules.	Wide angle camera	Aspect measurement for guide star identification and tracker error signals.
Optional Equipment:				
Fine Point, High Stability Gimbals	STA 1246 (external)	May be susceptible to particulates and VCM.		

Table XVIII. Payload AS-04-S 1m UV Diffraction Limited Telescope

Instrument	Location	Contamination Sensitivity	Description	Measurement Objective/Function
1m UV Telescope	STA 1246 (external)	Sensitive to scattering from atoms and molecules around spacecraft and to material of any size deposited on optical surfaces.	R.C f/16 Cassegrain 0.5° Field	Focuses diffraction limited image in 0.09 to 0.7 μ region into focal plane.
Guidestar Trackers	STA 1246 (included in telescope)	Sensitive to scattering from particles > 1 μ m; possibly to scattering from molecules.	Two star capability, 0.015 arc sec. angular	Provide error signals for gimbal control and adjustment for secondary focus.
Imaging Spectrograph	Sta 1246	Sensitive to scattering from particles and molecules around spacecraft.	Reflecting slit Spectrograph	Multiple range spectroscopy in 0.11 to 0.7 μ region with lambda/delta lambda ($\lambda/\Delta\lambda$) = 10,000.
Echelle Spectrograph	STA 1246	Sensitive to scattering from particles and molecules around spacecraft.	All reflecting Echelle $\tilde{w}/2$ gratings and 3 mirrors	High dispersion spectroscopy in region of 0.12 to 0.7 μ , 3 ranges, $\lambda/\Delta\lambda$ = 100,000.
Lyman Spectrograph	STA 1246	Sensitive to scattering from atoms and molecules around spacecraft, especially for observations of nebulous sources	Concave grating, mult. detector in row. cir. $\tilde{w}$/slit.	Moderate dispersion spectroscopy $\lambda/\Delta\lambda$ = 10,000 in Lyman Series 0.09 to 0.12 μ .
f/30 Film Camera	STA 1246	Sensitive to scattering from molecules and particles around spacecraft. Film is sensitive to radiation unless shielded.	40 mm film, remote control film advance, interference filters.	High resolution image recording, 9.17 E-7 rad (0.2 arc sec) in selected spectral bands.
Electronographic Image Converter	STA 1246	Used with film camera or field monitor; optical sensitivity will be same as the instrument with which it is used.	Electron optics & film cameras.	Achieve reasonable exposure times for faint sources.

Table XIX. Payload AS-20-S 2.5m Cryogenically Cooled IR Telescope

Instrument	Location	Contamination Sensitivity	Description	Measurement Objective/Function
2.5m IR Telescope	STA 951 (external)	Optics susceptible to particulates $>20\mu$ m and vacuum condensible materials (VCM). No hot objects within 2π sterad of aperture unless covered by sunshade.	f/2 cryo cooled, 10 to 1000 μ . Internal Temp $\approx 20^{o}$K.	Focuses 8.7 E-3 (0.5^{o}) field on Cassegrain image plane.
Broadband IR Filter Photometer	STA 951 (in telescope - external)	Optics susceptible to particulates $>20\mu$ m.	Solid State, LHe cooled detector	Selected broadband photometry in 10 to 1000μ range.
IR Photoconductor Array	STA 951	Optics susceptible to particulates $>20\mu$ m and VCM.	LHe cooled, doped Ge detector array	Measures flux distribution with high NEP and spatial resolution in 5 to 100μ region.
Fourier Interferometer - Spectrometer	STA 951 (in telescope - external)	Optics susceptible to particulates $>20\mu$ m and VCM.	LHe cooled, interferometer	Line profiles and position with medium resolution (0.1/cm, 25 to 1000μ)
Polarimeter	STA 951 (in telescope - external)	Optics susceptible to particulates $>20\mu$ m and VCM.	LHe cooled, Polarization Detectors	Measures amount of linear and circular polarization and angle.
Grating Spectrometer	STA 951 (in telescope - external)	Optics susceptible to VCM, possibly to particulates.	LHe cooled, Multichannel detector	Moderate dispersion, intermediate band IR Spectrophotometry, 50 to 100μ .
Spectrophotometer	STA 951 (in telescope - external)	Optics susceptible to VCM, possibly to particulates.	LHe cooled, 24 channel	Moderate dispersion spectrophotometer in the 10 to 50μ band.
Instrument Selector Mechanisms	STA 951 (in telescope - external)	May be susceptible to VCM.	LHe cooled.	
Aspect and Guide Star Tracker Optics and Sensors	STA 951 (outside telescope)	Sensitive to scattering from particles $>1\mu$m; possibly to scattering from molecules.	0.5m Aspect Telescope, TV field monitor, & guide star trackers	Provide error signals to gimbals with 0.485 E-6 rad (0.1 arc sec) resolution.
Optional Equipment:				
Fine Pointed Gimbal/ Mount	STA 951 (external)	May be susceptible to particulates and VCM.		

Table XX . Payload SO-01-5 Dedicated Solar Sortie Mission

Instrument	Location	Contamination Sensitivity	Description	Measurement Objective/Function
Externally Occulted Coronagraph	STA 1037 (external)	Very sensitive to scattering from molecules or particles in vicinity of spacecraft. Sensitive to material deposited on optical surfaces. Film sensitive to radiation.	Images corona by occulting solar disk.	Observe coronal brightness 2000 - 7000 Å; 1.5 to 6 solar radii.
100-cm Photoheliograph	STA 936 (external)	Sensitive to scattering from molecules or particles in vicinity of spacecraft. Sensitive to material deposited on optical surfaces. Film sensitive to radiation.	Telescope with spectrograph.	High spatial & spectral resolution images of sun.
Soft X-Ray Spectrometer/ Spectroheliograph	STA 1159 (external)	Susceptible to scattering from small particulates in range 0.01 μ m and larger.	Ods collimators, grazing telescope, flat crystals	Coronal maps and line profiles, 0.5 - 25 Å.
Grid Collimator Acquisition Photometer	STA 1127 (external)	Susceptible to scattering from small particulates and condensates in range of 0.01 μ m and larger.	2 aligned grids Photon counters	Locate flare to 2 arc sec in 10 - 30 sec.
Solar Gamma Ray Detector	STA 1190	May be sensitive to particulates and condensates, with reduced sensitivity due to scattering.	Spark Chamber	Decay Gamma Rays from flare pions.
Bragg Reflection Polarimeter	STA 1239 (external)	Susceptible to scattering from small particulates and condensates of sizes $\geq$0.01 μ m; condensate crystal lattices act as unwanted grating for Bragg reflections.	Crystal Reflector, Photon counter	Polarization of soft X-rays from flares 1 - 10 Kev.

Table XXI. Payload CN-01-S Communications/Navigation Sortie Mission

Instrument	Location	Contamination Sensitivity	Description	Measurement Objective/Function
Note: Experiments located inside Sortie Lab are not tabulated.				
Optical Antenna	STA 1208	Possible sensitivity, depending on design.	30-meter Parabolic Antenna	Determine the structural, thermal and electromagnetic performance of a 30 meter antenna reflector in space.
Gas Analyzer	STA 1292	Sensitivity to gases and perhaps to particles is expected; exact values are not known.		
STARS Platform and Sensor System	STA 1152	Susceptible to scattering from molecules and particulates in vicinity of spacecraft (particle sizes $\leq 100\mu$). Sensitive to material deposited on optical surfaces.	Stellar Tracking Attitude Reference System	Evaluate the precision of star trackers.
PADS Sensor System	STA 1208	Sensitivity will depend on design; at worst, will be same as for STARS system.	Precision Attitude Determination System	Evaluate the precision of the rate gyro systems.
Optical instruments located inside will be susceptible to scattering from molecules and particles in vicinity of spacecraft.				

Table XXII. Payload AP-01-A Upper Atmosphere Explorer

Instrument	Location	Contamination Sensitivity	Description	Measurement Objective/Function
Electron Analyzer	STA 1210	Specific design may impose contamination limits. Inside spacecraft.	Solid State of Channeltron	Measure electronic current present.
Current Collector/ Analyzer	STA 1210	See above.	Gridded Faraday Cup	Measure electric ion current present.
Ion Spectrometer	STA 1210	May detect charged contaminants.		Analyze ambient ion mass species.
VLF Receiver plus Antenna	STA 1210	Specific design may impose contamination limits.	Low Noise Model	Pick up VLF radio waves present.
Mass Spectrometer	STA 1210	Require contaminant gas pressure less than 10^{-6} atm; no organic molecules are permissible.	Calibrated for H, He, O	Analyze ambient atmosphere mass species.
UV Detector	STA 1210	May be susceptible to particulate contaminant down to 0.1 micrometer and Vacuum Condensable Materials (VCM). Ambient temperature and pressures will not be constant over orbit.	Photomultiplier	Measure Ambient UV Flux.
Electric Field Detector	STA 1210	Specific design may impose contamination limits.	Capacitive Solid State	Measure ambient electric fields.
Magnetometer	STA 1210	See above.	Rb vapor, triaxial	Measure geomagnetic fields.
Drag Analyzer	STA 1210	See above.		Measure atmospheric drag.
Pressure Gauge	STA 1210	Will be susceptible to gaseous effluents, water vapor, and possibly to particulates.	Ruggedized ion gauge.	Measure ambient atmosphere pressure

Table XXIII. Payload AS-01-A Large Space Telescope

Instrument	Location	Contamination Sensitivity	Description	Measurement Objective/Function
Optical Telescope Assembly (AS100)	STA 749	Exposed optical surfaces susceptible to contamination by condensed gaseous effluents, water vapor, and particulates. Telescope should be covered and repressurized with clean air at small positive pressures for reentry and for service visits by Shuttle.	f/12 Ritchey-Chretien 3m aperture.	Collects & focuses energy & images to instruments, 0.09 to 5 μ .
f/12 Camera Assembly (AS105)	STA 1146 Inside LST	Assembly is located inside LST; will not be directly exposed to space but will be exposed to effluents, products of outgassing, and particulates trapped in instrument area. Image tube optical surfaces must be protected from water vapor.	Camera plus filters	Images: .115 to .555 μ with 1.37 E-3 rad. field.
f/96 Camera Assembly (AS110)	STA 1146 Inside LST	See above.	3 cameras plus filters.	Images: .115 - .340, .165 to .55, .45 - 1.1 μ with 1.7 E-4 rad. field.
FO Spectrograph I (AS121)	STA 1146 Inside LST	See above.	4 instruments, 6 spectral ranges	Faint resolution spectroscope: .115 - .16, .16 - .22, .22 - .352, .352 - .66, .66 - 1.0, 1.0 - 5.0 μ .
FO Spectrograph II (AS122)	STA 1146 Inside LST	See above.		
FO Spectrograph III (AS123)	STA 1146 Inside LST	See above.		
Mid IR Interferometer (AS124)	STA 1146 Inside LST	See above.		
High Resolution Spectrometer I (AS131)	STA 1146 Inside LST	See above.	Echelle Type	High resolution spectroscopy: .115 to .180 μ .
High Resolution Spectrometer II (AS132)	STA 1146 Inside LST	See above.	Echelle Type	High resolution spectroscopy: .180 to .350 μ .
Optional Instrument (AS140)	STA 1146 Inside LST	See above.		
Slit Jaw Camera Assembly (AS170)	STA 1146 Inside LST	See above.		
Instrument Support Equipment (AS180)	STA 1146 Inside LST	See above.	Includes Louver Control Thermal Control System	Maintains constant $293^{\circ} \pm 2^{\circ}$ K in science instrument area.

Table XXIII. Payload AS-01-A Large Space Telescope (Concluded)

Instrument	Location	Contamination Sensitivity	Description	Measurement Objective/Function
Guidance, Navigation, Stabilization Subsystem (SM-101) - Star Tracker	STA 1200 Inside LST	Susceptible to large sporadic particles (100 micrometer) in field of view, which may reflect enough sunlight for the tracker to mistake them for guide stars. Smaller particles (1 micrometer) may scatter enough light to increase background levels and make detection of objects more difficult.	Inertial Reference Unit, CMG Actuators	OTA directed to 4.9 E-6 rad. Provides backup attitude to 1.46 E-4 rad.

Table XXIV. Payload AS-02-A Lyman Alpha Explorer

Instrument	Location	Contamination Susceptibility	Description	Measurement Objective/Function
UV Telescope (AS-210)	STA 1128	Highly susceptible to contamination from condensed gases on optical surfaces and to scattering from small particles (~0.1 micrometer in size) in field of view. Telescope assembly should be covered and pressurized with clean air to slight positive pressure for ascent and reentry.	0.45m, f/15 cassegrain	Collect and focus energy in the 0.115 to 0.320 μ band.
Spectrograph Assembly (AS-211)	STA 1187 Inside spacecraft	Susceptible to gaseous effluents and particulates; image tube must be protected from water vapor.	High dispersion Echelle spectrograph	Resolution: 0.1 Å in 0.08 to 0.15 μ range, measure spectra from comets, planets, stars, earth exosphere.
Lyman Alpha Resonance Absorption Cell (AS-212)	STA 1187 Inside spacecraft	May be less sensitive than other instruments to light scattered over broad wavelength range. Scattering from molecules and particles .1 micrometer in size will tend to reduce signal-to-noise ratio; condensation of gaseous effluents may be important. Telescope and instrument optics are to be maintained at 273°K, so condensation can occur very early in lifetime of satellite.		Detection & intensity measurements of faint source Lyman Alpha radiation. 0.09 to 0.150 μ .
Acquisition Field Camera (AS-213)	STA 1187 Inside spacecraft	Susceptible to large sporadic particles (~100 micrometers) in field of view which may reflect enough sunlight for the tracker to mistake them for guide stars. Smaller particles (~0.1 micrometer) may scatter enough light to increase background levels and make detection of objects more difficult.		

Table XXV. Payload HE-01-A Large X-Ray Telescope Facility

Instrument	Location	Contamination Susceptibility	Description	Measurement Objective/Function
X-Ray Telescope (HE100A)	STA 616 Closure	Particulates and condensate deposited on surfaces and in line-of-sight will degrade performance by scattering.	Nested array of X-ray reflecting mirrors (structure - 3m dia x 15m long - 5000 cm^2 area)	Collect and focus 0.1 to 4 Kev X-ray in a 1° field-of-view with resolution of 2.57 E-6 rad (0.5 arc sec.)
Field Monitor Camera (HE101A)	STA 620	Sensitive to scattering by small particles (~1 micrometer) and by large particles (~100 micrometer) on optics and in line-of-sight. Image tube must be protected from water vapor.	In conjunction with aspect sensor telescope	Monitor X-ray field of view in UV/VL range .40 to .12 μ.
Guide Star Trackers (HE103A)	STA 1210 Inside payload	See above.		Provide offset tracking of two or more guide stars.
Aspect Sensor Telescope (HE105A)	STA 620 Inside payload	See above.	0.3m D x 12m optical scope with above field mon. & star tracker with detector below.	Monitor X-ray field of view in UV/VL range .40 to .12 μ.
Proportional Counter (HE111A)	STA 1210 Inside payload	Specific design may impose contamination limits.		
Image Detector/ Intensifier (HE121A)	STA 1210	See above.	Proportional counter at focal plane with spatial readout.	Provide images in 0.1 to 4 Kev band with resolution of 2.43 E-6 rad (0.5 arc sec).
Crystal Spectrometer (HE131A)	STA 1210 Inside payload	See above.	Crystal array mounted on gimbal and prop. counter.	Provide high resolution spectral measurements in 0.1 to 4 Kev range.
Transmission Grating and Filter (HE143A)	STA 1128 Inside payload	Susceptible to particulates and condensate on surfaces; less sensitive to material floating in line-of-sight.		

Table XXVI. Payload PL-04-A Mars Hard Lander

Instrument	Location	Contamination Susceptibility	Description	Measurement Objective/Function
Multispectral Line Scan Camera	STA 782	On spacecraft bus. Avoid deposition of VCM and particulate on optical surfaces.		Photograph planet surface.
IR Radiometer	STA 782	See above.		Planetary atmosphere temperature, pressure, composition.
UV Photometer	STA 782	See above.		Planetary internal structure.
Magnetometer	STA 782	See above.		Solar wind/atmosphere interaction
Solar Wind Analyzer	STA 782	See above.		Atmospheric composition.
Neutral Mass Spectrometer	STA 835	On Lander. Must be sterile and clean to assure probability of less than 0.001 of one earth organism on Mars.	Quadrupole	Atmospheric temperature.
Temperature Gauge	STA 835	See above.	Thermocouple	Atmospheric pressure.
Pressure Gauge	STA 835	See above.	Transducer	Atmospheric density.
Accelerometer	STA 835	See above.	3 Axis	

Although the Shuttle Payloads may differ in design or sensitivity or offer a wider spectral range of performance than many of the individual experiments on Skylab, some are similar in nature and limited correlation can be attained.

Table XXVII presents a matrix which identifies a proposed Shuttle Payload and similar Skylab experiments. For each Skylab experiment, the spectral range of the experiment, the maximum allowable signal attenuation and the maximum scattering or background noise, the tolerable particle densities are presented. The sensitivities presented for the Skylab experiments were obtained from each of the Skylab experiment's Principal Investigators.

5.5.3 Shuttle Payload Induced Environment - Table XXVIII summarizes the extent of the predictions resulting from the previous sections and the impact on each payload.

The first 3 columns address the range of total mass column densities, number column densities, and maximum return flux when all sources are contributing for all lines-of-sight. The mass and number column densities do not directly concern Free Flying Payloads while in the bay area and are considered not applicable. The return flux values can impact the deployable systems while in the experiment bay during pre-deployment preparation.

The particle emission/scattering column relates to the predicted particle densities background to infrared systems as an emission source and to ultraviolet systems as a scattering source. The signal wavelength λ, particle radius r, and resulting signal strength in watts/micron or brightness in terms of star magnitude are included.

The signal absorption resulting from deposition is listed for a 7 and 30 day mission taken from the deposition per orbit column for the typical sortie mission exposure time for the representative payload surface. The absorption loss is based on attenuation data used for Skylab evaluation for the ultraviolet systems and infrared signal losses from quoted sources that indicate a 0.1 micron deposit will result in a 1% signal loss.(1) The signal wavelength considered, λ, is also included.

(1) Witteborn, F. C.: "Infrared Telescope for a Space Observatory," - Preliminary Draft, July 31, 1973.

Table XXVII. Shuttle Payload Correlation with Skylab Experiment Susceptibilities

Shuttle Payload Designation	Similar Skylab Experiments	Spectral Region	Maximum Allowable Signal Attenuation	Maximum Scattering or Background Noise	Tolerable Particle Densities
A) 1.5m IR Telescope	S191 IR Spectrometer	0.4-15.4 μm	10% Known Degradation 1-3% Unknown Degradation	$B/B_o = 4.0 \times 10^{-9}$	Not Specified
	S192 Multispectral-Scanner	0.4-12.5 μm	< 5% Degradation	$B/B_o = 4.4 \times 10^{-9}$	Not Specified
	Star Tracker	S-20 Visible	Not Specified	S-20 Visible Mag. of 1.16 (is 1/2 Mag. Below Dimmest Target Star)	Particles >10μ Exceed Threshold & Are Trackable as Stars
B) Deep Sky UV Telescope	S019 (UV Stellar Astronomy)	1300-3000Å	< 10% @ 1300Å, 1700Å & 3000Å Correspond to Deposition of 9, 17, or 72Å @ 30° Reflection Respectively	Not Specified	$12.5 \times 10^6/cm^2$ (.01 to .2μm) $5.0 \times 10^5/cm^2$ (.2 to 1.0μm) $2.5 \times 10^4/cm^2$ (1.0 to 5.0μm)
	S183 (UV Panorama)	1500-2100Å 2800-3400Å	Any Attenuation but 50% Will Make Data Useless	Not Specified	Same as S019
	S063 (UV Airglow Horizon Photography)	2400-6500Å	Any Attenuation Between 2350-3450Å but 50% Will Make Data Useless	$B/B_o = 3.3 \times 10^{-10}$	Not Specified
C) 1m UV Diffraction Limited Telescope	Same as B	Same as B	Same as B	Same as B	Same as B
D) 2.5m Cooled IR Telescope	Same as A	Same as A	Same as A	Same as A	Same as A
E) Dedicated Solar Sortie Mission	S020 X-Ray/UV Solar Photography	10-100Å 20-200Å	10% of Incoming Signal Will Be Harmful (Corresponds to ~ 4200Å of O_2)	$B/B_o = 1.2 \times 10^{-8}$	Particles Greater Than ~ 10μ Could Possibly Clog Entrance Slit
	S054 X-Ray Spectrographic Telescope	3-60Å 2-10Å	< 10% Grating is Vulnerable & Film Deposits on Reflecting Surfaces Can Cause Scattering	$B/B_o < 1 \times 10^{-3}$	Not Specified
	S056 XUV & X-Ray Telescope	2-20Å 5-33Å	40Å in 6-60Å λ on Primary Mirror	$B/B_o < 10^{-3}$	Not Specified
	S082-UV Spectrograph and XUV Monitor	970-3940Å 170-550Å	Deposits on MgF_2 Surface Can Cause Scattering & Absorption	$B/B_o < 10^{-4}$	Not Specified
F) Communications/ Navigation Sortie Mission	S193 Microwave Radiometer Scatterometer Altimeter	13.9 GHz	0.5% @ 13.9 GHz ~ 2.54×10^4 μgm/cm^2 or .01 Inch Deposition	Not Specified	Outgassing Creating Increased Pressures (~ 10^{-4} Torr) Could Create Corona Problems
	Star Tracker	Same as A	Same as A	Same as A	Same as A

Table XXVII. Shuttle Payload Correlation with Skylab Experiment Susceptibilities (Continued)

Shuttle Payload Designation	Similar Skylab Experiments	Spectral Region	Maximum Allowable Signal Attenuation	Maximum Scattering or Background Noise	Tolerable Particle Densities
G) Upper Atmosphere Explorer	S019	Same as B	Same as B	Same as B	Same as B
	S063	Same as B	Same as B	Same as B	Same as B
	S183	Same as B	Same as B	Same as B	Same as B
H) Large Space Telescope	S019	Same as B	Same as B	Same as B	Same as B
	S063	Same as B	Same as B	Same as B	Same as B
	S183	Same as B	Same as B	Same as B	Same as B
	S190A Multi-Spectral Photographic Camera S190B Earth Terrain Camera	400-900 nm (Visible) 400-900 nm (Visible)	0.5% @ 400 nm 0.5% @ 650 nm 0.5% @ 900 nm Fluid & Semi-Solid Shall Not Cause Greater Than 0.5% Loss of Transmitted Incident Radiation at 0^{o}-15^{o} Incident Angle @ 400, 650, 900 nm	Equivalent Optical Flare Increase Shall Not Exceed 0.4%, $B/B_{\odot} = 3.7 \times 10^{-9}$	Not Specified
	S191	Same as A	Same as A	Same as A	Same as A
	S192	Same as A	Same as A	Same as A	Same as A
I) Extra Corona Lyman Alpha Explorer	S055	296-1350Å	10% @ 300Å-1350Å	$B/B_{\odot} < 10^{-4}$	10^{14} H, 10^{16} N or O Atoms/cm^2
	S082	170-550Å 970-3940Å	10% @ 170-600Å	$B/B_{\odot} < 10^{-4}$	$10^{10}/cm^2$ All Species
J) Large X-ray Telescope	S020	Same as E	Same as E	Same as E	Same as E
	S054	Same as E	Same as E	Same as E	Same as E
	S056	Same as E	Same as E	Same as E	Same as E
	S150	1-60Å	< 10% @ 60Å < 5% @ 15Å < 1% @ 1Å	Not Specified	Not Specified
	Star Tracker	Same as A	Same as A	Same as A	Same as A
K) Mars Hard Lander	S019	Same as B	Same as B	Same as B	Same as B
	S063	Same as B	Same as B	Same as B	Same as B
	S183	Same as B	Same as B	Same as B	Same as B
	S190A & B	Same as H	Same as H	Same as H	Same as H
	S191	Same as A	Same as A	Same as A	Same as A
	S192	Same as A	Same as A	Same as A	Same as A

Table XXVIII. Payload Contamination Summary

PAYLOAD CLASSES / PARAMETER	TOTAL MASS COLUMN DENSITY (g/cm^2)	NUMBER COLUMN DENSITY (molecules/cm^2)	RETURNED FLUX (MAX) (g/cm^2/sec) 435 Km	RETURNED FLUX (MAX) (g/cm^2/sec) 200 Km	PARTICLE EMISSION/ SCATTERING	MOLECULAR SCATTER/ ABSORPTION	DEPOSITION ABSORPTION 435 Km	DEPOSITION ABSORPTION 200 Km	FLUX ON DEPLOYED SYSTEM AT DISTANCE (Z) (g/cm^2/sec)	DEPOSITION PER ORBIT FOR TYPICAL SORTIE MISSION EXPOSURE TIME FOR REPRESENTATIVE SURFACE (g/cm^2) 435 Km	DEPOSITION PER ORBIT FOR TYPICAL SORTIE MISSION EXPOSURE TIME FOR REPRESENTATIVE SURFACE (g/cm^2) 200 Km
1. Deep Space Payloads	1(-9) to 1(-8)	1(13) to 1(15)	1(-12) to 1(-10)	1(-10) to 1(-8)	$\lambda = 10\mu$ $r = 10\mu$ 10^{-17} w/μ $r=100\mu$ 10^{-15} w/μ	$\lambda=1\mu$ 1(-14)to 1(-12)w/μ $\lambda=10\mu$ 1(-20)to 1(-18)w/μ T > 0.999	>1% (7 days)	>>1%	N/A	5.8(-8)	1.7(-6)
Deep Sky UV Survey Telescope	1(-9) to 1(-8)	1(13) to 1(15)	1(-12) to 1(-10)	1(-10) to 1(-8)	λ=0.1 to 0.3μ M_{uv}=25 to 37 r_{uv}= 10μ	λ=0.1μ M_{uv}=20 to 25 λ=0.3μ M_{uv}=15 to 20 T > 0.999	at 1000Å 7 days<1% 30 days<1%	at 1000Å 7 days<1% 30 days 1%	N/A	3.0(-12)	1.6(-10)
1m UV Diffraction Limited Telescope	1(-9) to 1(-8)	1(13) to 1(15)	1(-12) to 1(-10)	1(-10) to 1(-8)	λ=0.1 to 0.3μ M_{uv} = 37 to 40 r_{uv}= 10μ	λ=.1μ M_{uv}= 20 to 25 λ=.3μ M_{uv}= 15 to 20 T > 0.999	at 1000Å 7 days<1% 30 days<1%	at 1000Å 7 days<1% 30 days<1%	M/A	3.0_-12)	1.6(-10)
2.5m Cryogenically Cooled IR Telescope	1(-9) to 1(-8)	1(13) to 1(15)	1(-12) to 1(-10)	1(-10) to 1(-8)	λ= 10μ r=10μ 10^{-17} w/μ r=100μ 10^{-15} w/μ	λ=1μ 1(-14)to 1(-12)w/μ λ=10μ 1(-20)to 1(-18)w/μ T > 0.999	>1% (7 days)	>>1%	N/A	5.8(-8)	1.7(-6)
2. Solar Payloads Dedicated Solar Sortie Mission	1(-9) to 1(-8)	1(13) to 1(15)	1(-12) to 1(-10)	1(-10) to 1(-8)	λ = 0.5μ M_v=6 r=10μ Coronagraph	λ=0.5μ H_{fp}=1(-11) to 1(-9) (w/cm^2-μ)coronagraph T > 0.999	at 2000Å 7 days 6% 30 days 25%	at 2000Å 7 days<1% 30 days 1%	N/A	5.4(-9)	1.6(-10)
3. Communication Payloads Communications/Navigation Sortie Mission	1(-9) to 1(-8)	1(13) to 1(15)	1(-12) to 1(-10)	1(-10) to 1(-8)	N/A	N/A	N/A		N/A	5.4(-9)	1.6(-10)
4. Free Flying Payloads Upper Atmosphere Explorer	N/A	N/A	1(-12) to 1(-10)	1(-10) to 1(-8)	N/A	N/A	N/A		1.3(-7)at Z=19 ft 2.0(-7)at Z=129 ft 2.0(-9)at Z=1290 ft	N/A	
Large Space Telescope	N/A	N/A	1(-12) to 1(-10)	1(-10) to 1(-8)	N/A	N/A	N/A		1.3(-7)at Z=19 ft 2.0(-7)at Z=129 ft 2.0(-9)at Z=1290 ft	N/A	
Extra Corona Lyman Alpha Explorer	N/A	N/A	1(-12) to 1(-10)	1(-10) to 1(-8)	N/A	N/A	N/A		1.3(-7)at Z=19 ft 2.0(-7)at Z=129 ft 2.0(-9)at Z=1290 ft	N/A	
Large X-ray Telescope Facility	N/A	N/A	1(-12) to 1(-10)	1(-10) to 1(-8)	N/A	N/A	N/A		1.3(-7)at Z=19 ft 2.0(-7)at Z=129 ft 2.0(-9)at Z=1290 ft	N/A	
Mars Hard Lander	N/A	N/A	1(-12) to 1(-10)	1(-10) to 1(-8)	N/A	N/A	N/A		1.3(-7)at Z=19 ft 2.0(-7)at Z=129 ft 2.0(-9)at Z=1290 ft	N/A	

The flux levels on a deployed system are presented as a function of distance from the Orbiter. During deployment manuevers, three distances from the vehicle along the +Z axis were chosen to represent possible deposition at deployed system positions. These were Z = 19, 129, and 1,290 feet. The flux rates on a Payload at these positions are 1.3×10^{-7} g/cm^2/second, 2.0×10^{-7} g/cm^2/second, and 2×10^{-9} g/cm^2/second respectively. The flux levels between Z = 19 and 129 feet increase from Z = 19 and reach a maximum then fall to the level noted at 129 feet. Depending upon the deployment time, significant flux could occur but should present no immediate problem since the deploying payload is essentially closed up. However, RCS deposits can exist from attitude control manuevers and will essentially desorb over a 72 hour period at which time a residual deposit will remain. If the surfaces that have RCS deposits are in the field-of-view of critical surfaces in an operational mode, several days may be required before operation can commence. If the 900 lb thrust engines are employed during deployment, this could be a significant problem.

Particulate material generated by the Orbiter during deployment will experience atmospheric drag effects and should clear the vicinity of the deployed system for altitudes of 500 km or less in times small compared to the deployed system activation time.

At altitudes above 700 km, the drag effect may not be sufficient to clear particulates quickly since the acceleration a particle experiences will drop by two orders of magnitude for an altitude change from 400 km to 1000 km.

The particulates generated by the deployed Payload itself will be an area of concern at any altitude because of the particulates proximity to the Payload and the continuous capability of such particulate generation. The magnitude of the problem will be directly related to ground handling, experiment bay storage, and number of movable surfaces a deployed system will have.

The deposition per orbit values for the typical sortie missions presented in the previous section are based on the following assumptions.

For the infrared systems, all material impinging by return flux mechanisms is allowed to deposit because of the cold surface temperatures. The actual amount reaching all components of a specific configuration can be less than these values. However, these values do represent the possible deposition resulting on a surface at the lower end of the system.

The deep space ultraviolet systems at 435 km will have deposition from outgassing and vernier engine sources. The ultraviolet surface was assumed to be slightly colder than the outgassing sources thus not allowing total deposition to occur. Of the engine return flux, a factor of 0.002 was allowed to deposit and is based on RCS engine testing from the Skylab Program and Skylab flight data.

For the solar sortie missions, the experiment surface was assumed to be at 20°C and the average outgassing sources at 60°C, thus allowing 30% of the outgassing return flux to deposit at 435 km. The amount of engine deposits remaining as in the ultraviolet case is several orders of magnitude below the outgassing sources.

At 200 km, the outgassing molecules cannot reach the experiment line-of-sight to be reflected back since they experience approximately 400 collisions/second with the ambient atmosphere and thus have very short meanfree paths. The engine deposition at 200 km is the major source and has the same value as in the previous case.

For both the Deep Space Ultraviolet and Solar Sortie Payloads, the large amount of return flux from light gases, O_2, N_2, CO_2, CO and H_2O were not allowed to condense on the relatively warm surfaces at 20°C.

The values from Table XXVIII were compared to the applicable Woods' Hole criteria (Table XXIX), GSFC astronomy sortie criteria (Table XXX) and Skylab limits so that a correlation or risk assessment can be made against available criteria or knowledge. The results of such an evaluation are presented in Table XXXI along with comments where applicable.

Table XXIX. Contamination Standards from Woods' Hole Summer Study Work Sheets (July 1973)*

(1) Contamination return rate from leakage and outgassing $\leq 10^{12}$ molecules/cm^2/second

(2) Particulate emission rate (particles 10 μ or larger) $< 10^{-4}$ particles/cm^2/second

(3) RCS fuel expended < 20 kg/day at 1% return

(4) No waste dumps

(5) Column density of $H_2O < 10^{10}$ to 10^{12} (molecules with dipole moment) molecules/cm^2

(6) < 1 ionizing event at detector/day, i.e. <1γ event of energy

>.5 Mev per cm^2 per sec; <100/cm^2 electrons of energy

>.5 Mev on outside of instrument. (per P. Dyal NASA/ARC-SSA phone (415) 965-5520)

* (Applicable document, ASD-PD-18743)

Table XXX. Astronomy Working Group Contamination Control Requirements
(Page 34, Astronomy Working Group Report of May 1973)*

Category (1), Atmosphere Around the Spacecraft

All absorption lines, UV, Optical, and IR, shall be optically thin. Possible exceptions would be lines such as L_α which exist naturally in the earth's upper atmosphere. Continuum emission or scattering shall not exceed 20th mag in the UV in a 1 arc sec circle, or 10^{-16} W noise equivalent power in a 10 arc sec circle (1M Telescope) for $\Delta\lambda / \lambda = 0.5$ bandwidth in the IR at wavelengths from 10 to a few hundred μm.

Category (2), Condensation on Optical Surfaces

Less than 1% loss due to absorption of radiation $\Delta\lambda / \lambda = 0.1$, by condensables on optical surfaces (UV, Optical, and IR) for the entire mission.

Category (3), "Artificial Stars" Produced by Small Particles

Less than one "Artificial Star" (i.e. 10 σ event above 10^{-16} W/$\sqrt{\text{Hz}}$ as seen by the detector for $\Delta\lambda/\lambda = 0.5$ bandwidth, 10 arc sec circle, and 1M telescope from 10 to a few hundred μm wavelength in the IR) per orbit.

* (Applicable document, ASD-PD-18743)

Table XXXI. Applicable Criteria Summary

CRITERIA * / PAYLOAD CLASSES	APPLICABLE WOODS' HOLE STANDARDS (REF. TABLE XXIX)			ASTRONOMY WORKING GROUP REQUIREMENTS (REF. TABLE XXX)			CORRELATION WITH SKYLAB EXPERIMENTS (REF. TABLE XXVII)
	1	2	5	1	2	3	
1. Deep Sky Payloads							
1.5m Cryogenically Cooled IR Telescope	E (1)	N	E (2)	E/N (3)	E (4)	M (5)	(8)
Deep Sky U.V. Survey Telescope	N/A (11)	N/A (11)	N/A (11)	E/N (6)	E (4)	N	(9)
1m U.V. Diffraction Limited Telescope	N/A (11)	N/A (11)	N/A (11)	E/N (6)	E (4)	N	(9)
2.5m Cryogenically Cooled I.R. Telescope	E (1)	N	E (2)	E/N (3)	E (4)	M (5)	(8)
2. Solar Payloads							
Dedicated Solar Sortie Mission	N/A (11)	N/A (11)	N/A (11)	N/A (12)	N/A (12)	N/A (12)	(10)
3. Communication Payloads							
Communication/Navgation Sortie Mission	N/A (11)	N/A (11)	N/A (11)	(7)	(7)	(7)	(7)
4. Free Flying Payloads							
Upper Atmosphere Explorer	N/A (13)	N/A (13)	N/A (13)	N/A (13)	N/A (13)	N/A (13)	N/A (13)
Large Space Telescope							
Extra Corona Lyman Alpha Explorer							
Large X-Ray Telescope Facility							
Mars Hard Lander							

NOTES: E = Exceeded N = Not Exceeded M = Marginal

* Application of these criteria to Shuttle Payloads and the resultant risk assessment should not be taken as absolute and/or as the final judgment. For those cases where criteria was exceeded, additional studies will be required to assess the specific impact.

Table XXXI. Applicable Criteria Summary (continued)

COMMENTS:

1. Exceeds return flux criteria of 10^{12} molecules/cm^2/second.

2. Exceeds column density criteria 10^{10} to 10^{12} molecules/cm^2.

3. Exceeds NEP criteria of 10^{-16} watts for $\lambda = 1\mu$ for $\Delta\lambda/\lambda = 0.5$.

4. Exceeds 1% absorption criteria.

5. False star appearance rate is acceptable (0.4 per/orbit). However large particles will exceed acceptable noise input of 10^{-16} watts for $\Delta\lambda/\lambda = 0.5$.

6. Scattered ultraviolet exceeds criteria M ≤ 20 for high column densities.

7. Insufficient experiment data.

8. Skylab infrared systems (S191,S192) had NEP of ~ 1×10^{-11} watts for $\Delta\lambda/\lambda$ ~0.2 to 1.5. Maximum molecular column densities were ~ 10^{13} molecules/cm^2. No degradation due to scattering or absorption has been identified to date. Shuttle infrared systems will have NEP of ~10^{-16} watts for $\Delta\lambda/\lambda$ ~0.5. Shuttle molecular column densities are predicted to be 10^{13} to 10^{15} molecules/cm^2. Consequently, the greater Shuttle column densities and higher instrument sensitivities have resulted in the previously indicated degradation for the Shuttle instruments whereas no degradation was predicted nor observed for the Skylab infrared instruments.

9. The Skylab ultraviolet experiments (S019,S183,S063) were designed with sensitivities to detect ultraviolet stars with magnitudes of ~7 to 9. Molecular column densities were ~10^{13}. These same instruments would not be degraded by the Shuttle column densities (10^{13} to 10^{15}). However, the Shuttle ultraviolet instruments are expected to detect stars with M_{uv} ~20. Therefore the greater sensitivity of the Shuttle instruments together with the higher column densities accounts for the predicted degradation.

Table XXXI. Applicable Criteria Summary (continued)

10. Significant numbers of particles were observed by the Skylab S052 coronagraph experiment, however, no significant loss of experiment data occurred. This condition is also expected for the Shuttle coronagraph.

11. Woods' Hole criteria are only applicable to infrared instruments.

12. No criteria established.

13. These payloads are not susceptible to Shuttle environment. Primary contamination impact will be caused by self-induced environment.

Specific experiment geometries and mission profiles will cause variations above and below those predicted values for this study presented in Table XXVIII. However, since a potential contamination problem does exist for a number of the Payloads evaluated, additional studies and meaningful criteria for each susceptible Shuttle Payload should be established in the near future to avoid overly restrictive design decisions as well as design deficiencies. Table XXXI shows that the applicability of the current standards or criteria and correlation from previous programs is limited. For those established criteria, the determined induced environment exceeds for all intent and purpose those standards or criteria identified. A requirement exists to assess the applicability of the current standards against those Payloads where sufficient detail exists and to develop criteria for those cases where none currently exists.

In this way, applicable risk factors can be accurately assigned so that timely design changes or operational requirements can be established for both the Payloads and the Orbiter. Until such meaningful criteria are developed for each Payload and until each Payload is modeled in detail with mission exposure profiles, the results of the preliminary contamination study should be taken to indicate a contamination problem appears to exist for all directly susceptible Payloads. Those recommendations given are basic in minimizing the determined affects upon these Payloads.

6. CONCLUSIONS AND RECOMMENDATIONS

6.1 General Discussion - The conclusions and recommendations presented in this study are based upon identified Shuttle Orbiter and Payload operational characteristics consistent to the time frame within which this study was conducted, to the relevant supportive data gained from the Skylab Program, and those typical mission profiles used to assess the affects of contamination. The results presented in Section 5 were established against those considerations where weighted worst case conditions would exist (e.g. during evaporator operation, during RCS 25 lb thrust engine firings and at the 10 hour offgassing rate point) for the sources evaluated. Depending upon actual mission profiles, attitude requirements, and specific Payload configurations; subsequent evaluations may produce conditions in excess or less than those indicated for this study.

The results presented are felt to be within an order of magnitude for those conditions modeled and the conclusions and recommendations presented below are weighted with this in mind along with anticipated program requirements and changes.

The closed form analytical model approach used for this study was shown on Skylab to be an effective tool in contamination evaluation and assessment. The effectiveness of this approach is highly dependent upon the quality of input data such as material characteristics, mission profiles and surface temperatures, vent characteristics, and the description of the physics involved in establishing how the induced molecular and particulate environment will interact with critical surfaces in question.

These types of limitations are inherent in all forms of modeling. However, they do not detract from the overall utility of such a model. An analysis of this nature allows basic parameters to be identifed, geometric considerations to be established, and formulates in a systematic perspective the trends that evolve from variations of important physical parameters. As either physical data concerning many of the complex functions becomes available along with improved definitions of mission requirements, the inherent model limitations can be minimized.

6.2 Study Conclusions and Recommendations - The following study conclusions and recommendations are made with respect to initiating necessary program requirements for contamination control on the identified Payloads and/or the Shuttle Orbiter/Payload interfaces.

6.2.1 Conclusions - By far, the infrared Payloads are recognized to be the most susceptible to contamination. The levels of contamination identified by this study from the major contaminant sources will present a problem to these types of Payloads. The cryogenic nature of these systems inherently make them susceptible to condensing practically every contaminant source effluent capable of impinging upon the cooled surfaces. Deposition as it results from the contaminant cloud is the primary influence on changing thermal backgrounds in cryogenically cooled telescopes. Thermal background changes occur in two basic areas. These are the active thermal control of the telescope as a whole and the specific properties of the critical optical and detector surfaces. Deposition effects on the optical properties of these surfaces are of great concern because of temperature rise in the thermal control surfaces and cooled optics. As a result, a change in emittance properties of these surfaces from deposited contaminants will increase the thermal background from the surfaces. Resultant changes in the telescope's thermal background will increase the usage rate of cryogens and severely limit its dynamic performance. Internal surfaces of an infrared telescope are generally highly reflective specular surfaces with low emittance and absorptance characteristics for both infrared and solar radiation. Doubling the emissivity of these surfaces from values of approximately 0.02 to 0.04 (typical of evaporated aluminum or gold) can cause a temperature change at the detector stage of 5 to 10 degrees Kelvin (depending upon telescope design) on passively cooled detectors operating in the 80 to 120 degree Kelvin range. Roughly 1 μ of ice buildup can raise the emissivity of these surfaces by 0.1 which represents an order of magnitude change in background signal for infrared telescopes. On actively cooled systems, temperatures will be only slightly affected and a slight emissivity change alone will not significantly change the thermal background from the telescope surfaces. However, this condition will significantly increase cryogenic cooling requirements.

From the study it has been shown that for the typical mission profile of seven days, the contaminants capable of condensing upon any exposed cooled surface is approximately 1 μ. Transmission and/or absorption losses can also be significant in that a deposit of 0.1 μ of H_2O can create approximately 1% absorption of signal as well as the net thermal changes previously identified.

The number column densities of polar molecules calculated will not absorb significant amounts of energy. However, the total number column densities are capable of scattering sufficient energy in the 1 to 10 μ spectral range to interfere with those measurements in this range.

Besides deposition, thermal emissions from particles 10 μ and larger will be the largest influence upon infrared type Payloads. NEPs of approximately 10^{-15} to 10^{-17} watts/$Hz^{\frac{1}{2}}$-μ for these systems will require the particulate production to be no more than that observed on Skylab or less. For observed Skylab particulate rates, the infrared Payloads potentially could have undesirable signal interference approximately every two to three orbits. The very nature of the Shuttle Orbiter, the gimbaled infrared Payloads, and the many large movable surfaces on the Orbiter which are not characteristic of a fixed system as Skylab will most likely increase the potential particulate production by an order of magnitude or two. In addition, particulates arising from the RCS engines firings every 5 to 15 seconds could significantly increase the particle environment and subsequently the observation of particulates.

The ultraviolet systems (Deep Sky and 1 meter Ultraviolet Payload) will also be susceptible to deposition from the returned flux. These systems degrade rapidly in the ultraviolet from the deposition of thin films. Deposition thickness of 2 to 3Å will result in approximately 1% signal degradation in the mid-ultraviolet regions (900Å to 1000Å). Deposition rates as a result of returned fluxes calculated in this study indicate that during a typical mission of seven days the deposition would be approximately 2Å, thus indicating a signal loss of nearly 1% for the assumed mission profile. However, the deposition is temperature dependent and for this study the optics or surfaces were considered to be at 20 degrees centigrade. A

decrease in surface temperature would increase the potential deposition.

Although the potential loss of signal due to deposition on ultraviolet systems is marginal for the conditions stated, the impact becomes even more significant if one takes into account the number of potential missions to be flown and the duration of any one mission increasing to 30 days. There is also an implied probable impact on similar Free Flying Payloads such as the LST which has a mission life time of 15 years with 2-1/2 year revisits.

An equal concern arises from the deposition of large particles on critical optical mirrors and surfaces. Dust and other particulates on the mirror surfaces can scatter off-axis stars and could greatly increase the noise background. This particulate matter is similar to that in the case of the infrared Payloads in that the quantity of particulates and the accumulative effect is hard to ascertain prior to a given mission.

For those molecular number column densities calculated in this study, absorption is not considered a problem. Scattering from the molecular column densities will be 20-25 M_{uv} in the mid-ultraviolet (1000Å) and 15-20 M_{uv} in the near ultraviolet (3000Å). Scattering could be a significant concern in the near ultraviolet.

Particulates in the size range of sensitivity for the infrared Payloads (10 μ to hundreds of microns) will not affect the ultraviolet Payloads. Extremely large particles or pieces of structure may be seen (S183 experiment on Skylab recorded an event which was tumbling and was thought to be a piece of space debris) but this affect would be transitory and should not degrade any data.

For those solar oriented Payloads, the main contamination concern may arise for the X-ray type systems. Preliminary Skylab data has shown that the S020 experiment incurred significant data loss below 110Å which is thought to be the result of H_2O. Mass or number column densities calculated in this study exceed those on Skylab in some instances by an order of magnitude or two and may indicate a potential problem for X-ray type systems. Depending upon the

types of solar experiments employed, they will probably detect particulates as observed on Skylab. Although particulates were observed on Skylab by various video displays and experiments such as the white light coronagraph, these particle sightings did not overly influence the quality of data. However, if for the Orbiter, these particle rates increase, this could be an overall concern.

The Communications and Navigation Payload is not anticipated to be affected directly by any of the mass and column densities calculated in this study. Concern for potential corona exists for these systems when the offgassing rates are very high. Delay in on orbit operational activities would minimize this effect. However, the potential delay period may be significant if the offgassing characteristic is predominant.

Contamination as a result of deposition on sensitive antenna cones may be a problem but limited information is available to assess this. Implied to a lesser degree would be long term deposition on thermal control surfaces and the subsequent change in solar absorbtivity of these surfaces. This ultimately could factor into a decision process on refurbishing requirements on the thermal control surfaces. This latter point is inherent for all Payloads which require thermal control paints for passive or active cooling.

As with the thermal control paints, any Star Tracker system required to support the individual Payloads will be affected by particulate sightings. Until Star Tracker operational procedures were changed on Skylab, the Star Tracker failure to track because of random particles became a concern. The number of particle or false star sightings will influence the fidelity of measurement programs where long target dwell times are required to see dim objects (e.g. infrared and ultraviolet observations). The only system which appears to be sensitive to the particulate rate of false stars (as observed on Skylab) is the 0.75 meter ultraviolet survey telescope (42 particles per orbit). A factor of 2 or 3 increase in false star sightings may equally impact other systems.

Contamination of Free Flying Payloads on orbit as a result of the near Orbiter induced environment is not considered a significant problem. The relative short deployment times and the flux

levels of contaminants calculated will not affect these systems. For all intent and purpose, these systems will be closed and protected while stowed in the experiment bay and during deployment and their critical surfaces will not be exposed.

Of particular importance for the Free Flying Payloads is the offgassing nature of the Orbiter and the Payload itself. In order to gain maximum protection for these Payloads, they should be exposed by opening the experiment bay doors and held in a solar mode for a minimum time to insure or allow as much offgassing of the Orbiter/Payload combination as possible. This would also be true for those Payloads which will employ automatic aperture doors such as the LST Payload. Maximum time should be used in assuring that these systems have at least offgassed to anticipated normal levels after being deployed before activation.

Hold periods of this nature will basically assure that particles that arise from deployment will be swept away. However, for the high orbits (e.g. 700 km) particles could reside for days. In any case, after deployment, the Free Flying Payload will in itself produce particulates and depending upon operational activities will have its own environment to be concerned with and not that of the Orbiter.

This latter point is extremely important in that this study addressed only the Orbiter and its major sources. Each individual Payload whether Free Flying or in the Spacelab configuration will represent a large system many times the size and complexity of unmanned satellites which themselves have incurred performance loss as a result of various contamination affects. Although this study begins to address major program contamination problems, specific systems will be required to be assessed in detail both in the automated mode and in the sortie mode.

Free Flying Payload life times may be further decreased from contamination during those periods where on orbit attending is required. This latter condition will impact these systems both from the near induced environment from the Orbiter and as a result of manned activities that require EVA to support. This may require control of active overboard dumping during deployment and/or attending operations.

Any direct impingement from the Orbiter RCS upon deployed payloads must be avoided. Skylab results have shown that RCS engines are capable of physically deflecting operational surfaces such as solar arrays from hundreds of feet distance. This momentum transfer from RCS impingement may cause physical failures in solar arrays, antenna, and low strength doors or windows employed on a payload. In addition, the resulting deposition of RCS engines have been shown to result in long term effects which may increase the on orbit operational activation time to minimize the affect. The residual deposition from RCS engines will most likely decrease operational life times of critical operational surfaces (e.g. solar arrays, thermal control surfaces, windows, antenna, etc.) as a function of the number of impingements and the amount deposited.

No interaction of the contaminants with solar radiation was considered for this study. However, on Skylab it was shown to be an important concern. The combined affects of contamination and solar radiation could conceivably present a condition where the resulting affect is more pronounced than the individual affects separately.

Insufficient detail is available concerning the environment seen by the Orbiter and subsequently the stowed Payload during launch and reentry. Inherently there are basic protective measures that can be employed. These include:

a. purged systems,
b. protective covers,
c. protective doors,
d. stowage design,
e. operational constraints such as delayed cooling.

Further evaluation of these phases along with more specific details concerning individual Payload design philosophy and operational activities will be required to attain more responsive and definitive requirements.

In summary, the infrared Payloads are recognized to be the most susceptible Payload to contamination. In one sense, the cryogenic nature of these systems are unique in that they will trap all of

the contaminants reaching these critical surfaces. This will not occur for other payloads. Common to the infrared Payloads and a number of other Payloads is the particulate environment. The infrared Payloads should set many of the requirements for contamination controls for the Orbiter and other Payloads. Limiting the impact of the on orbit induced environment upon infrared Payloads will essentially set the basis for minimizing the affects upon any other Payload system. The infrared Payloads should be considered fundamentally the pacing system for contamination control especially for the ground handling and the launch and reentry phases of operation.

An important consequence of this study indicates that all the sources considered impact the Payloads in one condition or the other. On Skylab, experiment viewing requirements were essentially unidirectional and the location of vents or directional sources could be established or constrained to meet operational needs. The multi-directional viewing requirements of some Payloads and the positioning of all major vent sources on the same side of the Orbiter (where they directly impact lines-of-sight by their forward flow fields or be reflected into the lines-of-sight) decreases the ability to provide unique control on these sources.

The elimination or reasonable reduction in rate of any one source considered does not necessarily present acceptable environments for those affected Payloads. Improvements in those sources which cannot be controlled and combined with improvements and/or elimination of those controllable sources will be the basic requirement needed to minimize the contaminant impact upon those Shuttle Payloads where the contaminant affect has been identified as a potential problem. Design changes in the Orbiter and/or the individual Payloads along with yet identified new requirements will no doubt increase the demands upon such contaminant sources as the evaporator and the RCS attitude control system. Improved sensitivities for Payloads will also drive contamination requirements to tighter controls. Therefore, where sources can be eliminated, recommendation should be made early in the design phases to eliminate these sources. This would eliminate the potential of unknown future program requirements dictating late and costly hardware changes.

6.2.2 Recommendations - As a result of this study, the following recommendations are made with respect to identifying the necessary program considerations for initiating contamination control on those Shuttle Payloads studied and the Shuttle Orbiter/Payload interfaces.

a. All liquid and/or large molecular overboard venting such as the evaporator should be studied in detail to select a position that venting will have no impact upon those critical lines-of-sight or critical Payload surfaces. The three positions considered for this study all contribute significantly to the induced environment and subsequent critical lines-of-sight. In advent this cannot be accomplished, containment of these sources must be considered. During deployment periods of Free Flying Payloads, all liquid and/or large overboard venting should be contained.

b. Attitude control other than the defined RCS bipropellant vernier engine system should be considered for those impacted Payloads. CMG control and cold gas thruster systems on Skylab worked effectively.

c. The leakage characteristics for the Orbiter should be reviewed. Although Skylab leakages were less than those anticipated, Orbiter leakages could be higher as a result of repeated launchings and landings (not to say the least for hard landing impact upon the seal integrity of the cabin).

d. Particulate control through design and manufacturing of the Shuttle Orbiter and Payloads and ground handling must be maintained at least at Skylab levels if not better.

e. Vacuum and vibration testing should be initiated for representative Shuttle Orbiter external surface geometries to establish a characteristic outgassing rate, an offgassing duration characteristic, and the particle production characteristics.

f. During final ground handling and installation into the Orbiter experiment bay and until just prior to initiation of operational activities, consideration should be given to using a break away protective bag or envelope to protect the Payload during ground, launch, and early on orbit environment.

g. Where feasible, all sensitive Payloads should have the capability to hold positive purges against the ambient environment during launch and reentry.

h. Maximum design considerations should be given for sensitive Payloads while stowed during launch and reentry to use the experiment tie down hardware on the pallet as a protective device for contamination control.

i. Deployment and initiation of operations for Free Flying Payloads should be deferred until the initial offgassing rate of both the Orbiter and the Payload reach near steady state acceptable conditions.

j. Free Flying Payload systems should include a cold gas thruster system or employ special rendezvous techniques which would allow the Payload to deploy from the Orbiter vicinity and thus minimizing or eliminating RCS usage for the Orbiter.

6.3 Future Study Activity Recommendations - The following future study activities are identified. These study recommendations are based upon those areas identified as a result of this study that require further investigation and those which their scope were beyond this study or insufficient detail information was available.

a. Review the Woods' Hole standards and the Goddard Space Flight Center criteria and establish meaningful criteria for basic Payload classes which would reflect their sensitivity to different contamination affects.

b. For those Payloads where sufficient design detail is available for review, establish

   1) a Payload susceptibility analysis,
   2) detailed Payload configurations
   3) mission profiles
   4) a model of each Payload whether in the sortie or free flyer mode
   5) the influence of each Payload on its own contamination environment and to the Orbiter and Orbiter experiment bay area.

c. Initiate a study to identify the launch and reentry environment so that quantitative assessment of these phases can be made.

d. Determine types, locations, and sensitivity ranges of contamination detection instrumentation required to monitor real time assessment of specific Payloads on orbit and during ground handling phases.

e. Continue to increase the fidelity of the existing model and develop a generalized model for all mission profiles including temperature profiles, surface mapping capability, and material identification capability.

f. Based upon a more applicable Payload sensitivity criteria and the modeling of the Orbiter induced environment, establish a Shuttle Payload contamination design handbook.

7. NOTES

7.1 Abstracts - The following abstracts are presented where applicable in support of technical footnotes contained in this report.

a. Chirivella, J. E. and Simon, E.: "Molecular Flux Measurements in the Back Flow Region of a Nozzle Plume," J.P.L., JANNAF 7th Plume Technology Meeting, April 1973.

Abstract - A series of tests were conducted at JPL to measure the mass flux in the far field of a nozzle plume in a high vacuum with emphasis on the back flow region. Existing theories to predict the far field of a plume are not adequate for large angular departures from the plume axis. The measurements presented in this report provide fairly accurate data for off-axis angles as large as 140° (i.e., in the back flow region). This region, since it is well behind the exist plane, is of particular interest to those concerned with instrument contamination. Usually sensitive spacecraft surfaces are located in the region affected by the back flow.

The tests, which utilized five different nozzles, were performed at the JPL Molsink facility. Parameters such as expansion ratio, throat diameter, nozzle lip shape, and plenum (chamber) pressure were varied. Carbon dioxide and nitrogen gases were flowed and mass flux measurements were taken using quartz crystal microbalances in as many as nine different locations relative to the test nozzle.

The tests have resulted in a large matrix of data that were correlated and compared to the Hill and Draper flow prediction theory. These tests are a continuation of earlier attempts to provide quantitative data, the results of which were previously published in two JPL reports.

Several conclusions with respect to the effect of nozzle and gas parameters on the amount of back flow mass flux are offered, and it was demonstrated that gaseous mass fluxes, which are not predictable by present theories, are encountered in the region behind the nozzle exit plane. This knowledge is significant if materials incompatible with the gaseous exhaust products are used in this region.

b. Simons, G. A.: "Effect of Nozzle Boundary Layers on Rocket Exhaust Plumes," AIAA Journal, Vol. 10, No. 11, November 1972.

Conclusion - It has been shown that the density in the plume at large angles from the centerline is a sensitive function of the ratio of the nozzle boundary-layer thickness to the exit radius. Analytic expressions have been developed which relate the gas density to the rocket nozzle and boundary-layer properties. However, these relations possess an arbitrary constant (U_{lave}/U_2), the value of which lies between 0.5 and 1. Further numerical experiments are required to confirm the existence and the value of this constant.

The angular distribution of the boundary-layer streamlines in the rocket plume has been obtained, and it has been demonstrated that only a very small portion of the boundary-layer gas expands beyond the inviscid turning angle θ_∞. The primary effect of viscosity at the walls of the rocket nozzle is to raise the density of the expanding boundary-layer gas and reduce its velocity.

These conclusions are valid only if the "exponential" density profile is a universal result. Additional numerical computations are necessary to establish this assumption and confirm the present results for the plume density.

c. Ratliff, A. W.; Audeh, B. J.; and Thornhill, D. D.: "Analysis of Exhaust Plumes from Skylab - Configuration R-4D Attitude Control Motors," LMSC/HREC D162171, March 1970.

Summary - The exhaust plume flow field of the Skylab (formerly AAP) configuration reaction control system (RCS) engines has been determined analytically as a preliminary step in the prediction of heating rates, forces and contamination effects due to these plumes. The engine utilized, which is designated R-4D, burns nitrogen tetroxide and monomethlyhydrazine (N_2O_4/MMH) propellant.

Engine configurations, nozzle geometries, propellant description, and operating conditions were supplied by three agencies: (1) NASA-Marshall Space Flight Center, Huntsville, Alabama; (2) the Marquardt Corporation, Van Nuys, California; and (3) NASA-Manned Spacecraft Center, Houston, Texas.

Plume flow fields in a vacuum environment were calculated for the engine used on the Command Service Module. Calculations began in the combustion chamber extended through the nozzle and continued into the plume to about 50 feet axially and radially from the engine.

Flow striations (oxidizer-to-fuel variations) were considered in the analysis based on injector information supplied by the Manned Spacecraft Center. A thermochemical program was used to define combustion product specie concentrations and thermodynamic properties of the propellant system. A one-dimensional streamtube solution was used to define the physical and thermodynamic properties after equilibrium combustion. An equilibrium chemistry ducted mixing analysis was made through the combustion chamber. A time-dependent transonic solution was used to describe the two dimensionality of the flow in the convergent section of the nozzle and through the nozzle throat. A method-of-characteristics solution was begun at the nozzle throat using equilibrium thermochemical properties up to a point in the flow at which a kinetic analysis indicated that the flow was chemically frozen. The plume was then generated using the nozzle exit conditions as starting information. The nozzle boundary layer effect on the plume was included and the region where non-continuum conditions may exist is indicated.

Two shock waves were considered and treated in this analysis. The nozzle shock and its reflection from the nozzle axis were computed as integral parts of the total flow field. Also included in this analysis is a correlation study of several R-4D engine and plume parameters. This information provides justification for the particular oxygen-to-fuel gradient used as well as verification of the general analysis procedure.

d. Naumann, R. J.: "Column Densities Resulting from Shuttle Sublimator/Evaporator Operation," NASA-TM-X-64794, October 1973.

Abstract - The proposed disposal of H_2O from the Shuttle fuel cell operation by ejecting it in vapor form through a supersonic nozzle at the rate of 100 lb/day has been investigated from the point of view of the possible interference to astronomical experiments. If the nozzle is located at the tail and directly along the shuttle longitudinal axis, the resulting column density will be less than 10 to the 12th power molecules/sq. cm at viewing angles larger than 48 deg. above the longitudinal axis. The molecules in the trail will diffuse rapidly. The column density contribution from molecules expelled on the previous orbit is 1.3 X 10 to the 8th power molecules/sq. cm. This contribution diminishes by the inverse square root of the number of orbits since the molecules were expelled. The molecular backscatter from atmospheric molecules is also calculated. If the plume is directed into the flight path, the column density along a perpendicular is found to be 1.5 X 10 to the 11th power molecules/sq. cm. The return flux is estimated to be of the order of 10 to the 12th power molecules/sq. cm/sec at the stagnation point. With reasonable care in design of experiments to protect them from the backscatter flux of water molecules, the expulsion of 100 lb/day does not appear to create an insurmountable difficulty for the shuttle experiments.

7.2 Abbreviations - The following abbreviations were used in this report and represent terminology relevant to this study and programs used to obtain supportive data for this study.

ABPS	-	Air Breathing Propulsion System
APU	-	Auxiliary Power Unit
ATM	-	Apollo Telescope Mount
CDC	-	Control Data Corporation
DOY	-	Day of Year
ECLSS	-	Environmental Control Life Support System
ESRO	-	European Space Research Organization
EVA	-	Extravehicular Activity
f/	-	Focal Ratio
GSFC	-	Goddard Space Flight Center
HRSI	-	High Temperature Reusable Surface Insulation
IML	-	Inner Mold Line
IR	-	Infrared
JP	-	Jet Propulsion
JSC	-	Lyndon B. Johnson Spacecraft Center
LOS	-	Line-of-sight
LRSI	-	Low Temperature Reusable Surface Insulation
MCD	-	Mass Column Density
MMH	-	Monomethyl Hydrazine
MSFC	-	George C. Marshall Space Flight Center
M_{uv}	-	Star Magnitude - Ultraviolet
M_{v}	-	Star Magnitude - Visible
NCD	-	Number Column Density
NEP	-	Noise Equivalent Power
OFR	-	Offgassing Rate
OGR	-	Outgassing Rate

7.2 Abbreviations - continued

OML	-	Outer Mold Line
OMS	-	Orbital Manuevering System
QCM	-	Quartz Crystal Microbalance
RCC	-	Reinforced Carbon-Carbon
RCS	-	Reaction Control Subsystem
RF	-	Returned Flux
RTV	-	Room Temperature Vulcanized
SL	-	Skylab
SRBM	-	Solid Rocket Booster Motor
TPS	-	Thermal Protection System
UV	-	Ultraviolet
VCM	-	Volatile Condensible Material
X-POP	-	X Axis Perpendicular to Orbital Plane
X-Z-IOP	-	X-Z Plane in Orbital Plane
Y-POP	-	Y Axis Perpendicular to Orbital Plane
Z-IOP	-	Z Axis in Orbital Plane
Z-POP	-	Z Axis Perpendicular to Orbital Plane

7.3 Definitions - The following definitions are presented to clarify terminology used in this report which reflect unique characterization of the principles, procedures, and methods of application that would be generally applicable to utilization of the results of this study.

a. Mass Column Density - The mass contained in a constant unit cross-sectional area extending from an origin to infinity, expressed in units of Mass/Unit Area.

b. Number Column Density - The number of molecules contained in a constant unit cross-sectional area extending from an origin to infinity, expressed in units of Molecules/Unit Area.

c. Flux - Mass flow through a unit area, expressed in units of Mass/Unit Area/Unit Time.

d. Line-of-Sight - The line being sighted from a critical surface and extending along a given direction of interest to infinity. Column densities are calculated along lines-of-sight.

e. View Factor - That fraction of the total mass leaving one surface that is capable of impinging upon another surface of interest in its field-of-view.

f. Interaction Sphere - Geometrically developed spheres along a given line-of-sight which establishes surface-to-surface relationships in its field-of-view such as distance, angular, and view factor.

g. Interaction Plane - Geometrically developed discs along a given line-of-sight which establishes surface-to-surface relationships in their fields-of-view such that for a calculated contaminant density at a given disc location the returned flux to a surface of interest from contaminant interaction with the ambient atmosphere can be calculated.

h. Returned Flux - The mass flow of contaminants through a unit area reflected back to a surface of interest as a result of collisions with the ambient atmosphere expressed in Mass/Unit Area/Unit Time.

i. Outgassing - That contribution to contamination which comes from the material bulk characteristics and is long term in nature.

k. Offgassing - That contribution to contamination which is related to the volatiles which are either adsorbed to the material and/or carried in the preparation of a material and boil off very rapidly when exposed to vacuum.

l. Beta Angle - That angle between the orbit plane and the earth-sun line.